Numerical studies on the phase transformation and crack generation of hypo peritectic steel during continuous casting

연속 주조 공정 중 아포정강의 상변화 거동

및 크랙 발생에 관한 수치해석 연구

2021년 2월

서울대학교 대학원

재 료 공 학 부

조 준 현

Numerical studies on the phase transformation and crack generation of hypo peritectic steel during continuous casting
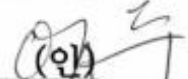
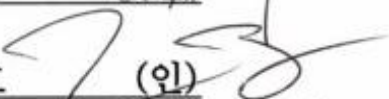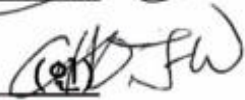지도 교수 이 경 우

이 논문을 공학박사 학위논문으로 제출함
2021년 2월

서울대학교 대학원
재 료 공 학 부
조 준 현

조준현의 공학박사 학위논문을 인준함
2021년 2월

위 원 장 _____ 이 명 규 _____ (인)

부위원장 _____ 이 경 우 _____ (인)

위   원 _____ 정 인 호 _____ (인)

위   원 _____ 조 중 욱 _____ (인)

위   원 _____ 이 중 의 _____ (인)

Abstract

In the continuous casting process, hypo peritectic steel has a complex phase change and a high cracking ratio. So, first, we develop a model of phase transformation that can simulate the phase change behaviors of the hypo peritectic steel. This new model is suggested to predict the behaviors of phase transformation during continuous cooling by considering the thermodynamics, empirical formulas, and carbon diffusion. Particularly, massive transformation from δ phase to γ phase and undercooling from the peritectic temperature to the formation of γ phase (dT_p) are included in this model. As a result, it is showed that the phase change behaviors of the hypo peritectic steel have two paths. When the solidification is completed without the peritectic transformation to all δ phases before the temperature reaches T_{ps} ($=T_p$ (peritectic temperature) $-dT_p$), the solidified δ phase is transformed to the γ phase by the massive transformation. On the other hand, when the peritectic transformation at the L/δ interface starts at T_{ps}, the growth of the γ phase by the peritectic transformation is generated by the carbon diffusion.

Using the results of the phase change model of hypo peritectic steel, the mechanisms of crack generation in the

continuous casting process were investigated. So, new models are developed, such as strain rates in solid, volume contraction rates with liquid, and pore formation susceptibilities. In addition, stress model is developed for calculating the stress distribution in the solidified shell. As a result, it can be suggested that the massive transformation in solid and peritectic transformation during solidification are the main mechanisms of crack generation. In addition, it is showed that these two crack mechanisms are divided based on the linear relation between carbon contents and dT_p, and that the probability of crack generation is high near the transition boundary between the two mechanisms.

The crack generation ratios are analyzed by using the results of models for predicting crack generation. In order to apply the results of the models to alloying steel, an equation of effective carbon composition is suggested. As a result, it is possible to analyze the behaviors of the crack generation ratio according to the effective carbon contents at various experiments by using the temperature at which massive transformation starts and the pore formation susceptibilities at a specific dT_p. Furthermore, the effects of silicon, manganese and casting speed on the behaviors of crack generation are analyzed. Casting speed, silicon concentration, and manganese

concentration shifted the effective carbon composition with the maximum crack ratio. These behaviors of crack ratios according to casting speed, silicon, and manganese can be understood by the difference of δ/γ interfacial energy as the energy to overcome to generate γ phase. As a results, because the casting speed, silicon contents, and manganese contents can change the dT_p by affecting the nucleation of the γ phase, it can be suggested that they can change the carbon contents with the maximum crack ratio.

Table of Contents

List of Figures

dT$_p$ is 20K.

List of Tables

Chapter. 1 Introduction

1.1 Continuous casting

Steel is one of the most used materials in the worlds, and the production of steel has been increasing continuously since the 1960's. Today, about 1800 million tons of crude steels are produced worldwide.[1] Especially, about 96.4% of the steel produced in the world was produced by a continuous casting process in 2019.

The continuous casting process began to be used as a method for non−ferrous metals from the 1930s. And in the 1960s, steel was produced by using continuous casting process.[2] In the 1980s, steel was produced the most through continuous casting process. The continuous casting process has many advantages such as high productivity, energy saving, and high quality of steel. These advantages are the reason why most steels are produced by continuous casting process instead of ingot casting.

Fig. 1.1 is a schematic diagram of the equipment of continuous casting process. [3] The steel producting process through the continuous casting process and the roles of each equipment are as follows.[2] Liquid steel with a specific composition in the ladle is transferred through the nozzle to the turndish. The turndish is used to properly control the amount of liquid steel transferred to the mold. The liquid steel flows to the mold through the submerged entry nozzle

(SEN). The SEN is used to prevent pickup of oxygen by molten steel and control flow conditions in the mold. The liquid steel begins to solidify in the mold. Copper molds are generally used, and heat is transferred through water flowing inside the mold to solidify the liquid steel. When the liquid steel is solidified in the mold, mold flux is also added to control lubrication and heat transfer. Liquid steel is solidified from the surface of mold, and the thickness of the solidified shell gradually increases through the mold. At the end of the mold, solidification of steel is not completed. However, the thickness of the shell is sufficient to sustain the pressure by liquid steel inside. This cooling in the mold is called primary cooling. After primary cooling, water is directly sprayed onto the surface of the steel to solidify. This process is called secondary cooling. The solidified steel by continuous casting is cut to certain size and transferred to a rolling meal.
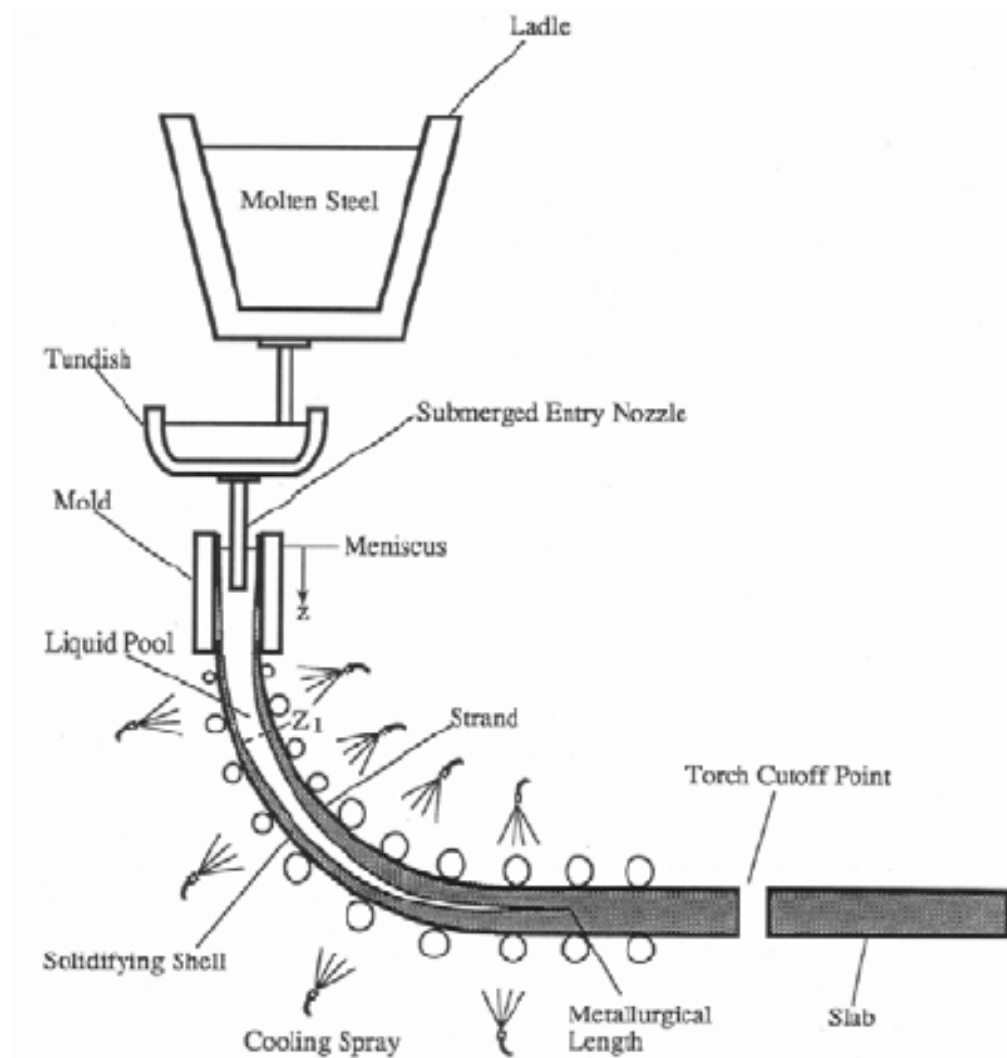
Fig. 1.1 A schematic diagram of continuous casting process [3]

1.2 Problems of continuous casting

There are many problems in the continuous casting process as shown at Fig. 1.2. [4] These problems can be roughly divided non-uniformity of surface of shell and crack generation.

One of problems of continuous casting process is a transversal cracking. And, the transversal cracking can be divided into transversal corner cracking and transversal facial cracking. The transversal cracking occurs by sticking in the mold by friction between mold and strand, severe cooling, and bending at too low temperature. [5] Additionally, Composition of alloy elements, uneven cooling in the mold, and flow and temperature of water can generate the transversal cracking. [6, 7]

In the continuous casting process, longitudinal cracking can be generated. Longitudinal cracking is mainly affected by improper mold design, irregular solidification due to irregular cooling, and casting speed, and steel compositions.[8] Longitudinal cracking can be divided into longitudinal corner cracking and longitudinal facial cracking. Longitudinal corner cracking is caused by wear or deformation of the mold, or uneven solidification by heat transfer that affected by gap formed at the corner of mold. [5, 9] Longitudinal facial cracking

is known to be strongly influenced by iron grades. In particular, peritectic steel has large possibilities of longitudinal facial cracking.[7] In addition, excessive cooling and very fast or slow casting speeds can also cause longitudinal facial cracking.[7]

Unlike cracking on the surface, inclusion lowers the cleanliness of the surface of the shell. Inclusion can be generated by products of de-oxidation, or slag particles that are trapped. Also, pick up of carbon can generate inclusion by improper lubricating materials. [10] Occasionally, if a hot spot is generated on the shell surface by using an improper mold flux, the shell may stick as if it is welded to the mold. This is called sticking. When this phenomenon becomes severe, the shell breaks at the bottom of the mold and the liquid steel inside shell can flow out. This phenomenon is called break-out. [11] In addition, bleeding is the oozing of liquid steel from a broken surface. [5]
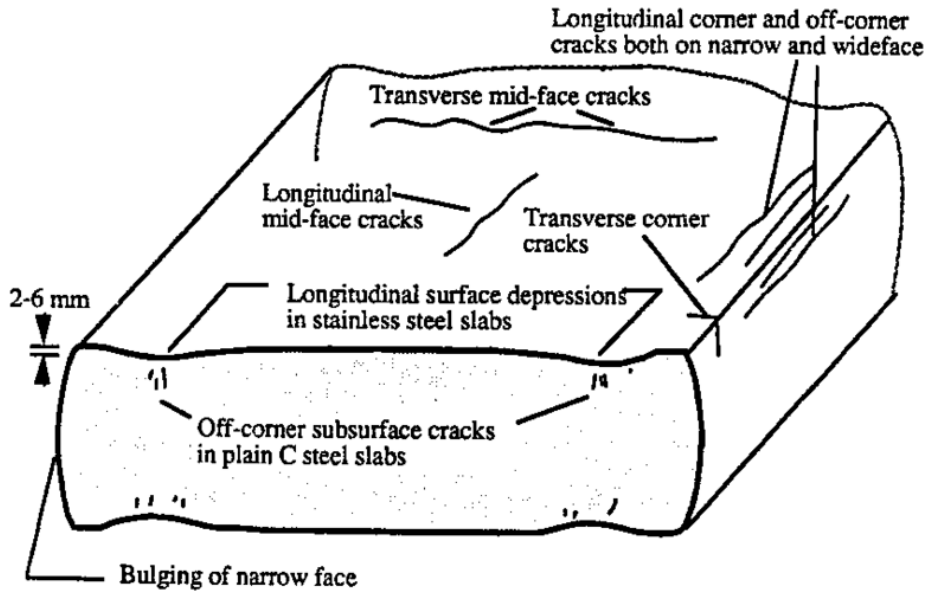
Fig. 1.2 Schematic diagram of surface defects during continuous casting process.[4]

1.3 Hypo peritectic steel

Hypo peritectic steel is a steel in the range of carbon contents between about 0.09wt%C and 0.17wt%C as shown at Fig. 1.3. The behaviors of phase transformation of hypo peritectic steel at equilibrium state are as follows. Hypo peritectic steel starts solidification to δ phase from liquid temperature, and starts peritectic solidification at the peritectic temperature. So, δ phase and liquid are transformed to γ phase, and solidification finishes at peritectic temperature. Below the peritectic temperature, remained δ phase is transformed to γ phase additionally.

The mechanisms of peritectic solidification were suggested from models and experiments of phase transformation of hypo peritectic steel. Peritectic solidification can be divided to peritectic reaction and peritectic transformation as shown at

Fig. 1.4. [12] Peritectic reaction is that γ phase grows along the L/δ interface. Growth of γ phase at the L/δ interface driven by super saturation at liquid. During peritectic reaction, carbon moves from γ phase, through liquid, to δ phase, and this rejected carbon dissolute δ phase. As a results, γ phase grows at triple points of δ phase, γ phase, and liquid. And the γ phase thicken, too. After δ phase and liquid are separated by formation

of γ phase, peritectic transformation starts. Peritectic transformation is that γ phase grows simultaneously into the δ phase and liquid. The δ phase transformed to γ phase by long range solid state diffusion in γ phase.

   At the previous section, there are many problems during continuous casting. Especially, hypo peritectic steels are known to have high crack generation ratios.[7, 13] This phenomenon are known to be affected by large volume contraction by peritectic transformation and cooling at the early stage of continuous casting. Because δ phase and liquid with low density are transformed to γ phase with large density simultaneously.
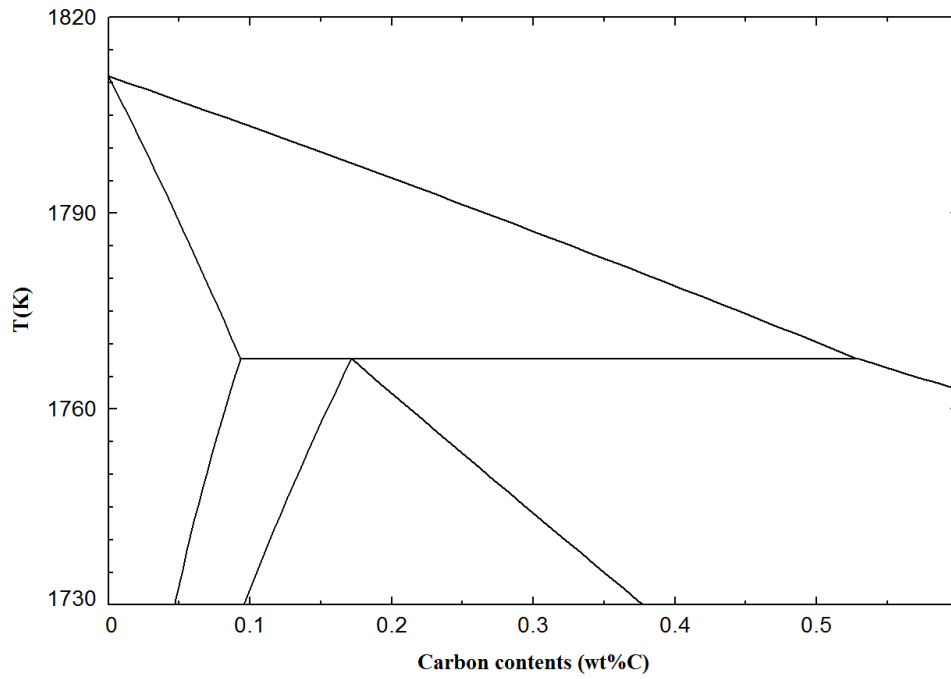
Fig. 1.3 Phase diagram of Fe−C system

peritectic transformation   peritectic reaction
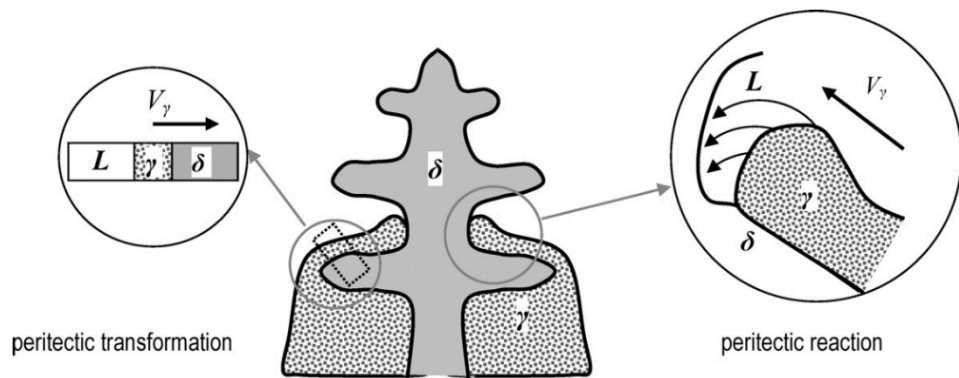
Fig. 1.4 Schematic diagram of peritectic solidification.[12]

Chapter. 2　Literature review of phase transformation and crack generation of hypo peritectic steel

2.1　Modeling of phase transformation for hypo peritectic steel

Several models have been developed to analyze the phase change behaviors of hypo peritectic steel based on the assumption that carbon diffusion is the controlling mechanism of phase transformation.[14−17] Also, it was assumed that peritectic transformation starts at the peritectic temperature, and peritectic transformation is generated at dendrite arm spacing. For calculating the peritectic transformation, the heat transfer at the dendrite arm spacing is first analyzed to calculate the temperature, and then the phase change behaviors are predicted by considering carbon diffusion and mass conservation of carbon.

Shibata et al. showed the speeds of the L/δ, L/γ and δ/γ interfaces comparing the results of phase transformation model and those of by a confocal scanning laser microscope and an infrared image furnace.[17] They calculated speeds of each interface using the models proposed by Uehima et al.[18] The plate−shaped domain is divided into Liquid, δ phase, and γ phase. The liquid phase and the d phase are located at both ends of the domain, and the g phase is in the middle. The main mechanism

8

of phase transformation is carbon diffusion from liquid to δ phase. The results of their experiments showed that the speeds of each interface by planar growth of γ phase growth were several μm/s. So, it was reported that the speeds of phase transformation of the hyper peritectic steel is the results of carbon diffusion by calculating the speeds of interface by phase transformation model.

Mizukami et al. calculated the behavior of phase transformation of peritectic steels by carbon diffusion as main mechanism of phase transformation for various carbon compositions, too.[15] They simulated the behaviors of phase transformation using 1-dimensional domain as shown at Fig. 2.1(a). So, they could show the different behaviors of phase transformation by low carbon steel, hypo peritectic steel, hyper peritectic steel, and high carbon steel. As a result, they could predict the possibility of crack generation by comparing the change of tensile strength and elongation applied to each phase.

Konish et al. calculated phase change behaviors assuming carbon diffusion controlled transformation according to heat flux. [16] They used a triangular 2-dimensional domain considering the shape of dendrites as shown at Fig. 2.1(b). By combining the results of phase transformation model with a finite-element stress model, the stress inside the solidified

shell could be calculated. So, it was suggested that cracks may occur if the stress of the solidified shell is greater than the ultimate tensile strength.
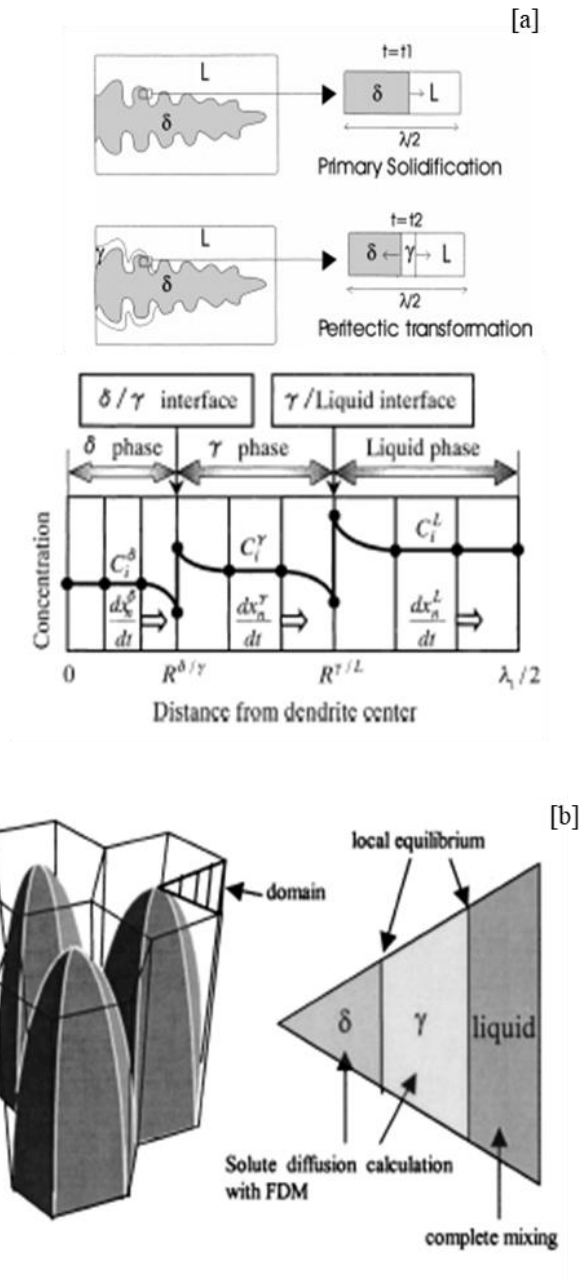
Fig. 2.1 Models of phase transformation of peritectic steel (a)1-dimension domain [15], (b)2-dimension domain[16]

2.2 Modeling of predicting crack generation during continuous casting

Many researchers reported that hypo peritectic steel has high crack ratio during continuous casting process. This phenomenon is generally believed to be influenced by local deformation of the solidified shell by peritectic solidification and cooling. These local deformations of the shell may cause uneven heat transfer in the mold or stress generation on the shell surface, which may cause cracks. [19] But, the exact mechanisms of crack generation are not still clarified. So, many researchers have suggested the mechanisms of crack generation for hypo peritectic steel. In this section, the mechanisms of crack generation suggested by many researchers are divided into two based on completion of solidification.

2.2.1 Internal stress and strain induce crack

Several groups suggested that the stress generated inside solidified shell by cooling and phase transformation is the main mechanism of crack generation of hypo peritectic steel.

Suzuki et al. suggested that index of stress by the product of the amount of volume change and the ratio of volume change during peritectic solidification, because stress is proportional to strain and strain rates. [19] So, they reported that hypo peritectic steel has large index of stress by peritectic transformation, and large cooling rate can cause large stress in solidified shell.

Several groups calculated stress distribution in solidified shell by using computational models.[20−22] They calculated the temperature inside the shell considering the phase change according to temperature. And then, the stress distributions inside the solidified shell were calculated by using the calculated temperature distribution in solidified shell. So, they suggested the location in shell and the compositions of steel with a high probability of crack generation.

Zappulla et al. calculated the distribution of temperature, stress and strain inside the solidified shell according to the heat flux and carbon composition.[20] In this model, They considered the strain affected by elasticity, plasticity, and

thermal deformation. In particular, the plastic deformation model was used considering the deformation of steel at high temperatures. As a result, when the high heat flux is high, and the steel grades are hypo peritectic steel, large stress is generated inside the shell.

2.2.2 Incomplete liquid filling with deformation

Many groups have studied the volume change with the remaining liquid fraction between dendritic arms during solidification. Because it was reported that crack generations in the continuous casting process were seen in the interdendrites.[23] These may be related to the inflow of liquid phase into the dendritic arm spacing during solidification. J. Borland suggested that it is difficult for liquid to penetrate into dendrite arm spacing during solidification, when fraction of liquid is 0.01 to 0.1.[24] So, if large stress due to phase change occurs with small liquid fraction, stress cannot be released by liquid. Therefore, cracks may occur during solidification.

On the basis of this suggestion, Clyne et al. suggested the cracking susceptibility coefficient by dividing time of the liquid feeding zone by time of the cracking zone.[25] They divided the mushy zone into liquid feeding zone (0.4<fs<0.9) and the cracking zone (0.9<fs<0.99). Liquid can penetrate into dendrite arm spacing in liquid feeding zone, so stress by phase change and cooling can be released by refilled liquid. But, in cracking zone, liquid cannot penetrate into dendrite arm spacing, because channel narrows with lower liquid fraction.

Several groups have interested the relationship between tensile strength and elongation of δ phase and γ phase with small

liquid fraction. [26, 27] Lopez et al. suggested that crack can occurs, when strain is generated at temperature lower than liquid impenetrable temperature. [26] The liquid impenetrable temperature was defined as a temperature at which solid fraction is 0.9 by suggestion of Clyne et al.[23] They suggested that the strain can be generated, when tensile strength and elongation of δ phase or γ phase are smaller than these of another phase. So, they reported that hypo peritectic steel has high crack susceptibility, because of the difference of mechanical properties of δ and γ phase, and the amount of conditions where strain can be generated is large at the temperature range below a liquid impenetrable temperature.

Xu et al. suggested that index of solidification shrinkage, which is the product of volume change of peritectic solidification and solid fraction after peritectic solidification, for predicting possibility of crack generation. [13] This is because the smaller the fraction of the liquid fraction is, the more difficult it is to release stress by incomplete liquid filling into dendrite arm spacing.

2.3 Complex behaviors of phase transformation of hypo peritectic steel

If the phase transformation of hypo peritectic steel occurs at the equilibrium state, the phase change behaviors are as follows. First, when the temperature reaches the liquidus temperature, primary δ starts to be formed and δ phase grows as temperature becomes lowering. And then, γ phase appears at the peritectic temperature, and liquid, δ phase and γ phase coexist. Also, the γ phase grows simultaneously into the liquid phase and the δ phase and liquid phase disappears at the peritectic temperature. As temperature drops lower than peritectic temperature, the δ phase transforms to the γ phase. When the temperature decreases lower more, only γ phase exists. However, various results of experiments showed that the phase change behaviors of hypo peritectic steel were different from those at equilibrium state in continuous cooling.

Lopez et al. analyzed the temperature change during cooling according to cooling rate, and calculated first and second derivatives of cooling curve for understand the behaviors of phase transformation. [26] The results showed that peritectic transformation starts at a temperature lower than peritectic temperature, and peritectic transformation occurs with temperature ranges.

Several groups showed the speeds of interface by peritectic transformation by using high-temperature laser-scanning confocal microscopy.[28-31] Their experiments showed that massive transformation can occur during peritectic transformation.

Moon et al. reported that the speeds of δ/γ interface are several mm/s, and increases with increasing cooling rate. Generally, the speeds of phase transformation by diffusion controlled transformation are several μm/s.[17] So, these speeds of δ/γ interface may be interpreted by the results of massive transformation.

Griesser et al. reported that the speeds of δ/γ interface according to steel grades, and the condition where massive transformation can occur.[29] They showed that phase transformation form δ phase to γ phase by peritectic transformation have three modes. Those are a planer growth by diffusion controlled transformation, a cellular/dendritic growth by diffusion controlled transformation, and massive transformation. Also, they suggested that massive transformation from δ phase to γ phase can occur at a temperature lower than T_0 where Gibbs energy of γ phase is same as that of δ phase.

2.4 Goals of the research

As explained at previous sections, experimental studies showed that phase transformations of peritectic steel are complex and deviated from the behaviors of phase transformation at equilibrium state. But, models suggested for the phase transformation of hypo peritectic steels assumed that only carbon diffusion is the main mechanism of phase transformation. And, it is assumed that peritectic transformation starts at peritectic temperature. Also, their models did not consider the massive transformation from δ phase to γ phase. This means that the previous studies were not sufficient to explain phase transformation of hypo peritectic steel. So, we developed a new model for understanding the complex behaviors of phase change of hypo peritectic steel by coupling thermodynamic analysis and kinetic simulation, first.

For estimating the crack susceptibility, we consider both mechanisms of crack generation, internal stress in solidified shell and volume contraction with incomplete liquid filling into dendrite arm spacing. So, we suggest the volume contractions during solidification and cooling, and strain rates and pore formation susceptibilities. For considering phase transformation of hypo peritectic steels to these parameters, the results of a new phase transformation model of hypo

peritectic steel are used. Additionally, Stress model is developed for calculating the stress distribution in solidified shell. As a result, quantitative prediction for crack generation can be calculated considering phase transformation and kinetics. So, it is suggested that the mechanisms of crack generation and the conditions with high possibility of crack generation.

Finally, the crack ratios of field data are analyzed using the results of new models for phase transformation and crack generation of hypo peritectic steel. So, the range of carbon contents with high possibilities and the effects of casting parameters on the behaviors of crack generation are suggested semi−quantitatively.

Chapter. 3 Modeling of phase transformation of hypo peritectic steel during cooling

3.1 Modeling procedure

3.1.1 Outline of the new model for peritectic transformation.

Phase transformation and solidification of hypo peritectic steel are generated at equilibrium state as shown at

Fig. 3.1. Liquid steel start solidifying to δ phase from liquid temperature (T_L). So, primary δ phase grows until peritectic temperature (T_p). At T_p, γ phase is nucleated and grows by peritectic transformation. And peritectic transformation finishes at T_p, and liquid phase disappears. As temperature decreases below T_p, remaining δ phase is transformed to γ phase in solid state. When the temperature becomes T_γ, phase transformation from δ phase to γ phase completes, so only γ phase exists.

But, the behaviors of phase transformation of hypo peritectic steel in a continuous cooling system is different to those in equilibrium conditions. In experiments with continuous cooling, the peritectic transformation did not complete at the peritectic temperature.[15, 32] The γ phase was generated at a temperature lower than T_p.[17, 28, 33] This phenomena

means that undercooling for formation of γ phase from T_p. So, we define that the amount of undercooling for formation of γ phase from T_p is dT_p. In addition, it was showed that phase transformation from δ phase to γ phase was generated by massive transformation in many experiments.[29, 30, 34] So, these different behaviors of phase transformation comparing those at equilibrium conditions are needed to be considered for the new model of phase transformation of hypo peritectic steel.

In this study, a new model to simulate the phase change behavior of hypo peritectic steel is developed. The model focuses on the initial part of the phase change during continuous casting, therefore we analyze the behaviors until all phases become the γ phase. The process is divided by five stages as shown in Fig. 3.2. The five stages are as follows: The solidification of primary δ starts at the liquidus temperature and δ phase is increasing until T_p. (stage 1) Then, δ phase is continuously growing until T_{ps} ($=T_p-dT_p$) without formation of γ phase. (stage 2) And then, γ phase is formed at δ/L interface and grows until solidification completes. (stage 3) After solidification finished, remaining δ phase is transformed to γ phase in the solid phase. (stage 4) Lastly, if δ phase remains below a temperature($T_{massive}$) at which massive transformation can occur, remaining δ phase is transformed to

γ phase by massive transformation, (stage 5)
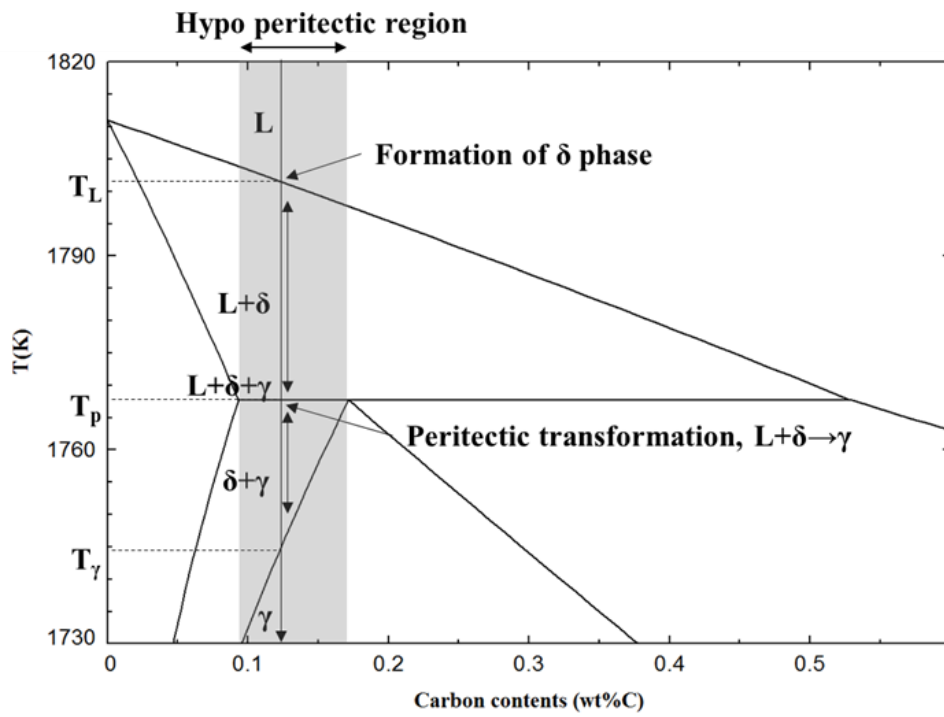
Fig. 3.1 Phase transformation of hypo peritectic steel at equilibrium state.
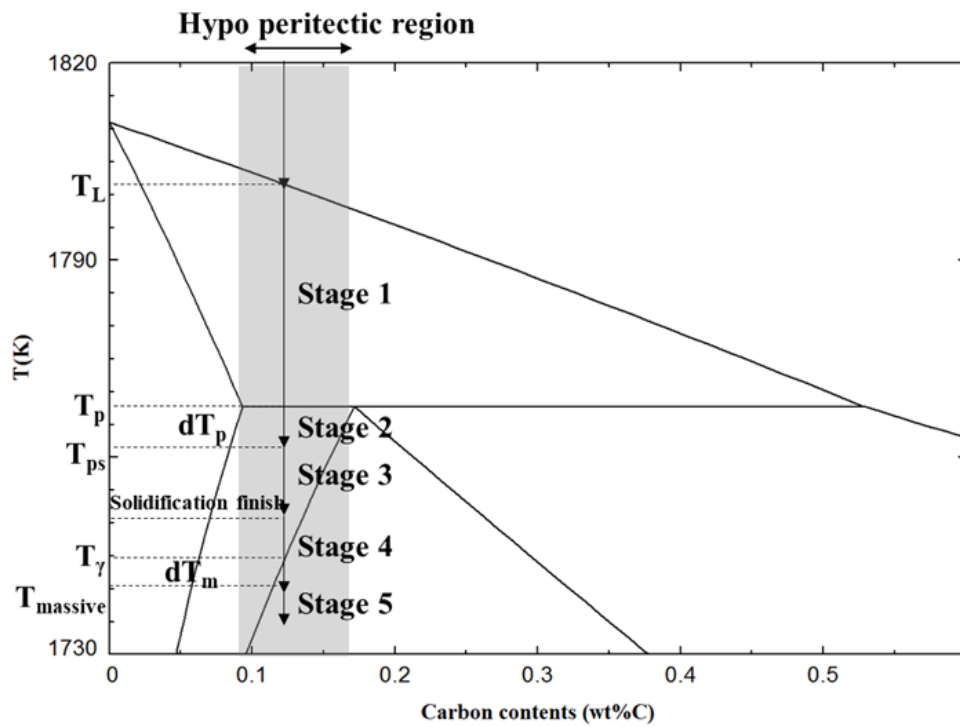
Fig. 3.2 Divide process of phase change of hypo peritectic steel with 5 stages and specific temperatures used for phase transformation of hypo peritectic steel

3.1.2 Thermodynamic analysis for the delay of formation of γ phase, dT_p, and massive transformation, dT_m

dT_p is the amount of undercooling for formation of γ phase from the peritectic temperature. In other words, the liquid is solidified to δ phase and the γ phase does not nucleate until T_{ps} ($=T_p-dT_p$). So, when dT_p is large, the amount of solidified δ phase increases. If dT_p is greater than a specific value, solidification can complete before peritectic transformation starts. Therefore, dT_p is a very important parameter for determining the phase change behavior.

The dT_p exists because of the energy barrier for the nucleation of γ phase. The nucleation and growth of the γ phase of peritectic reaction occurred at the δ/L interface.[12, 17] So, δ/γ and γ/L interfaces are generated, and δ/L interface disappears, when the nucleation of γ phase occurs at δ/L interface. Yoshiya et al. calculated the interface energy of δ/L, δ/γ, and γ/L interfaces according to the crystal structure using atomistic simulation and phase field modeling.[35] They suggested that interface energy can be generated by mis−orientation because of different crystal structures at δ(BCC)/γ(FCC) interface. They obtained the following values : $\sigma_{\delta/\gamma}$ = 0.56 ± 0.03 J/m^2, $\sigma_{L/\delta}$ = 0.29 ± 0.03 J/m^2, $\sigma_{L/\gamma}$ = 0.34 ± 0.03 J/m^2. By using these interface energy, the energy barriers for nucleation of δ phase and γ phase at 1755K (dT_p=10K) are calculated. For calculating energy barrier of each phase, Gibbs free energies of each phase (L, δ, and γ) are

calculated using Factsage. As a result, the energy barrier of δ phase (6.06×10^{-10} J for 2.1nm cube sized nucleus of δ phase) is smaller than the energy barrier of γ phase (1.84×10^{-9} J for 2.9nm cube sized nucleus of γ phase) as shown at Fig. 3.3. Therefore, additional energy is necessary to overcome the interfacial energy for γ nucleation. This is the reason why undercooling(dT_p) of formation of γ phase from T_p is necessary.

The value of dT_p is influenced by the free energy and interfacial energy generated during the phase change. Interfacial energy of formation of γ phase can decrease by the presence of an inclusion with the same or a similar crystal structure with γ phase, In addition, the presence of nucleation seeds, the segregation of carbon and alloying elements during solidification, and the cooling rate might also have a considerable impact on dT_p.

Similar to dT_p, dT_m should exists because additional energy is necessary for formation of γ phase at δ/δ interface. The difference is that dT_p is the amount of undercooling required when the γ phase is generated at the L/δ interface, and dT_m is the amount of undercooling required when the γ phase is generated at the δ/δ interface. Using the interfacial energies obtained by Yoshiya et al. [35], the changes of interfacial energies are calculated, when the γ phase of 1 nm hemisphere is formed. As a result, the calculated energy barriers for nucleation of γ phase is 7.54×10^{-19}J, when the γ phase is generated at the δ/δ interface. This value is three times smaller than the value of 2.51×10^{-18}J which is the additional energy when the γ phase is generated at the L/δ interface.

2 7

Therefore, dT_m might have a smaller value than dT_p. dT_m is very difficult to measure experimentally and the exact value is unknown. So, we assume that the value of dT_m is one third of dT_p. However, dT_m is the minimum condition that can cause massive transformation. Therefore, in the present model, if temperature becomes smaller than $T_{massive}$ by very large dT_p, it can be suggested that massive transformation starts at T_γ.
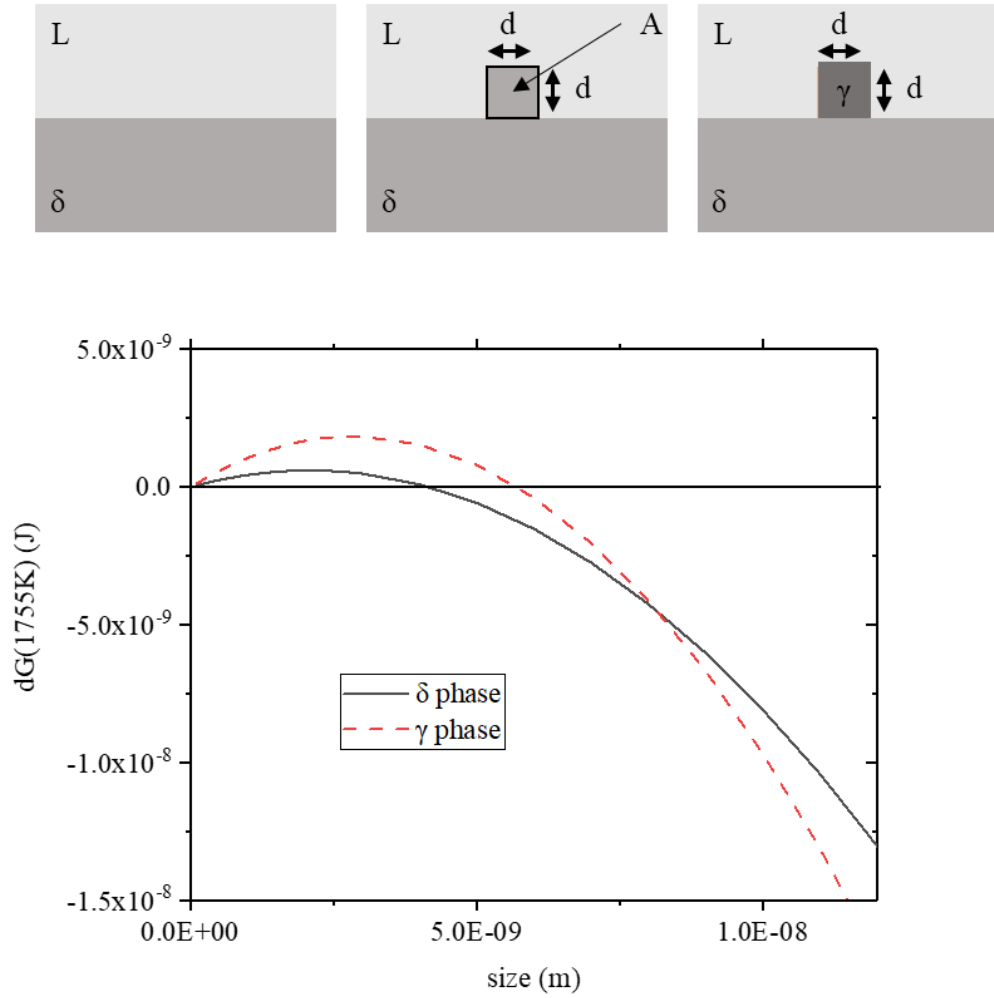
Fig. 3.3 Schematic diagram of nucleation at L/δ interface for calculating energy barrier, and change of Gibbs free energy for nucleation of δ and γ phase

3.1.3 Modeling procedure of phase transformation model

It is very important to consider the kinetics for phase transformation, because this model should simulate the phase change during continuous cooling. It is assumed that the kinetic behavior is mainly determined by the carbon diffusion controlled transformation during cooling in the present model. The diffusion coefficient of carbon in the δ and γ phase is a function of the temperature and the following equations are used. [36, 37]

$$D_\delta(cm^2/s) = 0.0127\exp(-19450 / RT) \qquad \text{Eq. (1)}$$

$$D_\gamma(cm^2/s) = 0.0761\exp(-32160 / RT) \qquad \text{Eq. (2)}$$

Generally, the carbon diffusivity in γ phase is much smaller than that of δ and liquid phase. At 1700K, the values of diffusivity of carbon in δ and γ phase are $4.01×10^{-5}$ cm²⁄s and $5.581×10^{-6}$ cm²⁄s respectively. In addition, the carbon diffusivity in molten steel at the temperature is $1.2×10^{-4}$cm²⁄s.[38] Therefore, it could be assumed that phase change is governed by the carbon diffusion in the γ phase.

During stage (1), solidification to the primary δ phase above T_p is assumed to follow equilibrium conditions predicted

by thermodynamics. So, phase fractions of δ and liquid phases are calculated using the lever rule. And the condition at T_p is the initial condition of this phase transformation model.

To model the behaviors of phase transformation of hypo peritectic steel, we solved the phase change at secondary arm spacing as Mondragon et al. [27] They modeled that peritectic transformation occurs at the volume of half of the secondary arm spacing, and this dendritic structure is proposed by Brody et al.[39] So, we use the secondary arm spacing as the diameter of the calculated domain. Eq. (3) shows that the length of dendrite arm spacing suggested by Cicutti et al.[40]

$$\lambda_2 = 26.1 t_s^{0.38} \qquad\qquad\qquad \text{Eq. (3)}$$

Where λ_2 is secondary arm spacing and t_s is time for cooling of primary δ until peritectic temperature. Fig. 3.4 shows the schematic diagram of the phase change behavior of hypo peritectic steel and carbon contents at each interface considering local equilibrium.

Solidification to the δ phase occurs additionally during Stage (2). During dT_p, the formation of γ phase is delayed by formation of new interface. Solidification from liquid to δ phase is calculated by diffusion of carbon and mass conservation using the local equilibrium contents at δ/L interface calculated by

Factsage.

Stage (3) starts at T_{ps}, so γ phase is nucleated at L/δ interface, and grows into liquid and δ phase simultaneously. We assume that carbon contents of δ/γ and γ/L interfaces are the values obtained from thermodynamic equilibrium during cooling. And the speeds of γ growth and solidification were calculated from the amount of transferred carbon through γ phase from γ/L interphase to δ/γ interphase, because the diffusivities of carbon in δ phase and liquid are larger than that of γ phase. We obtain the Eq. (4) by solving carbon diffusion in cylindrical domain with assumption that flux of carbon is steady in the γ phase and the boundary conditions are at local equilibrium.

$$C(r) = C_{\delta\gamma} + \frac{(C_{\delta\gamma} - C_{L\gamma})}{\ln(^{r_\delta}/_R)} \ln(\frac{r}{r_\delta}) \qquad \text{Eq. (4)}$$

Where r is the position from dendrite arm center, r_δ is the thickness of δ phase, R is the half of secondary dendrite arm spacing, and C_δ, $C_{L\gamma}$, and $C_{\delta\gamma}$ are carbon contents at δ phase, γ/L interface and δ/γ interface, respectively.

For δ phase to γ phase transformation, the movement of carbon from γ phase to δ phase is needed. In this case, the amount of carbon accumulated in δ phase for phase transformation is equal to the amount of carbon moving through

the δ/γ interface. Then, the flux of carbon is described as follow.

$$Q = D_\gamma \times \frac{dC}{dr} \times A$$

$$= D_\gamma \times \frac{(C_{\delta\gamma} - C_{L\gamma})}{\ln(^{r\delta}/_R)r} \times 2\pi r = \frac{l}{dt} \times 2\pi C_{\delta\gamma} \times (C_{\delta\gamma} - C_\delta)$$

Eq. (5)

Where Q is the flux of carbon through the δ/γ interface, A is the area between δ and γ phase, C_δ in the carbon contents in δ phase, dl is the thickness of transformed γ phase during dt, dt is the time step, and D_γ is the diffusivity of carbon in γ phase. As a results, the velocity of δ/γ interface is developed as follow.

$$\frac{dl}{dt} = D_\gamma \frac{(C_{\delta\gamma} - C_{L\gamma})}{r_\delta(C_{\delta\gamma} - C_\delta) \times \ln(^{r\delta}/_R)}$$

Eq. (6)

And speeds of γ/L interface are calculated through mass conservation of carbon, after fraction of δ phase is calculated using speeds of δ/γ interfaces.

At the beginning of stage (3), δ/γ interface velocity can be very fast, because the thickness of the γ phase is small. However, reassembling iron atoms is necessary for formation of γ phase from δ phase regardless of the amount of carbon diffusion. Therefore, we assume that the iron atoms must move in one lattice parameter for formation of γ phase, and this velocity is used as the maximum velocity of the growth of γ

phase. The maximum velocity of formation of γ phase was derived using the diffusivity of iron atom in the γ phase and lattice parameter of γ phase as follows.

$$D_{\gamma,Fe}(m^2/s) = 0.000049\exp(-\frac{284100}{RT})$$ Eq. (7)

$$v_{interface}(m/s) = D_{\gamma,Fe}/\Delta$$ Eq. (8)

When solidification finishes by peritectic transformation at Stage (3), phase transformation from δ phase to γ phase occurs at Stage (4). The speeds of phase change during stage (4) is also determined by the carbon diffusion in the γ phase on local equilibrium at the δ/γ interface and mass conservation. At this stage, the gradient of carbon concentration in γ phase continuously decreases because there is not inflow of carbon from the liquid phase. In Stage (4), δ phase can remain below a temperature at which single γ phase is most stable (T_γ). Because additional energy is necessary for formation of γ phase at δ/δ interface, as mentioned in the last section. So, Stage (4) finishes at $T_{massive}$ (=T_γ−dT_m), not T_γ.

In stage (5), the δ phase reaches a temperature, $T_{massive}$ (=T_γ−dT_m), massive transformation from δ phase to γ phase starts. Theoretically, massive transformation can occur any place in the δ phase. However, it is easier that massive

3 4

transformation occurs at δ/γ interphase, because additional energy barrier from new interphases at the interphase is far smaller than that of internal region.[41] So, it can be assumed that massive transformation is proceeded from δ/γ interface. If there are no δ/γ interface, γ phase preferably grows δ/δ interface, because of benefits of low energy barriers comparing nucleation at interior region. After new γ phase is formed, massive transformation may continue from the interphase of new δ/γ interphase.

But, it is difficult to obtain the value of the rates of massive transformation. In the present study, the speeds of massive transformation are assumed to the limited rates for phase change by same concept of peritectic reaction in stage 3, because this transformation also needs rearrangements of Fe atoms. But, the difference between the formation of γ phase at δ/L at initial peritectic transformation and massive transformation is that the γ phase forms at δ/δ phase and grows in the mixed phase of δ and γ phase. Considering this behavior of massive transformation, the diffusion coefficients of iron atoms are calculated from the effective diffusion coefficients in composite solids as follows.[42] The effective self−diffusion coefficients of iron atoms were calculated assuming that the fractions of δ and γ phases are 0.5. As a results, we calculated

the speeds of δ/γ interface by massive transformation. $D_{\gamma,Fe}$ is self−diffusivity of iron in δ phase and $v_{massive}$ is speed of δ/γ interface by massive transformation.

$$D_{\delta,Fe}(m^2/s) = 0.00019\exp(-\frac{238500}{RT}) \qquad \text{Eq. (9)}$$

$$D_{eff,Fe}$$
$$= D_{\delta,Fe}(1 + \frac{1.5}{(\frac{D_{\gamma,Fe}+2D_{\delta,Fe}}{D_{\gamma,Fe}-D_{\delta,Fe}})-0.5+1.569(\frac{D_{\gamma,Fe}-D_{\delta,Fe}}{D_{\gamma,Fe}-4D_{\delta,Fe}})0.5^{\frac{10}{3}}}) \qquad \text{Eq. (10)}$$

$$v_{massive}(m/s) = D_{eff,Fe}/\Delta \qquad \text{Eq. (11)}$$

In previous paragraphs, it is suggested that the phase transformation of hypo peritectic steel consists of five stages in this model. But, this does not mean that any compositions of hypo peritectic steels should pass all five stages during solidification and cooling. Stage 1 and 2 appear in any cases, but the other stages appear selectively depending on the situations. As an example, if phase change from δ phase to γ phase finishes during stage 4, then stage 5 does not appear. And for a special case, if the solidification finishes before temperature reaches T_{ps} ($=T_p-dT_p$), all solids exist as δ phase. Thermodynamically, this δ phase is unstable and can be decomposed to δ phase with lower carbon contents (C_δ) and γ phase with very higher carbon contents(C_γ) as shown at Fig. 3.5. However, this phase change might be very difficult because

of the following reasons. At first, interfacial energy between δ/γ interface is very large compared to the decreases of free energy by this decomposition. For example, when a hemispherical γ phase with a radius of 1 nm is generated at the δ / δ interface, the energy required for interfacial energy generation $(3.90 \times 10^{-18} \text{J})$ is about 7.4 times larger than the free energy decrease from δ phase to γ phase $(5.26 \times 10^{-19} \text{J})$. Another difficulty is that this transformation needs rearrangements of carbon. As an example, 0.13wt%C δ phase is decomposed, the resulting phases are 0.068wt%C δ phase and 0.272wt%C γ phase. When additional carbon is supplied from liquid, the γ phase with high carbon contents can be formed. However, if there are no external supply of carbon, it should be very difficult to form new γ phase because Fe atoms rearrangements and carbon enrichments should occur simultaneously. Therefore more possible way of transformation path is that transformation is delayed to $T_{massive}$ and then massive transformation occurs.

So, the flow chart of the phase change behavior of the hypo peritectic steel is obtained through the modeling process of phase change is shown in Fig. 3.6.
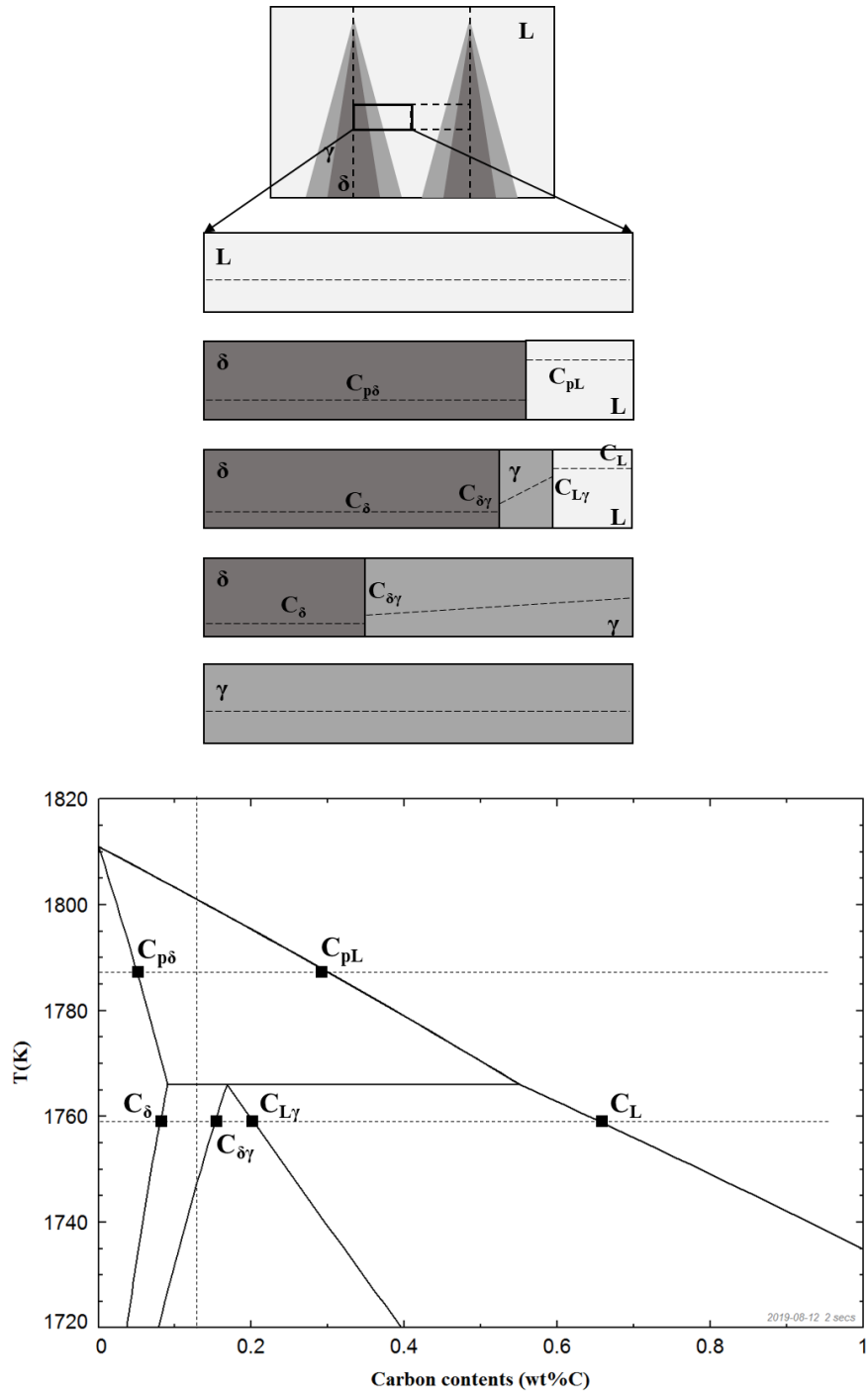
Fig. 3.4 Schematic diagram of the phase change behavior of hypo peritectic steel, and specific carbon contents for modeling of phase transformation.
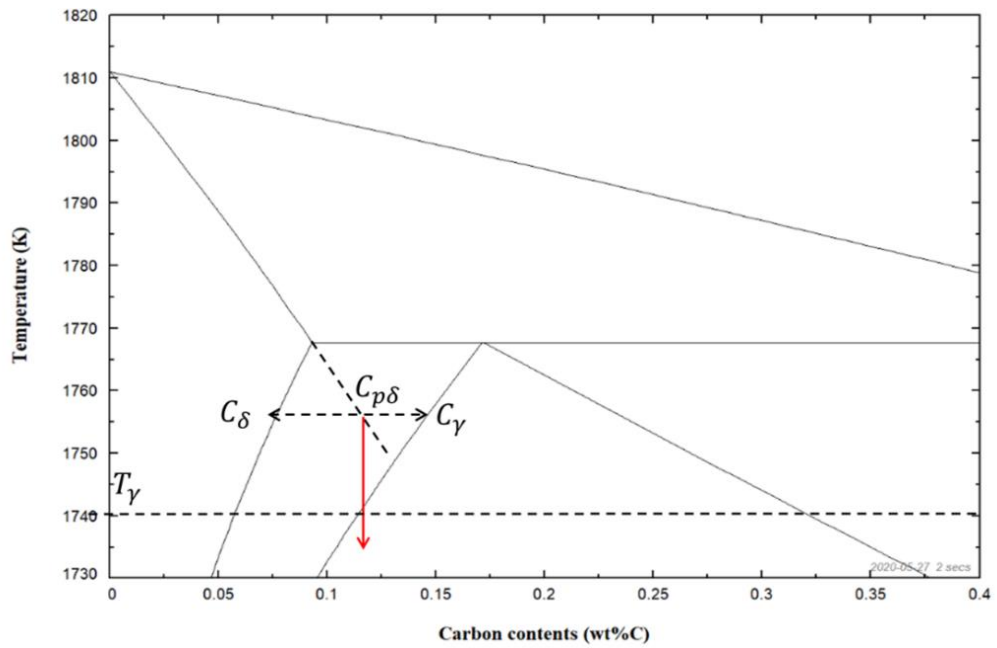
Fig. 3.5 Difficult phase transformation from δ phase to γ phase, when solidification completes to only δ phase during dT_p.
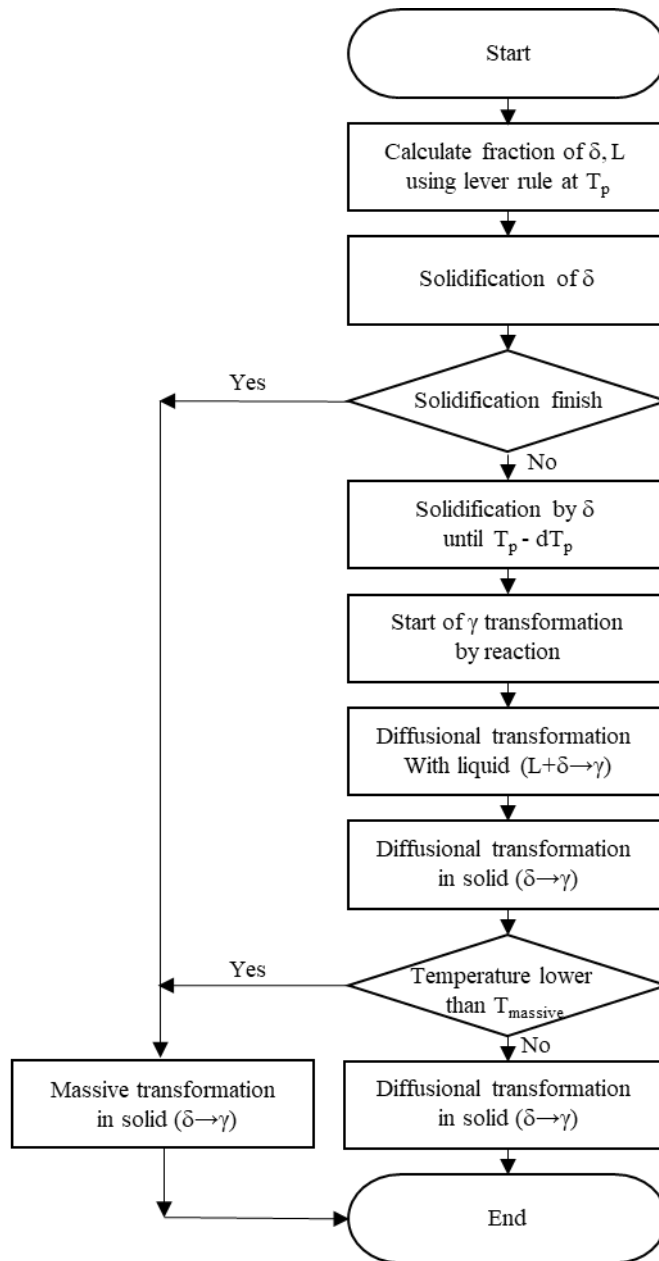
Fig. 3.6 Flow chart for phase change behaviors of hypo peritectic steel.

3.2 Results and discussion

3.2.1 Phase change of hypo peritectic steel during cooling

Using the new model of phase transformation for hypo peritectic steel, the phase changes of each phase are calculated according to cooling rate, carbon contents, and dT_p (undercooling of formation of γ phase from peritectic temperature) during continuous cooling as shown at Fig. 3.7 and Fig. 3.8. Cooling rate is set as 800K/min to simulate cooling behavior of continuous casting with casting speed, 2.2m/min. In the figures, the dotted lines are the fractions of each phase calculated using Factsage at equilibrium conditions, and the solid lines are the results of the model developed in this study. The behaviors of phase transformations in Fig. 3.7 are different from those in Fig. 3.8. In Fig. 3.8, liquid phase is solidified to δ phase until T_{ps}, and solidification does not completes. The formation of γ phase starts at L/δ interphase from T_{ps}, and γ phase grows into liquid and δ phase simultaneously. This phase transformation occurs by diffusion controlled transformation. After solidification completes by peritectic transformation, δ phase is transformed to γ phase by diffusion controlled transformation in solid phase. Unlike the behaviors of phase

transformation in Fig. 3.7, liquid phase is solidified to δ phase until T_{ps}, and solidification completes at a temperature above T_{ps} without peritectic transformation in Fig. 3.8. So, only δ phase exists at T_{ps}. This δ phase is cooled to $T_{massive}$, and δ phase is transformed to γ phase by massive transformation.

These different behaviors of phase transformation of hypo peritectic steel are affected by carbon contents and dT_p. Comparing Fig. 3.7(a), Fig. 3.7(b), and Fig. 3.8(a), the behaviors of phase transformation of Fe−0.09wt%C are different from those of Fe−0.107, 0.144wt%C, although dT_p is same. Because the amount of liquid phase solidifying to δ phase is small, when carbon contents is small. So, solidification of Fe−0.09wt%C finishes to only δ phase without peritectic transformation before T_{ps}. This solidified δ phase needs additional energies for formation at interphases and liquid phase for supply of carbon do not exists. Therefore, massive transformation starts after temperature reaches Tmassive. This phenomena can occur even in the higher carbon composition, when dT_p is larger. Comparing Fig. 3.7(b), and Fig. 3.8(b), massive transformation form δ phase to γ phase, when dT_p is large. Because the time to solidify to δ phase is longer, when dT_p is large. So, when dT_p is 5K, peritectic transformation of Fe−0.107wt%C can occur during solidification, and phase

transformation from δ phase to γ phase is generated by diffusion controlled transformation. On the other hands, when dT_p is 20K, solidification completes without peritectic transformation, and δ phase is transformed to γ phase by massive transformation.

(a)

(b)

4 4
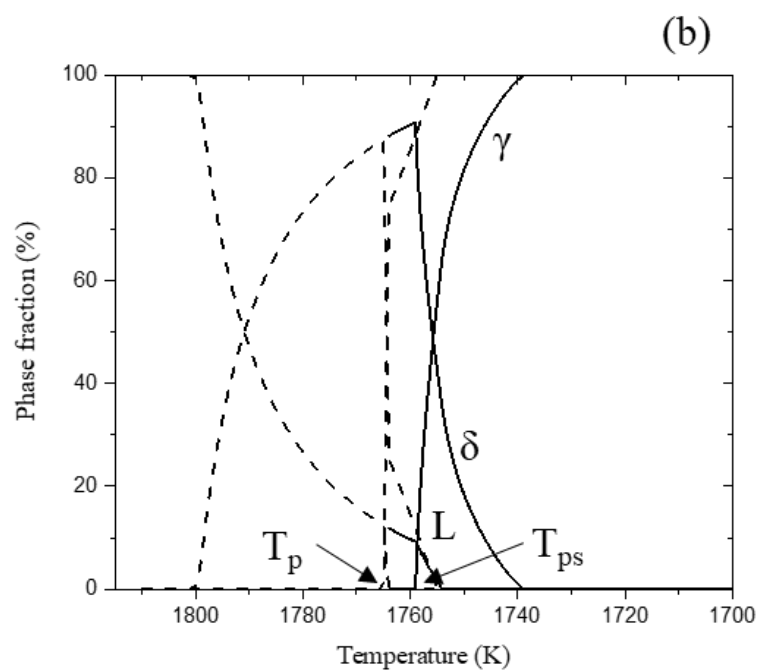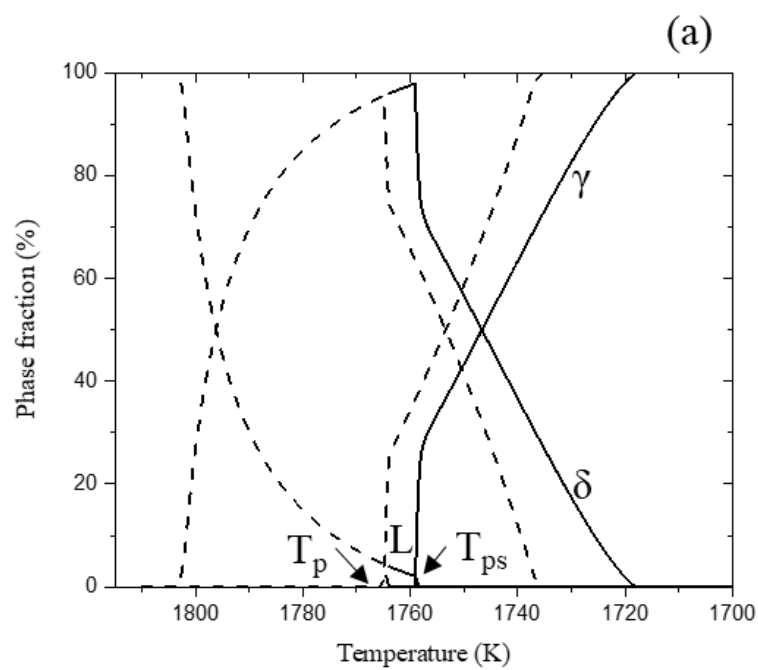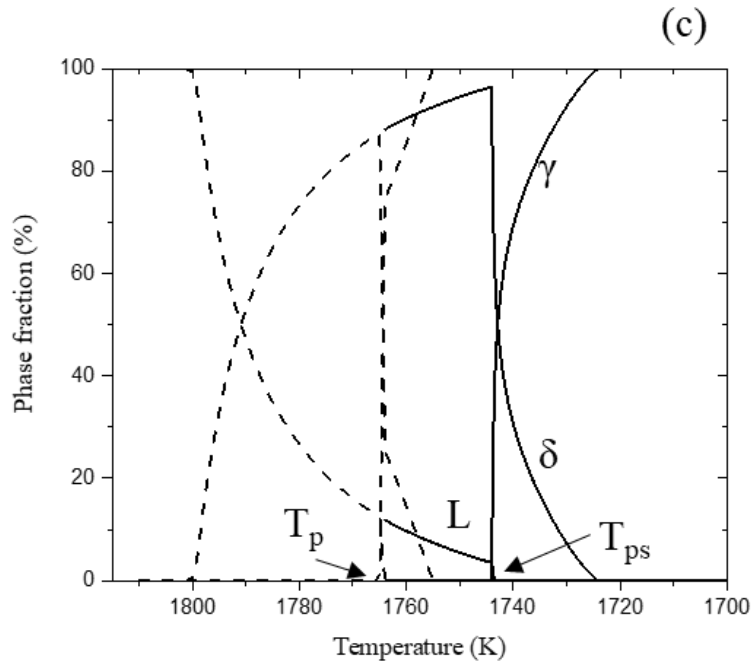
Fig. 3.7 Phase change with peritectic transformation by diffusion controlled transformation during continuous cooling (a) dTp=5K, Fe−0.107wt%C, (b) dTp=5K, Fe−0.144wt%C, (c)dTp=20K, Fe−0.144wt%C
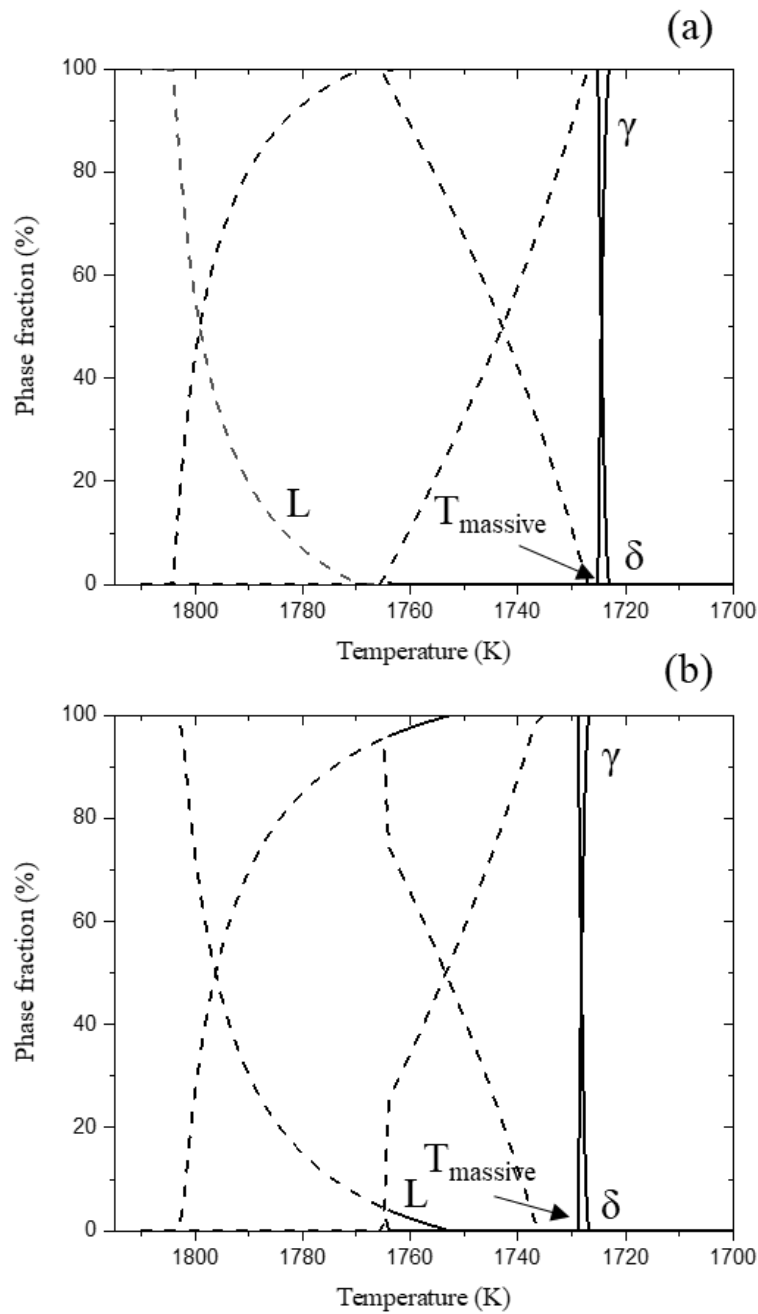
Fig. 3.8 Phase change with massive transformation from δ phase to γ phase during continuous cooling (a) dTp=5K, Fe−0.09wt%C, (b) dTp=20K, Fe−0.107wt%C

3.2.2 Speeds of interfaces during cooling

With various carbon compositions and dT_p, the speeds of the δ/γ interface are calculated. Fig. 3.9 is the results of the δ/γ interface speeds according to the growth of γ phase when cooling rate is 800K/min and dT_p is 5K. In case of Fe－0.107wt%C, the initial speed of δ/γ interface is very fast value of 500μm/s or more, after which the speed decreases rapidly. And the speed of δ/γ interface drastically decreases, when the fraction of γ phase is 22%. This is when the solidification completes at each condition. Based on this, the growth behavior of γ phase can be divided into two stages, which are stage(2) and stage(3) in this model, respectively. Before the solidification is completed, the phase change takes place at the local equilibrium on δ/γ and γ/L interface with carbon inflow from the liquid phase to the γ phase. So, the speeds of δ/γ interface is fast. On the contrary, there is no carbon inflow from the liquid phase after solidification is completed. Therefore, the carbon concentration gradient in γ phase decreases as time passes, so the speeds of δ/γ interface also decrease. The speeds of δ/γ interface of Fe－0.107wt%C are in the range of about 10μm/s except for last stage of formation of γ phase. This value is similar to the values reported by Shibata et. al.[17] At the last moment of the formation of γ phase, the speed of δ/γ

interface is very fast. This is geometrical phenomena because the area of δ/γ interphase is very small near the center region.

The speeds of δ/γ interface of Fe−0.107wt%C and Fe−0.144wt%C show different behavior. The reason why interface speeds decrease is that the length of carbon diffusion through γ phase increases for phase transformation from δ phase to γ phase. The speeds of δ/γ interface decrease considerably when the fractions of γ phase are 22% at Fe−0.107wt%C and 64% at Fe−0.144wt%C. And the speeds of δ/γ interface at Fe−0.144wt%C are about 30μm/s in stage(3).

The δ/γ interface speeds of Fe−0.09wt%C is approximately 1.20mm/s until the formation of γ phase is completed. Because the solidification is completed by the δ phase before T_{ps} and the growth of γ phase is proceeded by the massive transformation. The values slightly decrease from 1.20mm/s to 1.19mm/s as cooling proceeds. The decrease in interface speeds is due to the diffusivity of the iron atoms as the temperature decreases.

After the γ phase is generated at the δ/L interface, the γ phase grows simultaneously toward the liquid phase and the δ phase. The Fig. 3.10 is the results of the moving speed of δ/γ and γ/L interfaces when carbon contents is 0.107wt%C and dT_{p} is 5K. As a result, speeds of the γ/L interface are present only

until the fraction of the γ phase at which solidification is completed. The speeds of the γ/L interface are about 10 μm/s, which is very slow compared to the speeds of δ/γ interface. Moon et. al. [34] reported that growth rates of the γ phase in the δ phase were far faster than those in the liquid phase

If dT_p is increased to 20K, steels of higher carbon contents can be transformed by massive transformation as shown in Fig. 3.11. γ phase fraction at which the solidification of Fe− 0.144wt%C with dT_p of 20K completes is approximately 40%. This is because the amount of liquid phase remaining at 20K is less than when dT_p is 5K. The formation of γ phase of Fe− 0.107wt%C is generated by massive transformation, when dT_p is 20K. And, the speed of δ/γ interface is faster than that of Fe− 0.09wt%C. Because the temperatures of the massive transformation are 1725K and 1729K respectively, when carbon contents 0.09wt%C and 0.107wt%C with dT_p of 20K.

The results of these phase change model can explain the various dT_p and speeds of interface movements. The undercooling for formation of γ phase ranges from about 5K to about 100K and the speeds of δ/γ interface range from about 10μm/s to 15mm/s from experimental results.[17, 28, 33] First, the phase change behaviors of hypo peritectic steels can be calculated using various undercooling in this model. For

example of Fe-0.107wt%C with dTp=5K and 20K shown in Fig. 3.7(a), Fig. 3.8(b), Fig. 3.9, and Fig. 3.10, we could calculate the phase fractions and speeds of δ/γ interface as diffusional transformation or massive transformation depending on dT_p. In addition, the wide range of δ/γ interfacial speeds can also be explained by this model. The δ/γ interfacial speeds of several μm/s are the results from the slow phase change rate by diffusional transformation, and those of several mm/s are the results from the fast phase change rate by massive transformation.
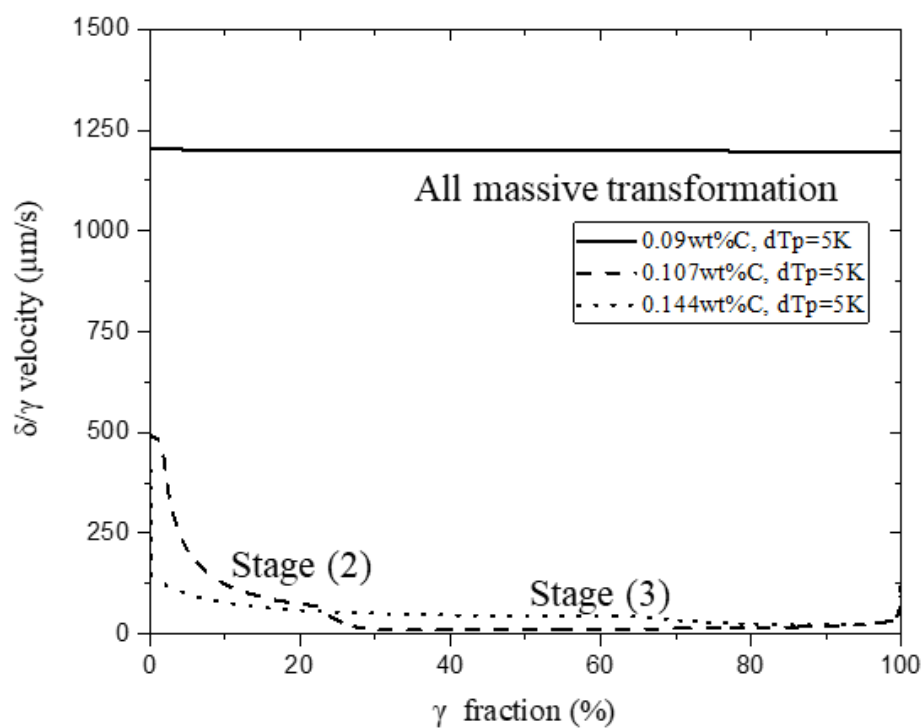
Fig. 3.9 The speeds of δ/γ interface according to carbon contents, when dT_p is 5K.
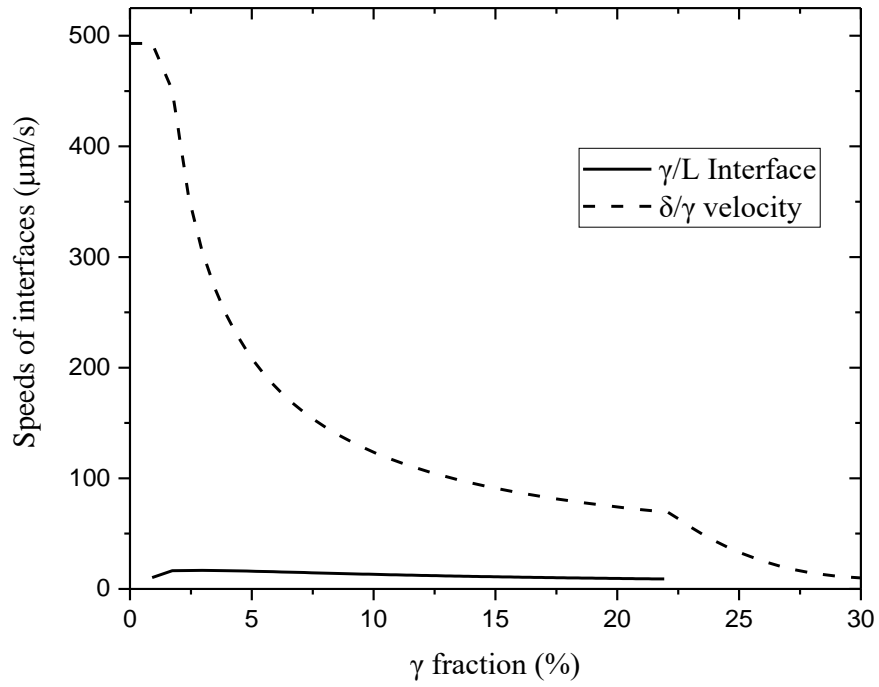
Fig. 3.10 The speeds of δ/γ and γ/L interface, when dT_p is 5K and carbon content is Fe−0.107wt%C
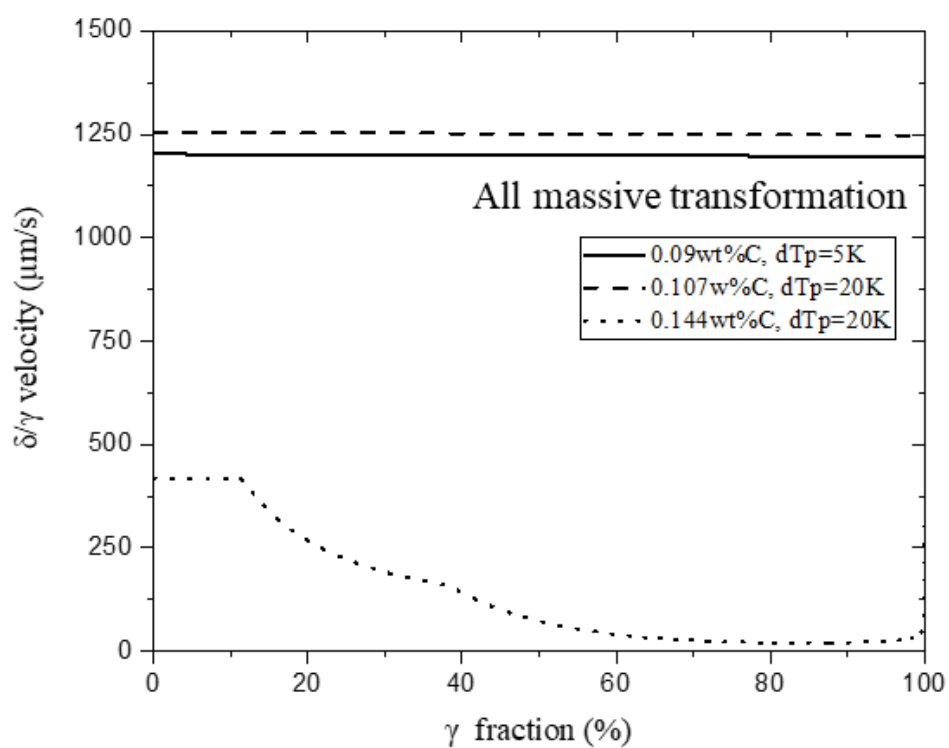
Fig. 3.11 The speeds of δ/γ interface according to carbon contents, when dT$_p$ is 20K.

3.2.3 Paths of phase transformation of hypo peritectic steel

Using the developed model, we showed that the phase change behavior occurred through several different paths. Fig. 3.12 shows the schematic diagram of the total phase change behavior of the hypo peritectic steel. If the solidification is not completed until T_{ps}, the γ phase is generated at the δ/L interface, and it will grow by carbon diffusion such as Fe$-$0.107wt%C and 5K of dT_p. On the other hand, if the solidification is completed by the δ phase before T_{ps} such as Fe$-$0.107wt%C and 20K of dT_p, the γ phase does not nucleate until T_{ps}. And then γ phase in the solid phase is generated by massive transformation at temperature lower than $T_{massive}$. In addition, there is also another possibility that the undercooled δ phase reaches a temperature below $T_{massive}$ and transform to γ phase by massive transformation. As a result, this model can show why previous experiments have reported that diffusional transformation occurred in some cases and massive transformation occurred in other cases, and suggest the conditions for occurring massive transformations.
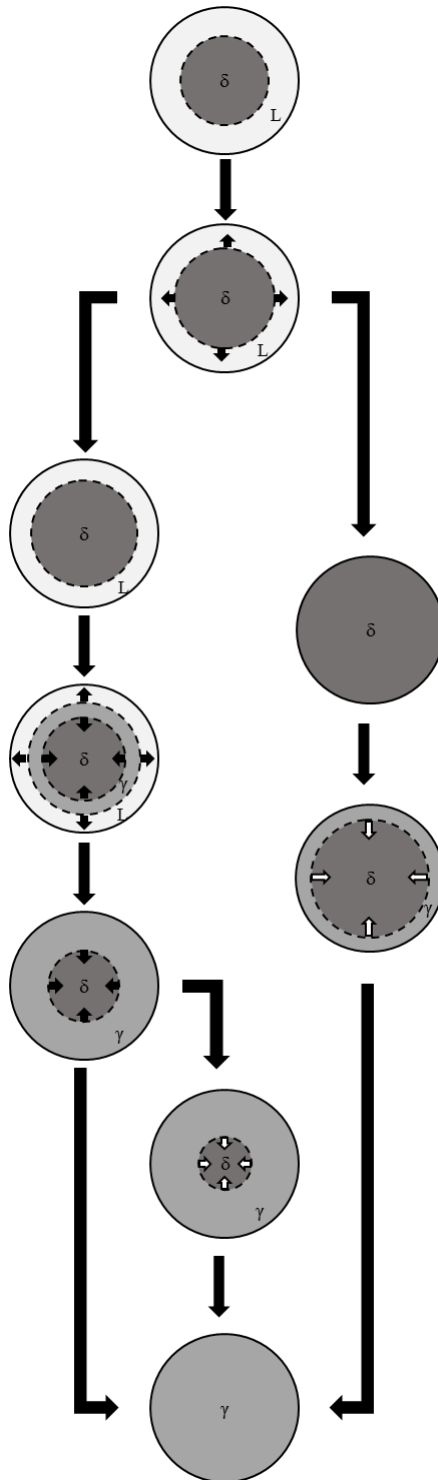
Fig. 3.12 Schematic diagram for several paths of phase transformation of hypo peritectic steel.

Chapter. 4 Predict crack generation of hypo peritectic steel during continuous casting

4.1 Modeling procedure for predicting crack generation considering phase transformation by new developed model

As mentioned at Chapter. 2, stress in shell can be generated by volume contraction because of cooling and phase transformation during and after solidification. So, calculating the amounts and speeds of volume contraction are important for understanding crack generation. To calculate volume contraction during solidification and phase transformation, we used the results of new developed model for phase transformation of hypo peritectic steel in Chapter 3.

These behaviors of phase change in cylindrical domain affects the volume change. The volume change by solidification and peritectic transformation is generated with different speeds according to the behaviors of phase change. Also, each phase is contracted by cooling. So, the effects of steel grades and temperature is need to be considered for volume contraction during continuous cooling. So, the results of phase fraction of each phase according to temperature by new developed model are used to consider volume change during continuous cooling. In this study, density is used for calculating volume at each time

step, and the density is affected by temperature and steel grades. Total density with liquid, δ phase and γ phase can be obtained by a simple mixture rule. The following equations are density according to carbon contents and temperature for each phase.[43−45]

$$\rho_{tot}(\frac{kg}{m^3}) = \rho_\delta f_\delta + \rho_\gamma f_\gamma + \rho_L f_L \qquad \text{Eq. (12)}$$

$$\rho_\delta = \frac{100(8011-0.47T(℃))}{(100-(wt\%C))(1+0.013(wt\%C))^3} \qquad \text{Eq. (13)}$$

$$\rho_\gamma = \frac{100(8106-0.51T(℃))}{(100-(wt\%C))(1+0.008(wt\%C))^3} \qquad \text{Eq. (14)}$$

$$\rho_L$$
$$= 7100 - 73(wt\%C) - (0.8 - 0.09(wt\%C))(T(℃) - 1550) \qquad \text{Eq. (15)}$$

$$V_{tot}\left(\frac{m^3}{kg}\right) = \frac{1}{\rho_{tot}} \qquad \text{Eq. (16)}$$

As mentioned at Chapter. 2., two mechanisms of crack generation during continuous casting process were suggested by previous studies. For the first mechanism of crack generation, the stress generated in the shell is main driving force. Stress can be generated in solidified shell by volume change of cooling and phase transformation. For predicting the crack generation considering this mechanism, many researchers have been calculating stress in solidified shell[20, 22, 46], or suggesting stress or unevenness index[17, 47]. Especially, Suzuki et al. suggested that stress generated at

solidifying shell is affected by the rates of phase transformation and the amount of volume change by cooling and phase transformation by using the equation of stress considering effects of strain and strain rates according to temperature.[19] The relationship between stress, strain, and strain rates at elevated temperature is as follow. [48]

$$\sigma = F \times \varepsilon^n \times \dot{\varepsilon}^m \times \exp(-Q/RT) \qquad \text{Eq. (17)}$$

where σ, ε, $\dot{\varepsilon}$, Q, R, T are the stress, strain, strain rates, activation energy, gas constant, and temperature. In present model, it is assumed that stress in solidified shell is mainly determined by strain rate.

The following equation is strain rate ($\dot{\varepsilon}$) in each time used to predict possibility of crack generation. The stress can be released when liquid exists together.[25] So, the strain rates are important, after solidification is completed. Volume per mass can be used for strain rate, because mass term is included at numerator and denominator. ε, V1, V2, and dt are strain rates, volume at previous time, volume at current time and time step respectively.

$$\dot{\varepsilon} = \frac{-(V_2 - V_1)/V_1}{dt} \qquad \text{Eq. (18)}$$

Second mechanism is related to the penetration of liquid into dendrite arm spacing. Many researchers interested in this behaviors suggested that thermal contraction and phase transformation can generate internal crack during cooling when liquid fraction is smaller than 0.1. [23, 25, 49] So, it is assumed that volume contraction rate is important for crack generation in present model, before solidification completes. Because the penetration ability of liquid becomes poor with large volume contraction rate. And stress cannot be released, when there is not liquid in dendrite arm spacing. So, crack can be generated with large volume contraction with liquid.

The following equation is volume contraction rate $(\dot{c_v})$ in each time for predicting crack generation during solidification. V_1, V_2, dt are volume contraction rate, volume at previous time, volume at current time and time step. These volumes are calculated by volume of each phase according to temperature. This equation of volume contraction rate is similar to the equation of strain rate after solidification because two equation consider the speeds of volume change. But, V_0 that normalized initial volume of the calculated domain is used at the denominator in volume contraction rate. Because it is need to consider volume maintained by penetrating of liquid into

dendrite arm spacing. Also, the volume change at the equation of volume contraction rate can consider the behaviors of peritectic transformation, solidification and cooling.

$$\dot{c}_v = \frac{{(V_1 - V_2)}/{V_0}}{dt}$$

Eq. (19)

When liquid fraction is small during solidification, volume contraction rates are suggested for the effects of the speeds of volume change by phase transformation and cooling. But, volume contraction rate with liquid is not enough to understand the behaviors at dendrites arm spacing for predicting possibility of crack generation. J. Xu et al. suggested that index of solidification shrinkage by volume change during peritectic transformation and remaining liquid fraction after solidification. And, it is showed that this value is proportional to crack ratio.[13] The following equation is index of solidification shrinkage $(R_v = \Delta V(1 - L))$ in his study. ΔV is the volume change by peritectic transformation and L is liquid fraction after peritectic transformation. They suggested that the crack susceptibility can increase by large volume shrinkage by peritectic solidification and small remaining liquid after solidification. Because the dendrite arm spacing becomes narrow by small liquid fraction, and it is difficult for liquid to

6 0

flow into dendrite arm spacing. Also, the stress cannot be released because there is not liquid at dendrite arm spacing.

In this study, when liquid fraction is small, pore formation susceptibility is suggested for important factor to crack generation as follow(Fig. 4.1). We focused on the difficulty of penetration of liquid into dendrite arm spacing, when the liquid fraction is small. Therefore, if the fraction of the liquid phase is small and the volume change is large, it can be assumed that there is a high possibility of generation of pores in the dendrite arm spacing. These pores can be a starting points for crack generation within the solidified shell.[23] This is because stresses by ferro-static pressure and phase transformation can be concentrated on the surface of the pores. Therefore, the pores generated during solidification can cause crack generation even under low stress.

Pore formation susceptibility

$$= \text{Maximum of } (\frac{Volume\ contraction\ rate\ with\ liquid}{Liquid\ fraction}) \qquad \text{Eq. (20)}$$

But, the effects of liquid unfilling for crack generation is considered differently from J.Xu et al. When the width of liquid channel is narrow by small liquid fraction, it can be assumed that the width of liquid channel is proportional to liquid fraction.

And, the pressure of fluid at the channel is inversely proportional to area of channel. So, it can be suggested that penetration ability of liquid into dendrite arm spacing is inversely proportional to liquid fraction. As a result, it is suggested that pore formation susceptibility is inversely proportional to liquid fraction. So we define pore formation susceptibility as the maximum value of volume contraction rate divided by liquid fraction as shown in Eq. (20). The reason why the maximum values are used for pore formation susceptibility is that the possibility of crack generation is maximized at this condition.
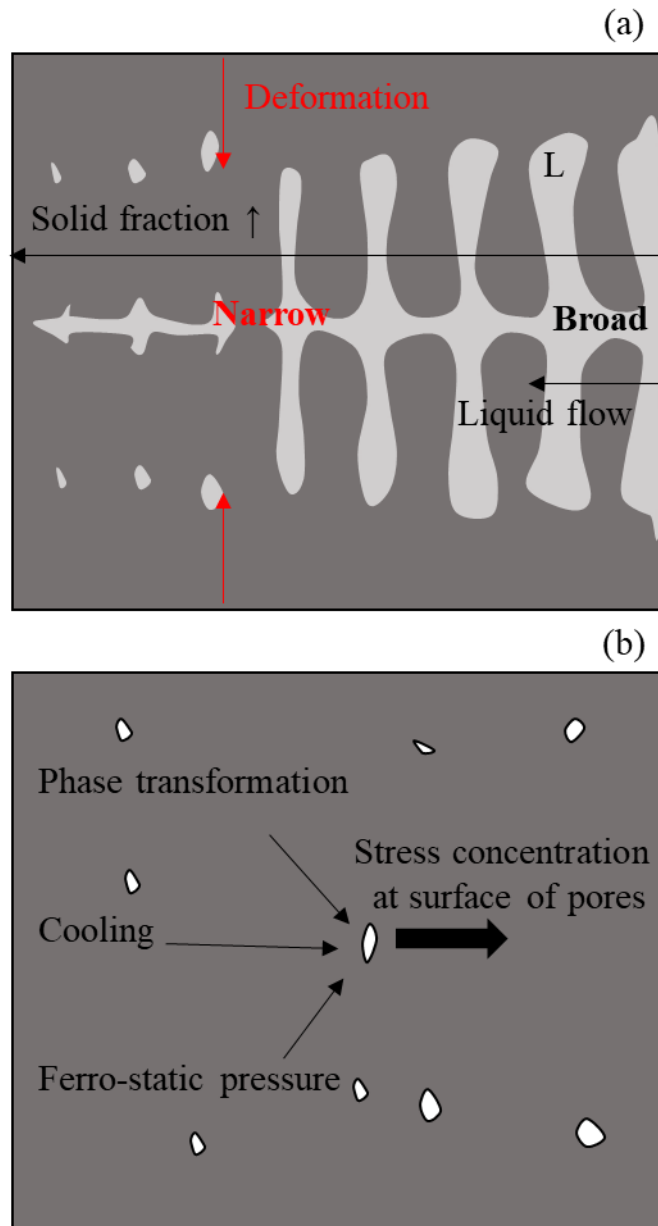
Fig. 4.1 Schematic diagram for crack generation by stress concentration on surface of pores. (a) difficult of penetration of liquid into dendrite arm spacing with small liquid fraction (b) Stress concentration on surface of pores

4.2 Modeling for stress in solidified shell

For predicting possibility of crack generation, we modeled strain rate after solidification, volume contraction rate with liquid, and pore formation susceptibility. Especially, the strain rate was modeled to predict the stress generation by the speeds of volume change inside the solidified shell. So, thermo−mechanical model is developed for calculating stress distribution at solidified shell for more quantitative analysis.

The constitutive model for stress inside the solidified shell by solidification and phase change during the continuous casting process has undergone many changes. The initial model was based on simple elastic–plastic laws.[50] They showed that compressive stress on the cooling surface and tensile stress on the inside are generated by considering the progress of solidification. Later, because the temperature at initial stage of continuous casting is very high, the behaviors at high temperature should be considered. So, the elastic−visco− plastic models were developed for consider the creep and plasticity at high temperature.[51−54] In the present study, the thermo−mechanical model is developed for calculating heat transfer and elastic−visco−plastic deformation.

4.2.1 The governing equations for thermal-mechanical model

First, heat transfer during cooling is calculated from a temperature at which there is the only liquid. So, the results of heat transfer model are applied to the stress model. The governing equation of heat transfer is as follow.[55]

$$\rho\left(\frac{\partial H}{\partial t}\right) = \nabla \cdot (k\nabla T) \qquad \text{Eq. (21)}$$

The mechanical behavior is governed by quasi−static momentum balance as follow. σ is the nominal stress tensor, and b is the body force density.

$$\nabla \cdot \underline{\underline{\sigma}} + b = 0 \qquad \text{Eq. (22)}$$

Also, the present model considers the elastic, plastic, and thermal deformation. So, the total strain rate is defined as follow. $\dot{\varepsilon}_{el}$, $\dot{\varepsilon}_{pl}$, $\dot{\varepsilon}_{ther}$ are the tensors of elastic, plastic, and thermal strain rate, respectively. $\dot{\varepsilon}_{pl}$ include the strain rates by deformation of plasticity and creep.

$$\dot{\varepsilon} = \dot{\varepsilon}_{el} + \dot{\varepsilon}_{pl} + \dot{\varepsilon}_{ther} \qquad \text{Eq. (23)}$$

At the early stage of continuous casting, temperatures at which solidification and phase transformation occurs are very high. So, visco-plastic model should be used for stress model. The visco-plastic strain consider strain rate independent plasticity and time dependent creep.[21] Kozlowski et al. suggested that the stress, temperature, strain rate, and carbon content in the austenite phase of steel affects the plastic strain rate.[56]

$$\dot{\overline{\varepsilon_{pl}}} = f(\bar{\sigma},\ T,\ \overline{\varepsilon_{pl}},\ \%C) \qquad\qquad \text{Eq. (24)}$$

where $\dot{\overline{\varepsilon_{pl}}}$, $\bar{\sigma}$, T, $\overline{\varepsilon_{pl}}$, $\%C$ are the equivalent plastic strain rate, equivalent stress, temperature, equivalent plastic strain, and carbon content of steel.

Visco-plastic strain model was proposed by various researchers, and in this study, the model presented by Anand and brown et al. is used for considering plasticity and creep.[57, 58]

$$\dot{\overline{\varepsilon_{pl}}} = A_A \exp\left(-\frac{Q_A}{T}\right) [\sinh(\xi \frac{\bar{\sigma}}{s})]^{1/m} \qquad\qquad \text{Eq. (25)}$$

$$\dot{s} = (h_0 \left|1 - \frac{s}{s^*}\right|^a \operatorname{sign}(1 - \frac{s}{s^*}))\dot{\overline{\varepsilon_{pl}}} \qquad\qquad \text{Eq. (26)}$$

$$s^* = \tilde{s}[\frac{\dot{\overline{\varepsilon_{pl}}}}{A_A}\exp(\frac{Q_A}{T})]^n \qquad\qquad \text{Eq. (27)}$$

where s, Q_A , A_A, ξ, m, h_0, $\tilde{s}$, n, a are the deformation resistance, activation energy over gas constant, pre－exponential factor, multiplier of stress, strain rate sensitivity of stress, hardening/softening constant, saturation value for s, strain rate sensitivity of saturation, and strain rate sensitivity of hardening or softening respectively.

The volume change can cause thermal strain by the different temperature according to positions and time during cooling. The governing equation of thermal strain is as follow.[59]

$$\varepsilon_{ther} = \alpha^{se}(T - T_{ref}) \qquad \text{Eq. (28)}$$

where ε_{ther} , α^{se} , T , and T_{ref} are thermal strain, secant coefficient of thermal expansion, temperature, and reference temperature at which thermal stress is free.

4.2.2 Modeling procedure of thermal-mechanical model

In the thermal−mechanical model, the 2−dimensional domain perpendicular to the casting direction is used as shown at Fig. 4.2. This domain moves in the casting direction during transient calculation, so we can calculate the 3−dimensional distribution of temperature and stress in the solidified shell. And the size of the domain is 0.03m in width (perpendicular to cooling surface) and 0.0001m in thickness (parallel to the cooling surface). The reason why the width is set to 0.03m is that the liquid can remain sufficiently during solidification. For calculating heat transfer and stress in solidifying shell, we use the commercial simulation programs, ANSYS FLUENT and ANSYS MECHANICAL.

Fig. 4.3 shows the boundary conditions of thermal – mechanical model. It is assumed that the three surfaces inside the mold are insulated and heat can be transferred only to the surface in contact with the mold. The heat flux at the surface is used to transfer heat to the left side of the domain at the heat transfer model. These values are measured by thermocouple measurements by Li et al.[22]

In the mechanical model, it is assumed that the upper side can be free to move only in the x−direction, and the left side

can be free to move only in the y-direction. Nodes at the bottom side have the same displacement in the y direction and do not move in the x direction. Lastly, the right side moves to maintain verticality on the upper and bottom sides. As a result, when volume changes occur during cooling, the domain remains rectangular. These boundary conditions are to obtain the same value as the result in 1-dimensional domain using a 2-dimensional domain. In order to apply these boundary conditions in ANSYS MECHANICAL, the right side and bottom side use the cp command. The cp command can determine the displacement of nodes on each side.
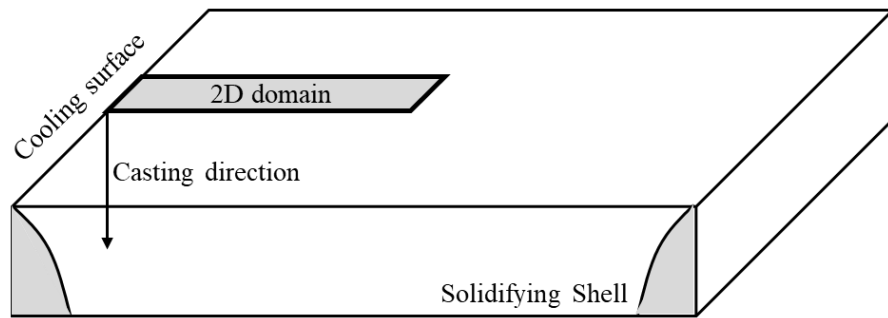
Fig. 4.2 2−dimensional domain of thermal−mechanical model perpendicular to the casting direction
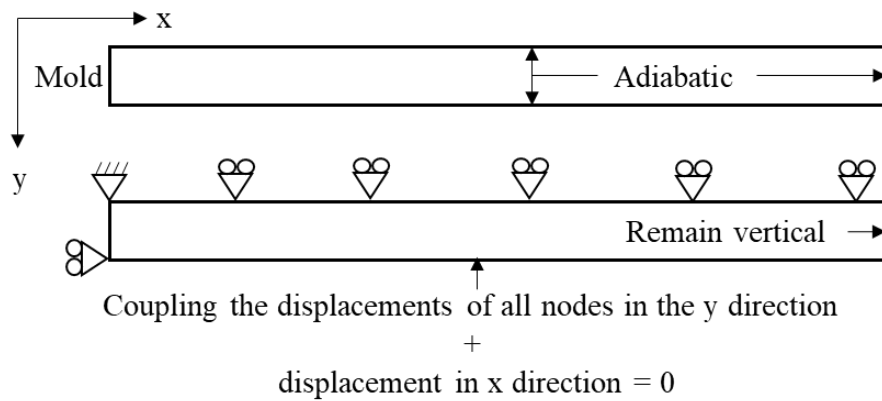
Fig. 4.3 Boundary condition of thermal−mechanical model

The changes of temperature and stress distributions in solidifying shell are affected by phase transformation. Because each phase has different material properties. So, material properties according to temperature and phase fractions of each phase should be used in the thermal−mechanical model. In the present model, the results of phase transformation model suggested in this study are used for calculating material properties by the phase change according to temperature. So, the liquidus temperature, solidus temperature, and peritectic temperature can be calculated by phase transformation model in this study.

The equation of thermal conductivity according to phase fraction and temperature was suggested by Harste et al. as follow.[45]

$$K(W/mK)=K_L f_L + K_\delta f_\delta + K_\gamma f_\gamma \qquad \text{Eq. (29)}$$

$$K_L = 39 \qquad \text{Eq. (30)}$$

$$K_\delta = (20.14 - 9.313 \times 10^{-3} T(℃))(1 - a_1 (pctC)^{a_2}) \qquad \text{Eq. (31)}$$

$$K_\gamma = (20.6 - 8.35 \times 10^{-3} T) \qquad \text{Eq. (32)}$$

$$a_1 = 0.425 - 4.385 \times 10^{-4} T(℃) \qquad \text{Eq. (33)}$$

$$a_2 = 0.209 - 1.09 \times 10^{-3} T(℃) \qquad \text{Eq. (34)}$$

The latent heat can be calculated by the enthalpy curve. So, the enthalpy according to phase fraction and temperature

was suggested by Harste et al. as follow.[45]

$$H(W/mK)=H_L f_L + H_\delta f_\delta + H_\gamma f_\gamma m \qquad \text{Eq. (35)}$$

$$H_L = 0.825T(K) - 105 \qquad \text{Eq. (36)}$$

$$H_\delta = 0.441T(K) + 8.87 \times 10^{-5}T(K)^2 + 51 + a_\delta \qquad \text{Eq. (37)}$$

$$H_\gamma = 0.43T(K) + 7.5 \times 10^{-5}T(K)^2 + 93 + a_\gamma \qquad \text{Eq. (38)}$$

$$a_\delta = \frac{(18(pctC)+2\times10^3(pctC)^2)}{(44(pctC)+1200)} \qquad \text{Eq. (39)}$$

$$a_\gamma = \frac{(37(pctC)+1.9\times10^3(pctC)^2)}{(44(pctC)+1200)} \qquad \text{Eq. (40)}$$

The equation of thermal linear expansion was suggested by using densities of liquid, δ, γ phases measured by Harste et al.[44, 45] and Jimbo et al.[43].

$$TLE = \sqrt[3]{\rho(T_0)\big/\rho(T)} - 1 \qquad \text{Eq. (41)}$$

$$\rho_L = 7100 - 73(pctC) - \big(0.8 - 0.09(pctC)\big)(T(℃) - 1550) \qquad \text{Eq. (42)}$$

$$\rho_\delta = \frac{100(8011-0.47T(℃))}{(100-(pctC))(1+0.013(pctC))^3} \qquad \text{Eq. (43)}$$

$$\rho_\gamma = \frac{100(8106-0.51T(℃))}{(100-(pctC))(1+0.008(pctC))^3} \qquad \text{Eq. (44)}$$

The elastic modulus according to temperature below the solidus temperature is used by a stepwise linear fit of measurements by Mizukami et al.[60] And it is assumed that the elastic modulus above solidus temperature is 50MPa for

convergence of calculations. The elastic modulus are shown at

Table 1.

In addition, some material properties are used as constant values. This is because these values did not significantly affect the stress distribution. These material properties are shown at

Table 2.

Last, the parameters in the Anand model are shown at

Table 3. [21] In particular, various values of s_0 have been proposed. Brown et al. suggested that it is a temperature dependent value. [61] It was suggested that s_0 is a value affected by temperature and strain rate, and has a range of about 35-52 MPa by Anand et al..[58] Then Huespe et al. used an average of 35 to 52, 43 MPa for s_0.[62] In this study, s_0 is 43 MPa at temperatures lower than the solidus temperature. Additionally, it is assumed that s_0 is 0.1 in the region where the liquid phase remains.

Temperature (K)	Elastic modulus (GPa)
273	200
573	185
773	165
973	130
1173	60
1373	25
1673	15

Table 1 The temperature dependent elastic modulus fitted by Mizukami et al.[60]

Thermal property	
Specific heat (J/kg K)	661
Mechanical property	
Density (kg/m^3)	7400
Poison's ratio	0.3

Table 2 Constant material properties for the thermal−mechanical model

Parameters	Value
Deformation resistance, $s_0(MPa)$	43 (below solidus T)
Deformation resistance, $s_0(MPa)$	0.1 (above solidus T)
Activation energy, $Q/R(K)$	32514
Pre−exponential factor, A	1e+11
Multiplier of stress, ξ	1.15
Strain rate sensitivity, m	0.147
Hardening constant, $h_0(MPa)$	1329
Saturation value, $\hat{s}(MPa)$	147.6
Strain rate sensitivity of saturation, n	0.06869
Strain rate sensitivity of hardening, a	1

Table 3 The parameters in the Anand model

4.3 Results

4.3.1 Volume contraction rates and pore formation susceptibilities during cooling

In the Chapter 3., a new model of phase transformation for hypo peritectic steel was developed. So, we can calculate the phase fraction of liquid, δ, and γ phase during continuous cooling for calculating volume contraction rates as shown at Fig. 4.4. These changes of phase fractions are calculated, when cooling rate is 800K/min and dT_p is 11K. When the carbon content is 0.12wt%C, the liquid is solidified to δ phase until peritectic temperature and the additional solidification to δ phase occurs. And then, the nucleation of γ phase starts at δ/L interface and γ phase grows during cooling. After solidification is completed, remained δ phase transformed to γ phase by diffusion controlled transformation. When the carbon content is 0.09wt%C, the solidification to δ phase starts from liquidus temperature and finishes without peritectic transformation before the formation of γ phase. After the solidified δ phase is cooled until $T_{massive}$, δ phase transforms to γ phase by massive transformation.

A notable difference between the results of the two steels is whether or not massive transformation in solid phase and peritectic transformation during solidification occur. Because,

the speed of growth of γ phase by massive transformation of Fe−0.09wt%C is faster than that that by diffusion controlled transformation of Fe−012wt%C. Also, the amount of phase transformation of Fe−0.12wt%C during solidification is larger than that of Fe−0.09wt%C, because peritectic transformation occurs during solidification.

Fig. 4.5 shows the volume contraction rates of Fe−0.09wt%C and Fe−0.12wt%C with liquid, when dT_p is 11K. The volume contraction rates of Fe−0.09wt%C are smaller than 0.004 /s. But, the volume contraction rates of Fe−0.12wt%C have a peak (1.81 /s) at 2.2% of liquid fraction. This is because of the behaviors of phase transformation during solidification. When carbon contents is 0.12wt%C, peritectic transformation occurs during solidification. So, the volume change is generated by cooling, solidification to γ phase, and peritectic transformation from δ phase to γ phase. However, peritectic transformation does not occur during solidification, when carbon contents is 0.09wt%C. So, the volume change of Fe−0.09wt%C is generated by cooling and solidification to δ phase. So, the amount of volume change of Fe−0.12wt%C is larger than that of Fe−0.09wt%C. Also, the speeds of peritectic transformation are very fast at the initial stage of peritectic transformation.[17, 33] As a result, the volume contraction

rates of Fe-0.12wt%C is larger than those of Fe-0.09wt%C.

Fig. 4.6 is the maximum volume contraction rates according to carbon contents, when dT_p is 11K. The graph of maximum volume contraction rates can be separated to two parts. When carbon contents is smaller than 0.105wt%C, maximum volume contraction rates are about 0.02 /s similar to result of Fe-0.09wt%C. However, when carbon contents is larger than 0.11wt%C, maximum volume contraction rates are about 1.7 /s similar to the results of Fe-0.12wt%C. This difference is generated by the presence of peritectic transformation according to carbon contents as mentioned about volume contraction rates at Fig. 4.5. As a result, it is showed that the behaviors of phase transformation change by a specific carbon content. This carbon content exists between 0.105wt%C and 0.11wt%C, when dT_p is 11K.

Fig. 4.7 shows the pore formation susceptibilities according to carbon contents and the liquid fractions with maximum volume contraction rates, when dT_p is 11K. When carbon contents are smaller than 0.105wt%C, the pore formation susceptibilities are about 0.2 /s, because there is no peritectic transformation during solidification. Pore formation susceptibilities increase rapidly upper to 280 /s at 0.11wt%C like maximum volume contraction rates, because large volume

contraction occurs by peritectic transformation during solidification and liquid fraction is very small at that time. So, the behaviors of pore formation susceptibilities are separated to two parts based of a carbon content between 0.105wt%C and 0.11wt%C, similar to the volume contraction rates. But, pore formation susceptibilities decrease rapidly after 0.115wt%C. This is because liquid fraction at which maximum volume contraction rates are generated increases, although peritectic transformation occurs during solidification. So, the steels with low carbon contents at which peritectic transformation starts may have high crack possibility by large volume contraction during solidification.
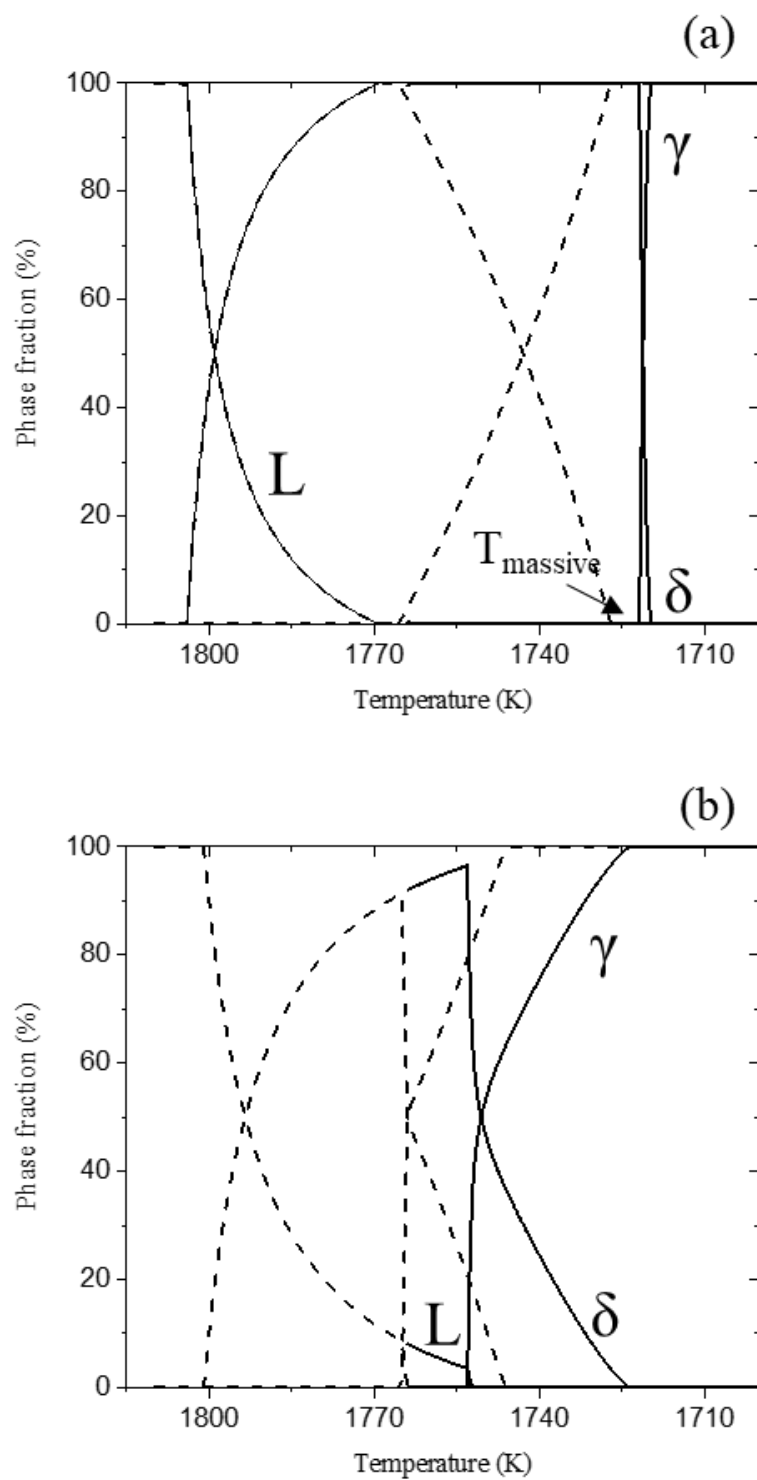
Fig. 4.4 Phase change during continuous cooling, when cooling rate is 800K/min and dT_p is 11K (a) Fe−0.09wt%C, (b) Fe−0.12wt%C

Fig. 4.5 Volume contraction rates of Fe−0.09wt%C and Fe−0.12wt%C, when dT$_p$ is 11K
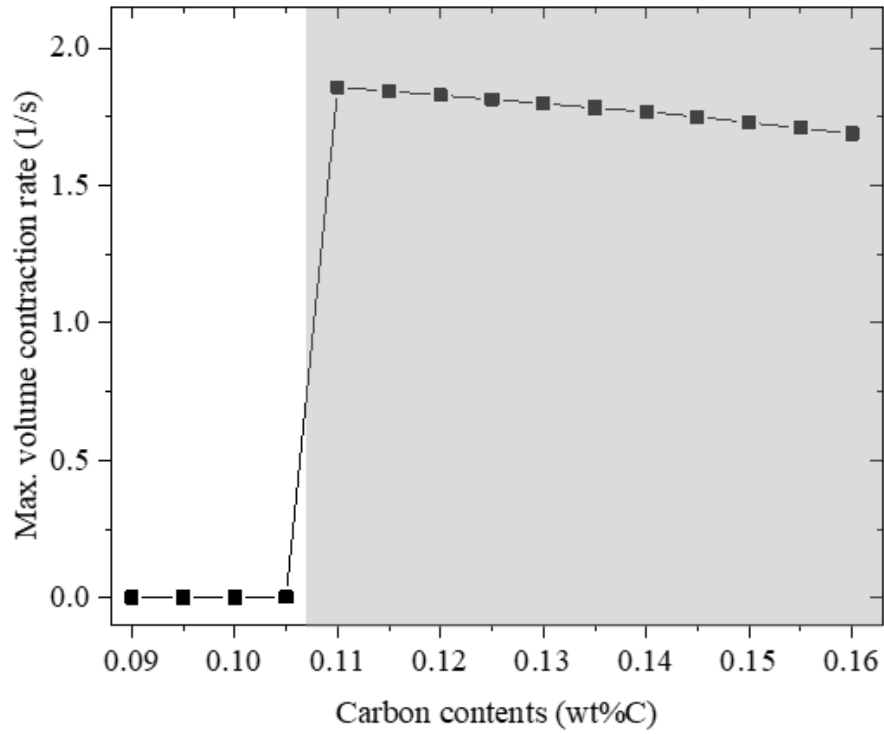
Fig. 4.6 Maximum volume contraction rates according to carbon contents, when dT_p is 11K

Fig. 4.7 (a) Liquid fractions when peritectic transformation starts, (b) Pore formation susceptibilities according to carbon contents

4.3.2 Strain rates in solid phase during cooling

It has been suggested that stress generated in solidified shell is mechanism of crack generation. So, we assumed that stress is mainly determined by strain rate. Fig. 4.8 shows that the strain rates of Fe−0.09wt%C and 0.12wt%C changes during phase transformation from δ phase to γ phase, when dT_p is 11K. The strain rates of Fe−0.09wt%C and Fe−0.12wt%C start at about 0% and 27% of γ fraction respectively, because solidification completes at these fractions of γ phase. In case of Fe−0.12wt%C, the strain rates decreases from 0.017 /s to 0.001/s, because the width of γ phase at which carbon diffuses for phase transformation increases and there is no inflow of carbon from liquid due to completion of solidification. In case of Fe−0.09wt%C, strain rates decrease from 0.06 /s to 0.001 /s. These values are larger than those of Fe−0.12wt%C. The strain rates in solid show different behaviors depending on whether the phase change to γ phase is diffusion controlled transformation or massive transformation. When carbon content is 0.12wt%C and dTp is 11K, peritectic transformation starts during solidification. So, after solidification completes by peritectic transformation, phase transformation from δ phase to γ phase occurs by diffusion controlled transformation. But, when carbon content is 0.09wt%C and dT_p is 11K, solidification

completes before T_{ps}, and it becomes δ phase only. This δ phase is cooled until $T_{massive}$ and transforms to γ phase by massive transformation. As a result, the mechanisms of phase transformation in solid are different according to carbon contents. And, the speeds of phase transformation by massive transformation are faster than those by diffusion controlled transformation. So, the strain rates of Fe−0.09wt%C are larger than those of Fe−0.12wt%C by difference of mechanisms of transformation in solid.

Large strain rates in solid can increase the possibility of crack generation. So, the maximum strain rates with 11K of dT_p are calculated according to carbon contents as shown at Fig. 4.9. When the carbon contents are smaller than 0.105wt%C, strain rates are about 0.23 /s. And when carbon contents are larger than 0.11wt%C, strain rates decrease to 0.035 /s rapidly and the values decrease to 0.01 /s additionally. The maximum strain rates can be separated to two parts according to the behavior of phase transformation like the maximum volume contraction rates. These difference of strain rates are caused by the mechanisms of phase transformation from δ phase to γ phase. When carbon contents are smaller than 0.105wt%C, phase transformation from δ phase to γ phase occurs by massive transformation. But, when carbon contents are larger

than 0.11wt%C, phase transformation from δ phase to γ phase occurs by diffusion controlled transformation. So, it can be suggested that the steels with carbon contents at which phase transformation from δ phase to γ phase occurs by massive transformation have high possibility of crack generation.
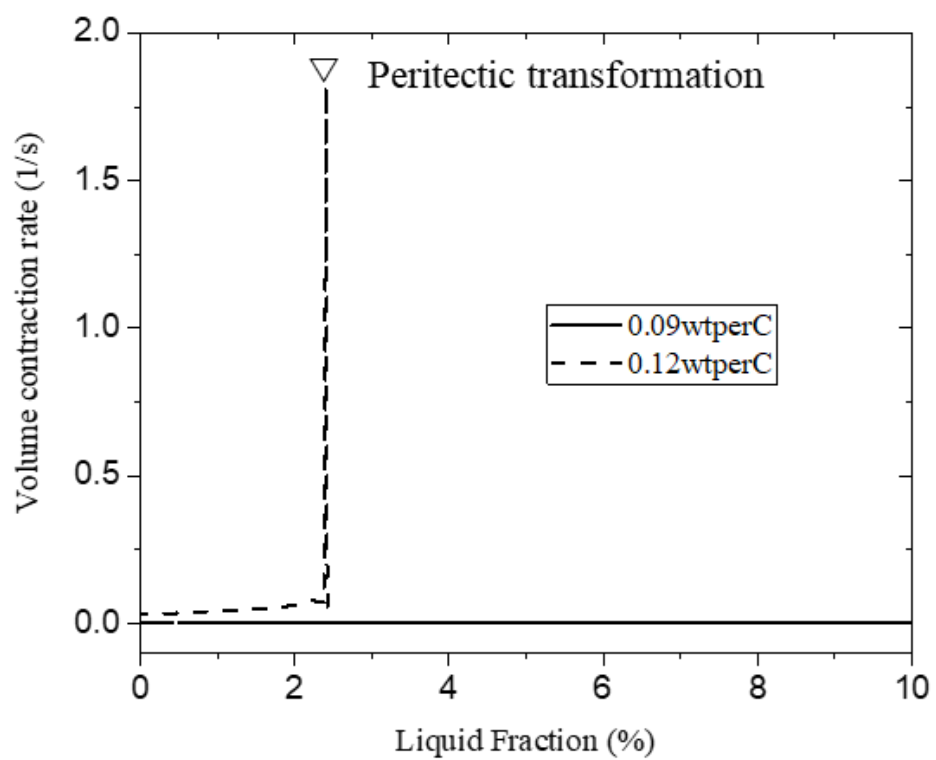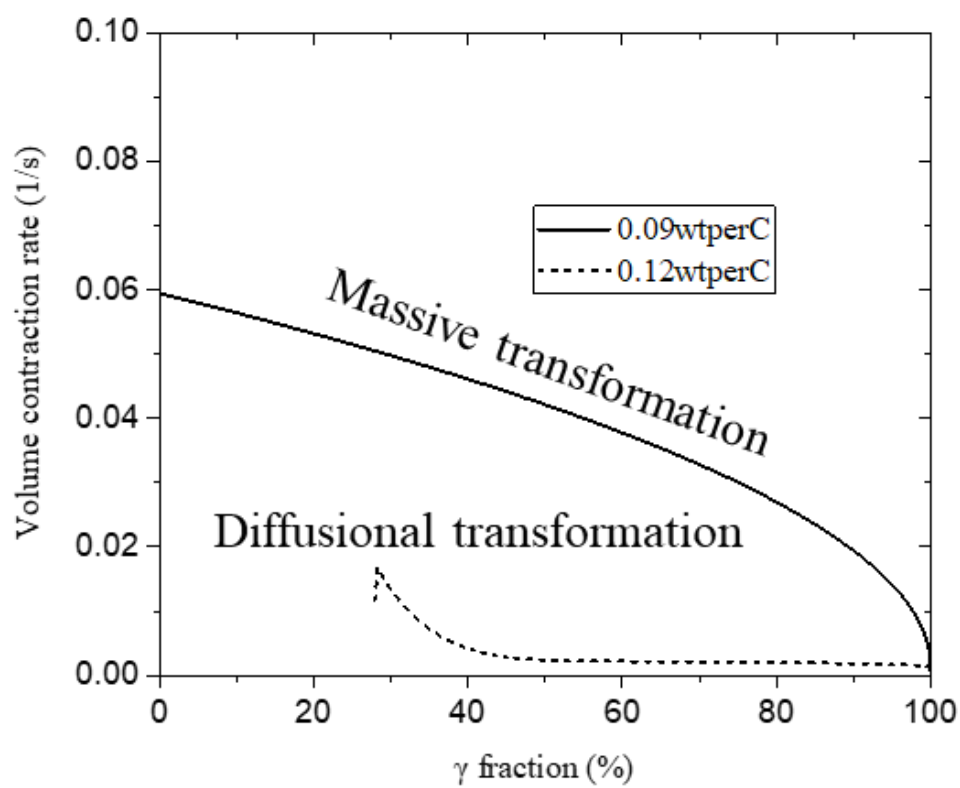
Fig. 4.8 Strain rates of Fe−0.09wt%C and Fe−0.12wt%C, when dT_p is 11K

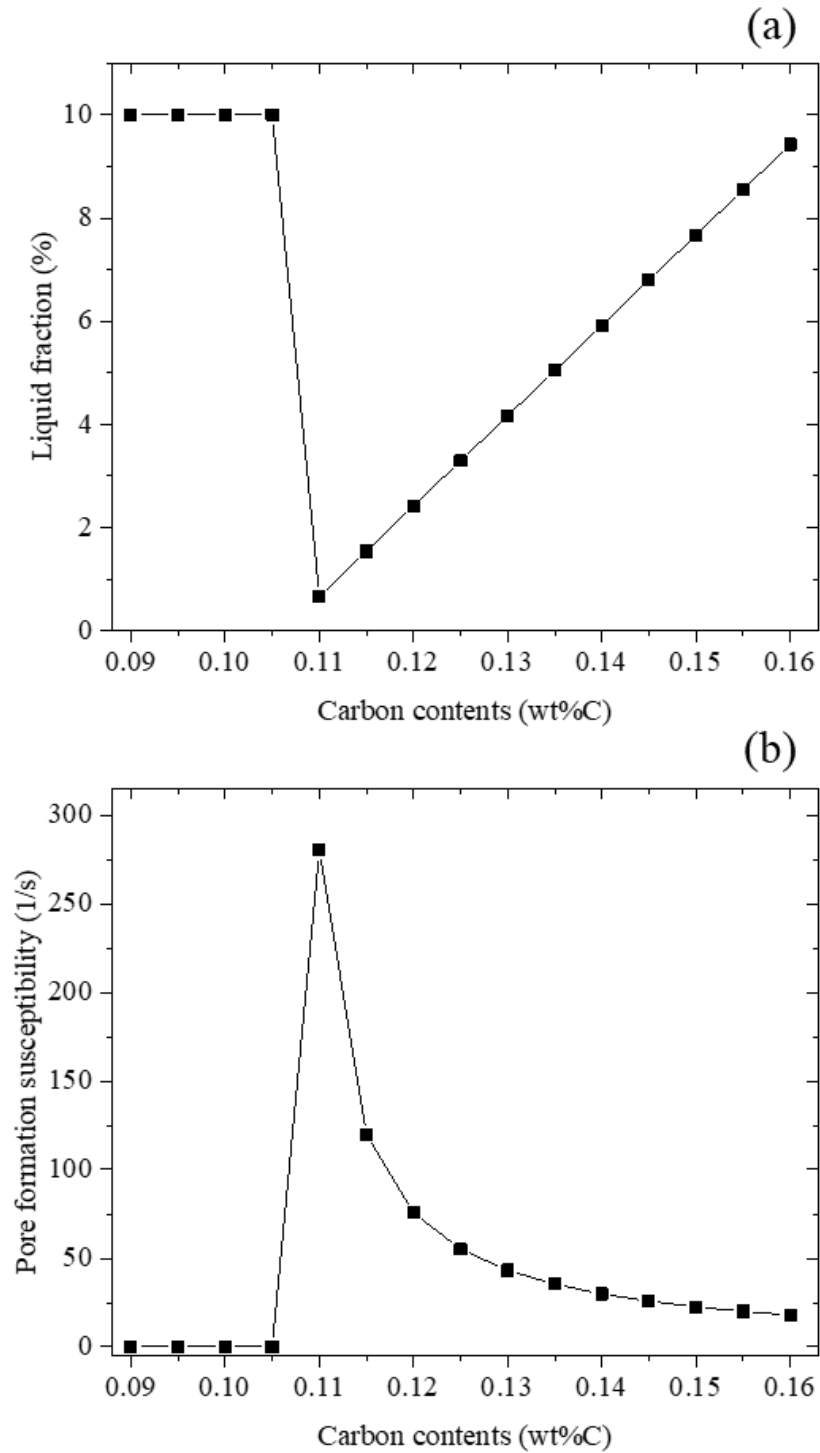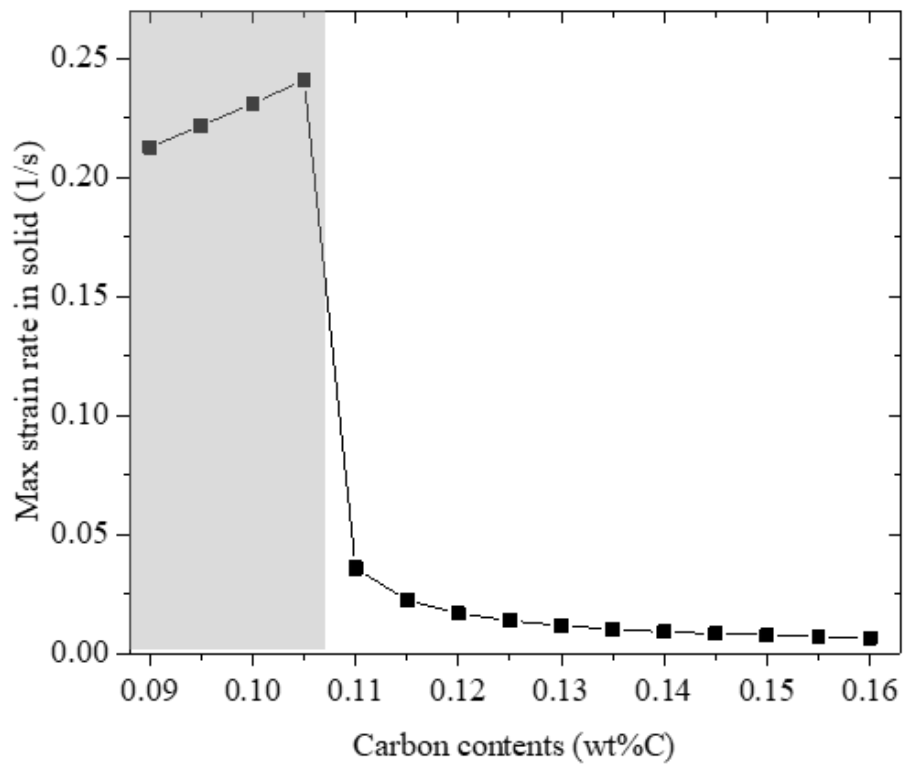Fig. 4.9 Maximum strain rates according to carbon contents, when dT$_p$ is 11K

4.3.3 Stress distribution in solidified shell

We calculate stress distributions for analyzing the effects of the behaviors of phase transformation to crack generation. First, we calculate the stress distribution, when carbon contents is 0.1wt%C and dT_p is 5K as shown at Fig. 4.10 and Fig. 4.11. The behaviors of phase transformation of this steel is similar to those of Fe−0.12wt%C with 11K of dT_p as shown at Fig. 4.4. Liquid is solidified to δ phase until T_{ps}, and peritectic transformation starts at T_{ps}. The formation of γ phase is generated by diffusion controlled transformation. After solidification completes by peritectic transformation, phase transformation from δ phase to γ phase is generated by diffusion controlled transformation.

First, the stress distribution in the direction perpendicular to the mold is calculated as shown at Fig. 4.10, when time is 1 and 1.8 seconds. Compressive stress is generated at surface, and tensile stress is generated inside the solidified shell. Also, the stress is hardly generated in the regions where temperatures are above the solidus temperature. So, it is possible to understand suggestion that cracks are generated by tensile stress inside the shell. However, it can be suggested that cracks may also occur on the surface of the shell through the results of stress distribution in the casting direction. Fig.

4.11 shows the stress distribution at the surface of shell in the casting direction. The stress distribution on the surface is as follows. Stress does not occur until solidification is complete. Immediately after solidification is completed at about 0.17 seconds, tensile stress occurs. Thereafter, about 6MPa of tensile stress is generated until 0.36 seconds due to peritectic transformation. Then, as the cooling progresses, the stress in solidified shell changes into compressive stress. As a result, the surface of the shell must have tensile stress at high temperatures. Therefore, cracks can occur not only inside the shell, but also on the surface of the shell.

Additionally, the stress distribution of Fe−0.1wt%C with 20K of dT_p in the casting direction at the surface of shell is calculated for analyzing the effects of the mechanism of phase transformation to stress in the solidified shell as shown at

Fig. 4.12. The behaviors of phase transformation of Fe−0.1wt%C with 20K of dT_p is showed at Fig. 3.8(b). Liquid is solidified to δ phase, and solidification completes before T_{ps} without peritectic transformation. So, only δ phase exists at T_{ps}. This δ phase is cooled to $T_{massive}$, and phase transformation from δ phase to γ phase is generated by massive transformation. So, the mechanism of phase transformation from δ phase to γ phase (massive transformation) is different to that of Fe−0.1wt%C

with 5K of dT_p (diffusion controlled transformation). So, the large tensile stress of about 8.76 MPa occurs in about 0.27 seconds by massive transformation. As a results, massive transformation in the solid phase can increase possibility of crack generation on the surface of shell.
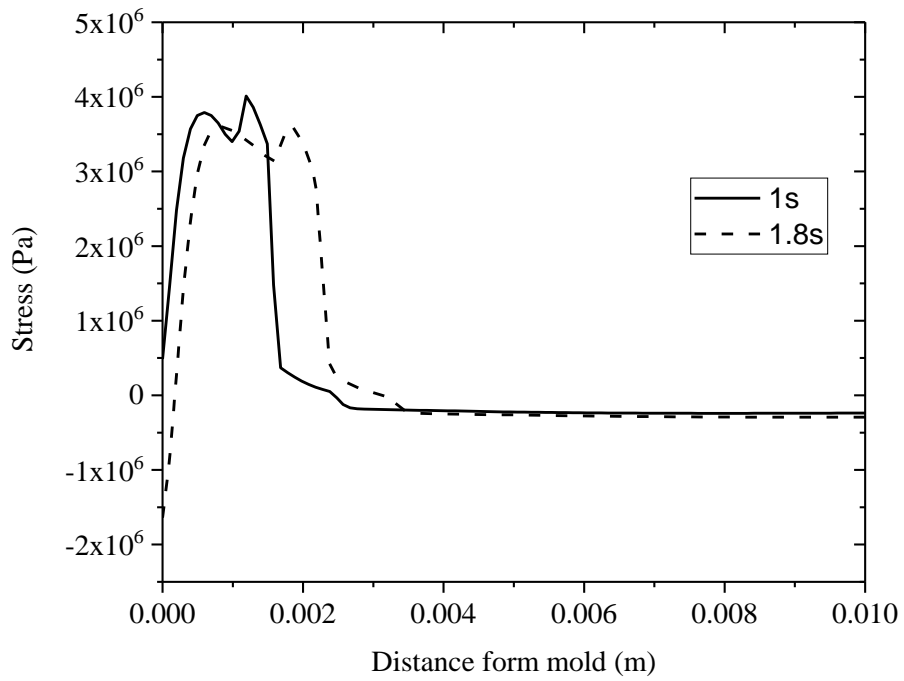
Fig. 4.10 Stress distribution in the direction perpendicular to the mold, when time is 1, 1.8 seconds ,when carbon contents are 0.1wt%C and dT$_p$ is 5K.
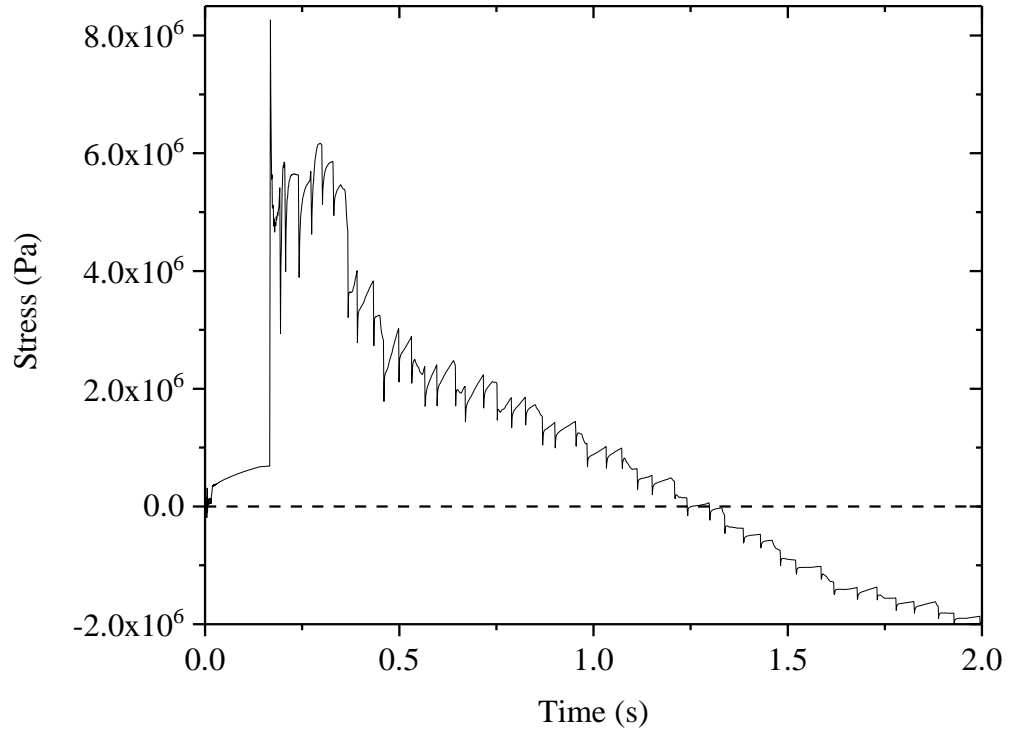
Fig. 4.11 Stress distribution in the casting direction at the surface of shell, when carbon contents are 0.1wt%C and dT_p is 5K.
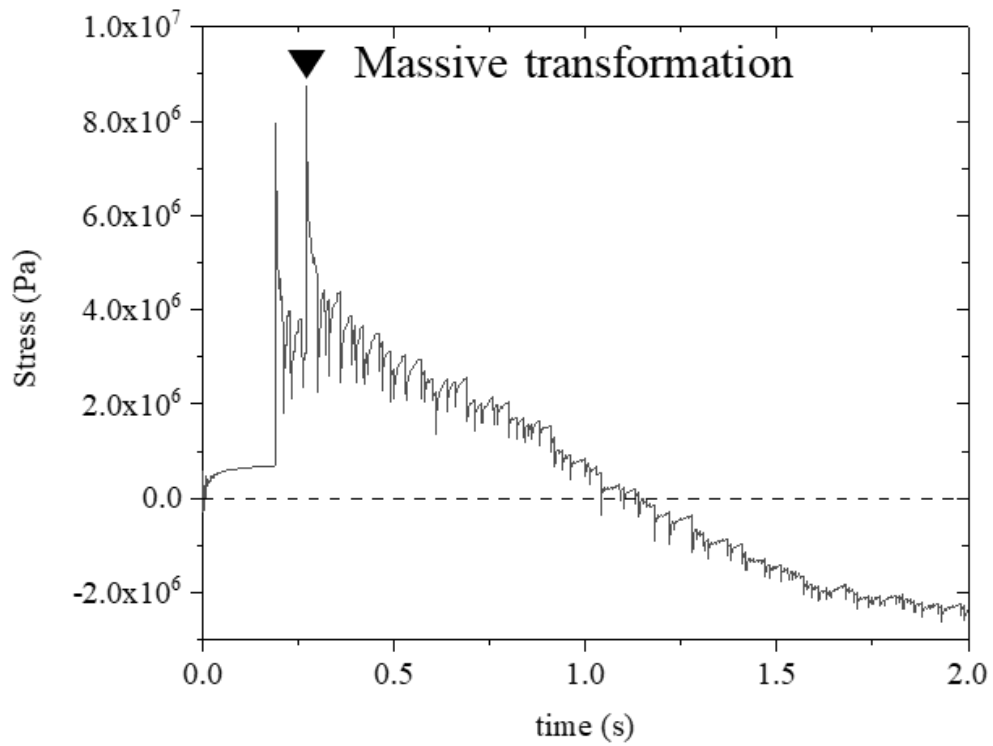
Fig. 4.12 Stress distribution in the casting direction at the surface of shell, when carbon contents are 0.1wt%C and dT_p is 20K.

4.4 Discussion

4.4.1 Crack mechanisms with relationship between delay of peritectic transformation, dT_p, and carbon contents

For predicting mechanisms and possibility of crack generation of hypo peritectic steel, pore formation susceptibilities and strain rates in solid were calculated as shown at Fig. 4.7(b) and Fig. 4.9. It is showed that the pore formation susceptibilities are small, when solidification to δ phase without peritectic transformation at low carbon contents. But, as carbon contents increase, pore formation susceptibilities increase rapidly by peritectic transformation with small liquid fraction , and decrease according to increasing liquid fraction at which peritectic transformation starts.

Strain rates in solid are large at low carbon contents by massive transformation from δ phase to γ phase, because of large and fast volume change in solid phase. But, as carbon contents increase, strain rates in solid phase decrease rapidly because phase transformation from δ phase to γ phase is generated by diffusion controlled transformation. So, it can be suggested that possibility of crack generation increase is high, when massive transformation occurs in solid phase.

We suggested that the possibilities of formation of pores

in dendrite arm spacing, when pore formation susceptibilities are large. These pores can be starting points of crack generation by stress concentrations. Also, it was suggested that stress in solidified shell is proportional to strain rates. So, the possibilities of crack generation increase by increasing strain rates in solid. So, we can suggest that peritectic transformation during solidification with small liquid fraction and massive transformation from δ phase to γ phase are main mechanisms for crack generation during continuous casting.

The pore formation susceptibilities and strain rates in the solid phase can be divided to two parts according to the behaviors of phase transformation at a specific carbon content. So, the pore formation susceptibilities and strain rates in the solid phase are calculated according to dT_p for analyze the carbon contents at which he pore formation susceptibilities and strain rates in the solid phase change rapidly as shown at Fig. 4.13 and Fig. 4.14.

When dT_p is 5K, 11K, and 20K, the carbon contents at which he pore formation susceptibilities and strain rates in the solid phase change rapidly are about 0.096wt%C, 0.107wt%C, and 0.125wt%C respectively. These behaviors are caused by the difference in phase change behavior due to whether solidification is completed without peritectic transformation

during dT_p. When carbon contents increase, the fraction of liquid increases at peritectic temperature. So, the more liquid can be solidified to δ phase during dT_p, when dT_p is large. Because dT_p is the delay of peritectic transformation from peritectic temperature. So, the time for solidification to δ phase increases with large dT_p. As a results, when dT_p increases, solidification can complete to only δ phase without peritectic transformation during dT_p in spite of increasing the carbon contents. So, in this case, phase transformation from δ phase to γ phase can be generated by massive transformation. On the contrary, when dT_p decreases, solidification cannot completes during dT_p, so peritectic transformation starts with liquid. Also, after solidification completes by peritectic transformation, phase transformation from δ phase to γ phase is solid can be generated by diffusion controlled transformation. As a results, the carbon contents at which pore formation susceptibilities and strain rates in the solid phase change rapidly increase, when dT_p increases. Fig. 4.15 is a results showing that there are relations between dT_p and carbon contents about mechanism of crack generation. For calculating this relationship, the median values of the two carbon contents in the region where the crack generation mechanisms are changed was used, when the dT_p was changed by 0.1K. In this study, the line representing the

relation between the carbon contents and dT_p is defined as transition line.

It is showed that the main mechanism of crack generation are different in the left and right side of the transition line by comparing Fig. 4.13, Fig. 4.14, and Fig. 4.15. On the left side of the transition line, the massive transformation with high transformation rates causes large strain rates after solidification. However, the solidification is completed without peritectic transformation, so pore formation susceptibilities are small. On the right side of the transition line, the pore formation susceptibilities are large because of peritectic transformation during solidification. But maximum strain rates in solid phase are small, because the phase change to γ phase occurs by diffusional transformation. In other words, if dT_p is determined under specific process conditions by cooling rate or alloy elements, main mechanism of crack generation can be selected according to carbon contents between stress generated in solid by massive transformation and pore formation by peritectic transformation during solidification. Also, it can be suggested that the possibility of crack generation is high near the transition line. Because the values of pore formation susceptibilities and maximum strain rates are the largest near the transition line.

(a)

(b)
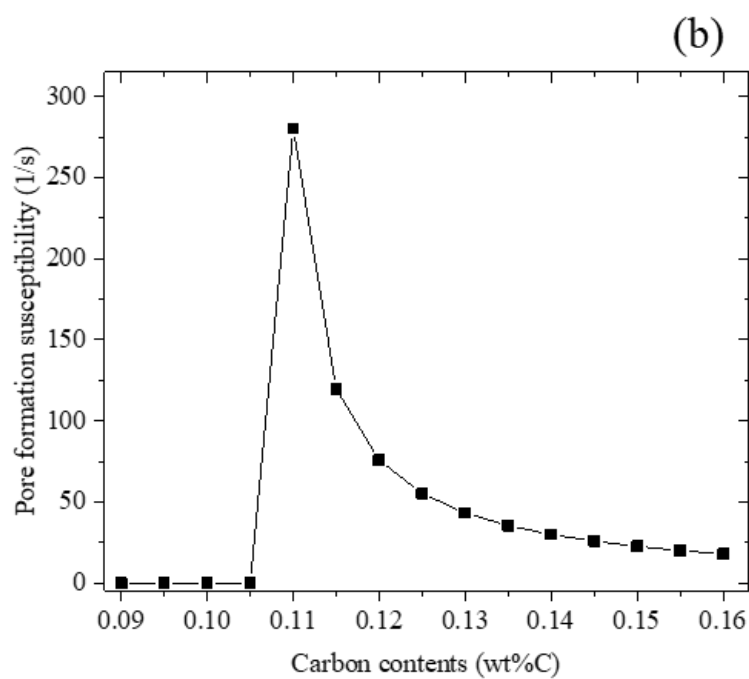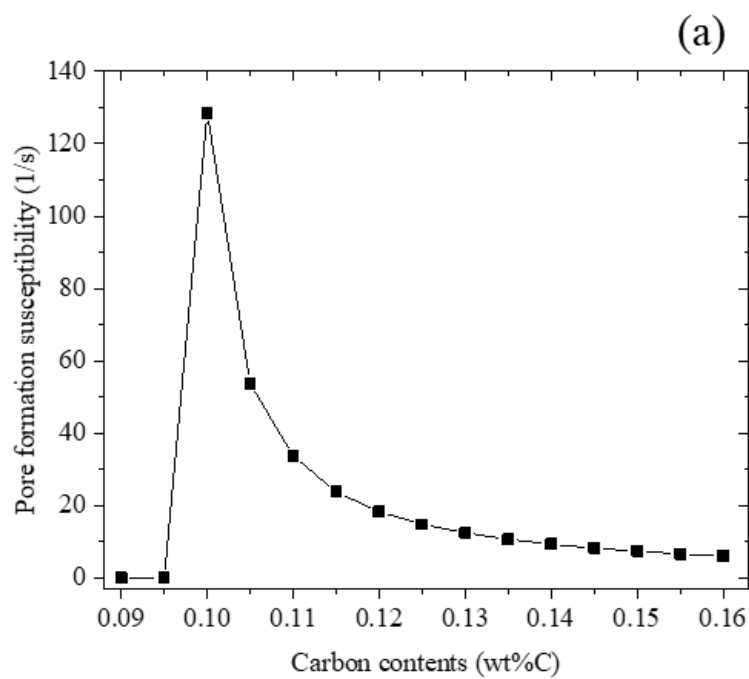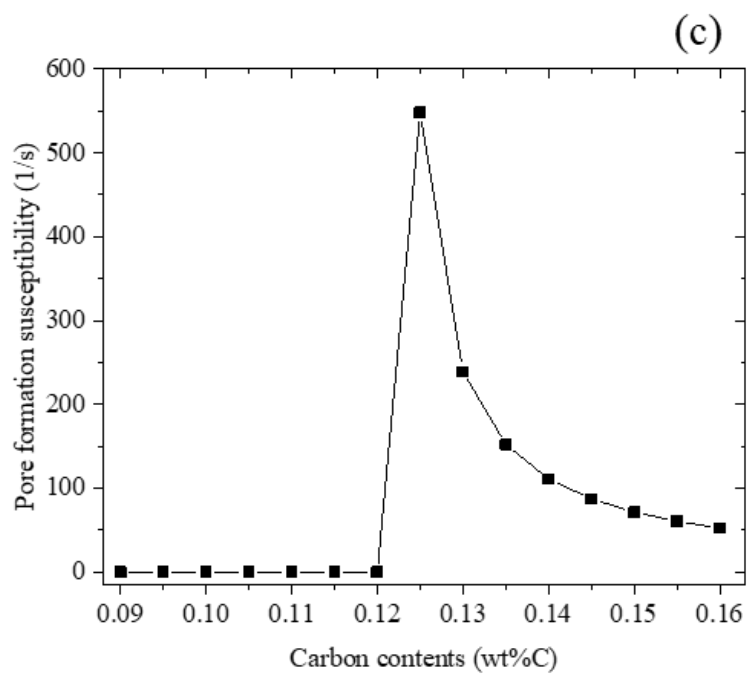
Fig. 4.13 Pore formation susceptibilities according to carbon contents

(a) dT_p = 5K, (b) dT_p = 11K, (c) dT_p = 20K

(a)

(b)
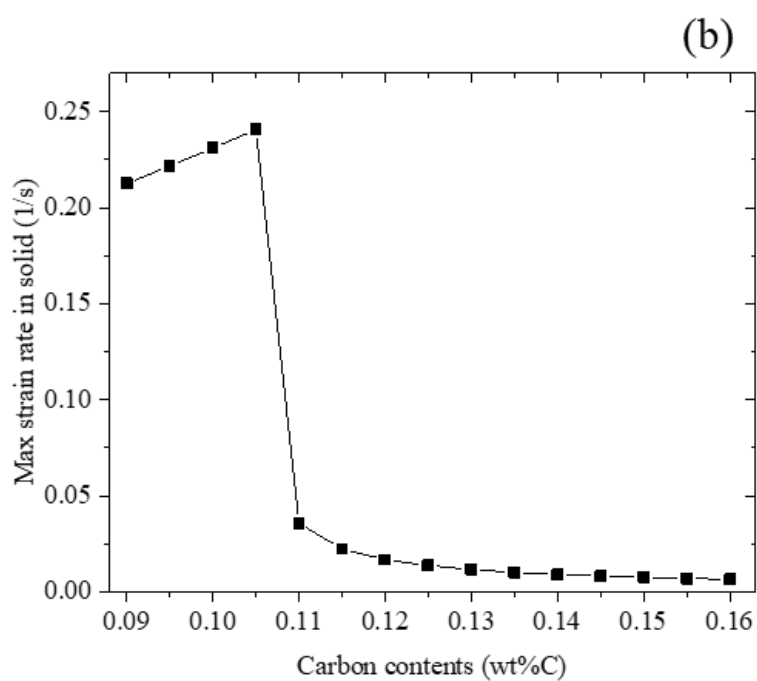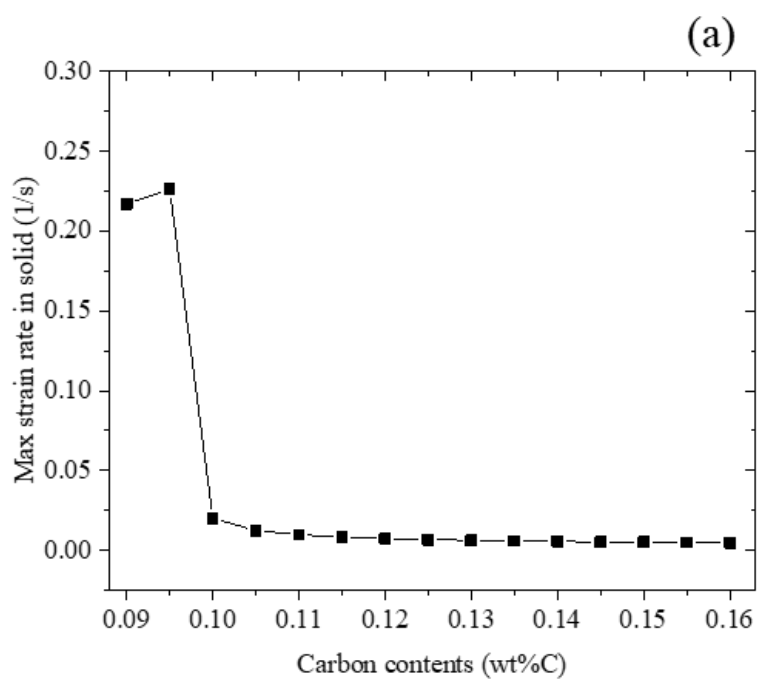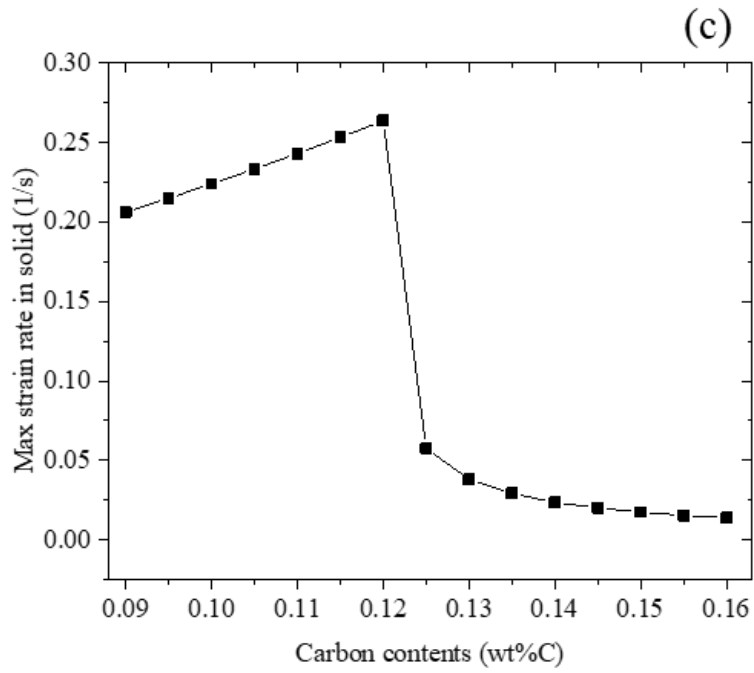
Fig. 4.14 Strain rates in solid phase according to carbon contents (a)
dT_p = 5K, (b) dT_p = 11K, (c) dT_p = 20K
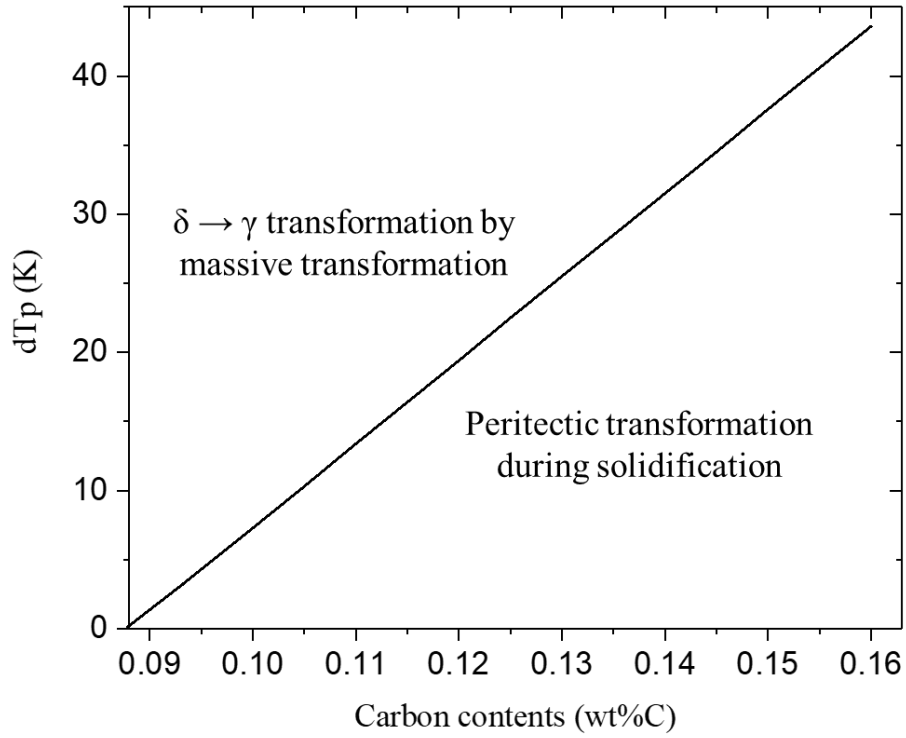
Fig. 4.15 The relation between carbon contents and dTp, and main mechanisms of crack generation according to carbon contents and dT_p.

4.4.2 Mapping of crack generation mechanisms

In the previous section, the relations between dT_p and carbon composition on crack generation and the mechanisms of crack generation were showed. In this section, the stress in the solidified shell and pore formation susceptibilities are mapped on carbon contents – dT_p graph as shown at Fig. 4.15 for analyzing quantitative analysis of crack generation.

First, the maximum stresses on solidified shell are calculated for analyzing the effects of the behaviors of phase transformation from δ phase to γ phase. Fig. 4.16 shows the maximum stress of Fe$-$0.11wt%C in solidified shell according to dT_p. These results are on the left side of transition line at carbon contents$-dT_p$ graph. In other words, the steels have small carbon contents and large dT_p. The maximum stresses of Fe$-$0.11wt%C are about 9MPa, although dT_p changes. Fig. 4.17 shows that the maximum stress of Fe$-$0.13wt%C, 0.14wt%C, and 0.15wt%C in solidified shell, when dT_p is 20K. These results are on the right side of transition line at carbon contents$-dT_p$ graph. In other words, the steels have large carbon contents and small dT_p. The maximum stresses of these steels are about 6MPa, although carbon contents changes. As a result, the maximum stresses in the condition on the left side of transition line are larger than those in the condition on the

right side of the transition line. This is because of the difference of the behaviors of phase transformation from δ phase to γ phase. On the left of transition line, the phase transformation occurs due to the massive transformation, so the maximum stresses are large by fast speeds of phase transformation. On the other hand, on the right side of transition line, the phase transformation occurs by diffusion controlled transformation, so the maximum stresses are small by slow speeds of phase transformation. So, it can be suggested that the massive transformation in solid phase can generate cracks in the solidified shell.

But, The maximum stresses due to the massive transformation are similar despite the change in dT_p. Therefore, the temperature at which maximum stress occurs due to the massive transformation is suggested as an important variable for crack generation instead of the maximum stress. Because the strength of steels decrease, when the temperature of steels increases. So, increasing the temperature at which massive transformation occurs can increase the possibility of crack generation.

The pore formation susceptibilities according to carbon contents and dT_p were calculated as shown at Fig. 4.13. From these results, the pore formation susceptibilities on the right

side of transition line are larger than the pore formation susceptibilities on the left side of transition line. Because, on the right side of transition line, peritectic transformation starts with liquid, so the large volume contractions are generated during solidification. But, on the left side of transition line, solidification completes without peritectic transformation during dT_p.

So, the temperatures at which massive transformation occurs and the pore formation susceptibilities are mapped on the carbon contents – dT_p graph as shown at Fig. 4.18. As a result, the temperature at which massive transformation starts are large near the transition line. Because the temperature at which massive transformation starts is high, when dT_p is small at the same carbon contents. Also, because the $T_{massive}$ is high, when carbon contents increase with same dT_p. The pore formation susceptibilities are large near the transition line like the temperature at which massive transformation starts. Because the liquid fractions are small near the transition line from the right side of the line. So, it can be suggested that the possibilities of crack generation are high near the transition line.
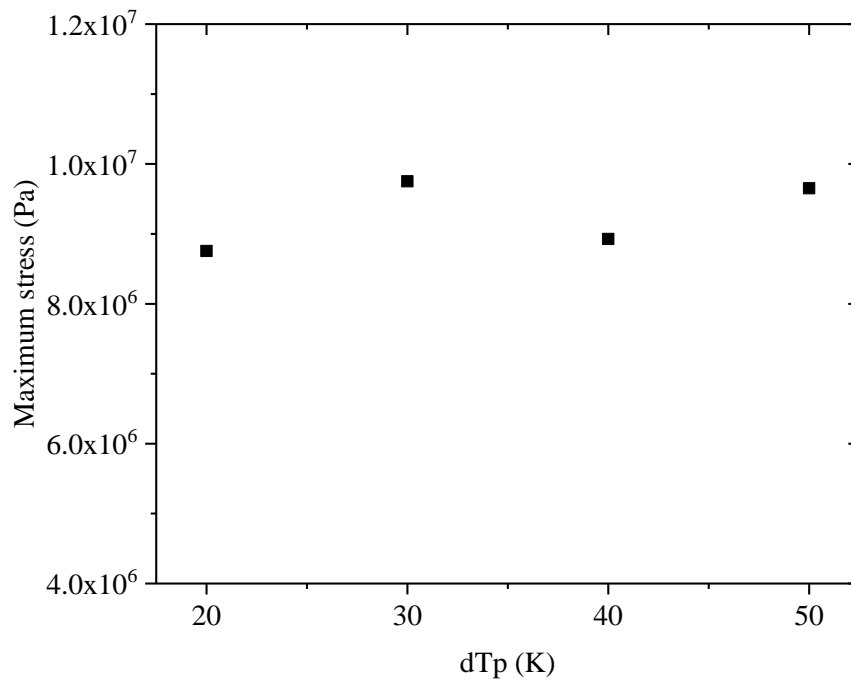
Fig. 4.16 The maximum stress of Fe−0.11wt%C in solidified shell according to dT_p. (On the left side of transition line)
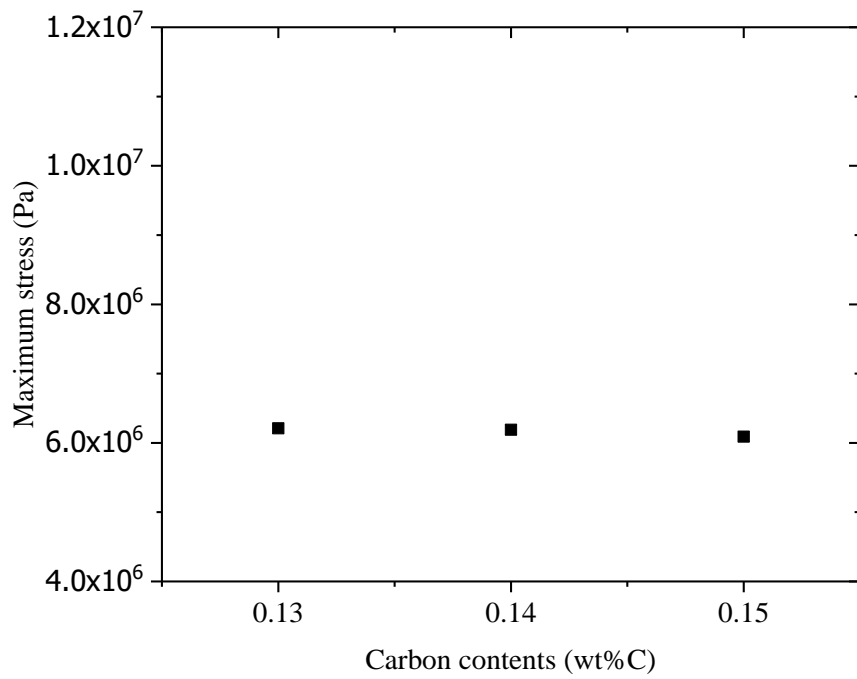
Fig. 4.17 The maximum stress in solidified shell according to carbon contents, when dT_p is 20K. (On the right side of transition line)
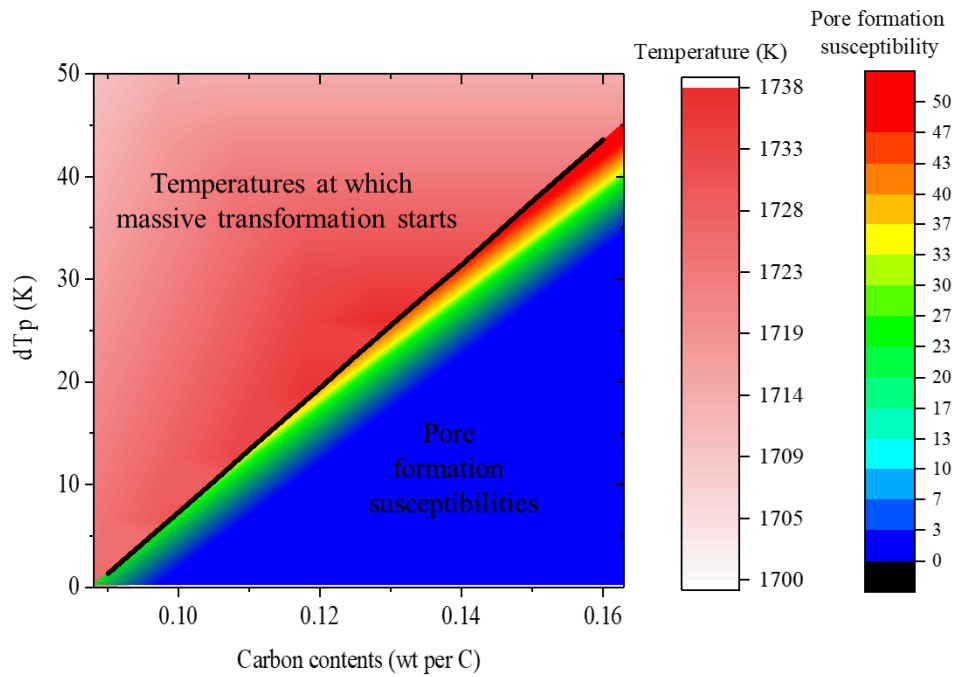
Fig. 4.18 Mapping the temperatures at which massive transformation starts and pore formation susceptibilities.

Chapter. 5 Analyze crack ratio of field data using the results of models for crack mechanisms

5.1 Longitudinal crack ratios according to effective carbon contents

Fig. 5.1 is normalized longitudinal crack ratio data of about 40000 continuous casting heats of a steel company at different carbon contents. These values were normalized based on the maximum longitudinal crack ratio. As a result, it is showed that the crack ratios of carbon contents between 0.05wt%C and 0.1wt%C are irregularly scattered in the carbon contents . However, these results include the effects of various alloying elements, such as S, Mn, etc. Therefore, in this study, relative position in the range of hypo peritectic steel (R) is proposed to apply crack data with various alloying elements to the results of phase change model. The reason for modeling newly the relative position in the range of hypo peritectic steel is to use a model that can be applied well in the composition ranges of alloying elements to be analyzed.

The method for calculating the relative position in the range of hypo peritectic steel is as follows. First, peritectic starting points and peritectic points of steels with various composition of alloy elements are calculated by using Factsage. And, peritectic starting points(a) and peritectic points(b) (as shown at

Fig. 5.2) are substituted into the equation of the relative position in the range of hypo peritectic steel as shown at Eq. (45). x is carbon content of steel used for calculate the relative position in the range of hypo peritectic steel.

$$R = \frac{x-a}{b-a} = \frac{1}{b-a}x + \frac{-a}{b-a} = Ax + B \qquad \text{Eq. (45)}$$

A and B are composed of pertectic points (a and b), so they can be also considered as values depending on the alloying element composition. So, It is necessary to understand the effects of alloying elements on A and B for analyzing the results of steels with various ratio of alloy elements. First, the equation considering the effects of alloying elements on A and B is as follows. The values in parentheses are the concentration (wt%) of each alloying element.

$$A(\text{or } B) = a(\text{Al}) + b(\text{S}) + c(\text{P}) + d(\text{Si}) + e(\text{Mn}) +$$
$$f(\text{S})(\text{Mn}) + g(\text{Si})(\text{Mn}) + h \qquad \text{Eq. (46)}$$

The influence of each alloy element on the change of peritectic points (a and b as shown in

Fig. 5.2) was suggested at the results of J.Xu et al.[63] They suggested that Al, P, S, Si, Mn, S have an individual effect to peritectic points, and interactions between S and Mn and

interactions between Si and Mn cause movements of peritectic points.

Using the Eq. (46), the coefficients of the Eq. (46) were fitted using peritectic points of 87 alloy steels calculated by Factsage. The composition range of the alloying elements used was 0 to 0.5 wt% for Si, 0 to 1.5 wt % for Mn, 0 to 0.05 wt % for P, 0 to 0.015 wt % for S, and 0 to 0.06 wt % for Al. The coefficients of the equations obtained by fitting are shown in the

Table 4. As a results of fitting the values, the R square values of A and B are 0.96 and 0.91. In addition, peritectic starting points and peritectic points are calculated with the compositions of randomly selected 20 alloy steels. It is showed that the differences between the results by fitting equation and the values calculated by thermodynamic calculation by Factsage are within 0.001wt%C. So, it shows that the relative position in the range of hypo peritectic steel can be used for comparing the crack ratio data of different alloying steels.

In addition, effective carbon contents (C_eff) can be calculated by peritectic points of carbon steel and relative position in hypo peritectic steel (R) by using Eq. (47).

$$C_{eff} = 0.09 + R(0.16 - 0.09) \qquad\qquad \text{Eq. (47)}$$

By using Eq. (45), Eq. (46), and Eq. (47), longitudinal crack ratio data at Fig. 5.1 can be transformed to longitudinal crack ratio data according to effective carbon contents. Fig. 5.3 is the values of longitudinal crack ratio every 0.04 interval of effective carbon contents. And these values are normalized based on the maximum longitudinal crack ratio. As a result, when the effective carbon contents is between 0.09wt%C and 0.115wt%C, most cracks occur. In addition, the longitudinal crack ratio gradually increases and then rapidly decreases thereafter, when carbon contents are from 0.09wt%C to 0.1135wt%C. When the effective carbon content is 0.106wt%C, the crack generation ratio has the maximum value.
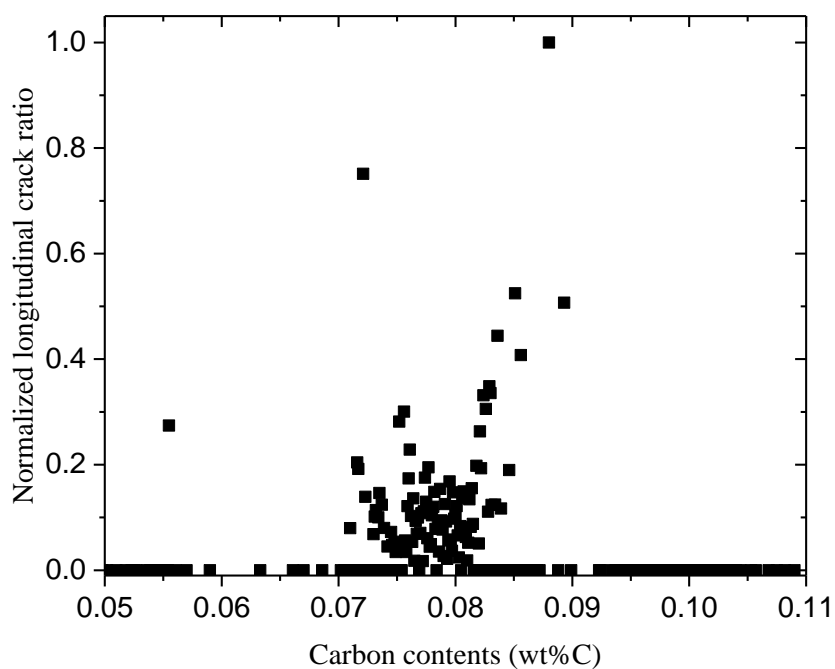
Fig. 5.1 Normalized longitudinal crack ratio of 19046 sheets. (The composition range of alloy elements : 0–0.5 wt% Si, 0–1.5 wt% Mn, 0–0.05 wt% P, 0–0.015 wt% S, 0–0.06 wt% Al)
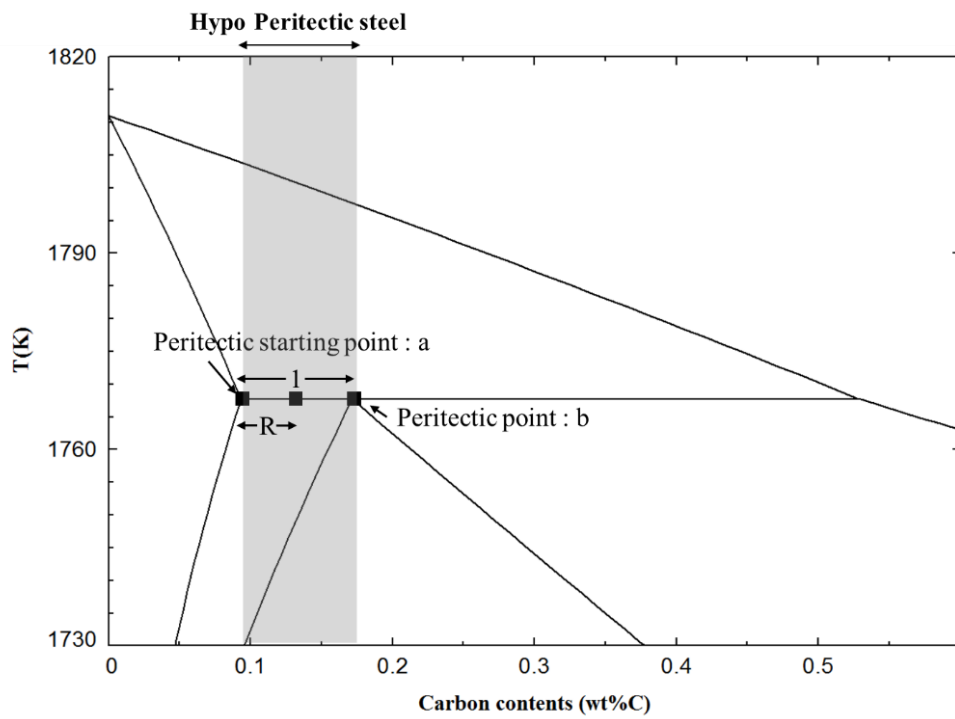
Fig. 5.2 Values for calculating relative position in the range of hypo peritectic steel (R)
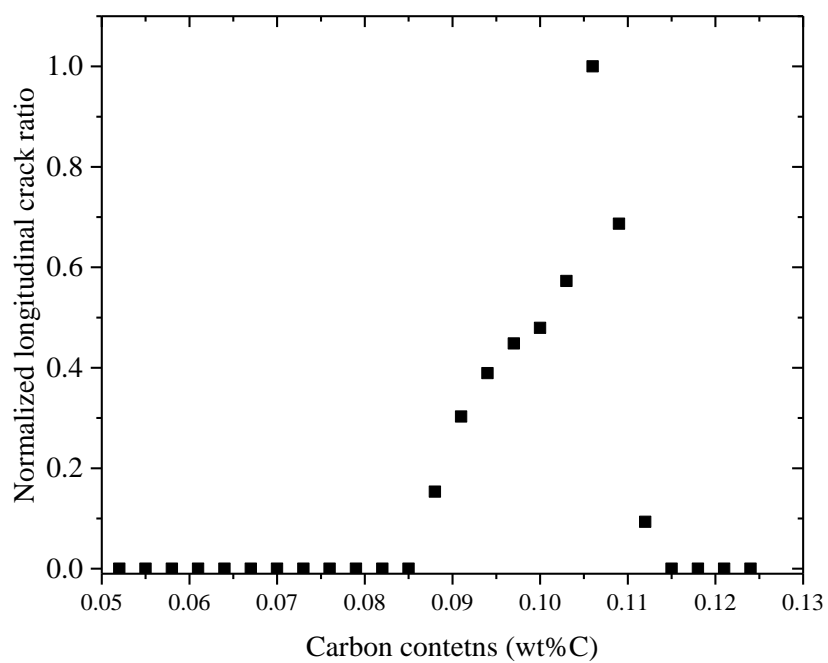
Fig. 5.3 Normalized longitudinal crack ratio every 0.04 relative position in hypo peritectic steel.

	A	B
a (Al)	3.9997	0.2476
b (S)	379.6260	−23.726
c (P)	−22.0576	1.472
d (Si)	−0.5573	0.0241
e (Mn)	2.1889	0.0197
f (S·Mn)	−148.275	15.5063
g (Si·Mn)	1.3074	0.1484
h (Constant)	12.3439	−1.1562
R square	0.9584	0.9117

Table 4 Coefficients of relative position in the region of hypo peritectic steel

5.2 Analyze distribution of crack ratio using results of crack generation model

For understanding the behaviors of longitudinal crack ratio and crack mechanisms, longitudinal crack ratio according to effective carbon contents is showed with temperature at which massive transformation starts and pore formation susceptibilities at

Fig. 5.4. The longitudinal crack ratio increase until 0.106wt%C at which maximum crack ratio is generated, and decrease rapidly as shown at

Fig. 5.4(a). In the previous section 4.4.2, it was suggested that there are two mechanisms of crack generation, massive transformation in solid and peritectic transformation during solidification, and the change of crack mechanisms occurs based on transition line. Also, it was showed that the possibility of crack generation can be maximized near the transition line by maximum strain rates and pore formation susceptibilities. So, dT_p can be calculated by transition line with the carbon contents at which maximum crack ratio is generated. As a result, dT_p of the results of this field data is 11K.

Additionally, we analyze the longitudinal crack ratio with temperatures at which massive transformation starts and pore formation susceptibilities, when dT_p is 11K as shown at

Fig. 5.4. The temperatures at which massive transformation increase to the carbon contents on the transition line, when dT_p is 11K. And the pore formation susceptibilities has maximum value near the carbon contents on transition line and decrease, when dT_p is 11K. These results can suggest quantitatively that the possibility of crack generation is maximized at a specific carbon contents and dT_p on transition line.

In other words, depending on the carbon composition and dT_p, the crack generation mechanisms are selectively acted between the massive transformation in the solid phase and pore formation by peritectic transformation during solidification. The behaviors of crack generation can be predicted according to carbon contents as follow. The possibility of crack generation increases up to the condition of carbon contents on transition line. And the possibility of crack generation is maximized at the carbon content near the condition on transition line. When carbon contents increase additionally, the possibility of crack generation decreases rapidly.

Many researchers showed longitudinal crack ratio according to carbon contents and analyzed the behaviors of crack ratio with their models of crack mechanisms.[13, 64, 65] In these studies, crack ratio increases, and decreases again

after reaching the maximum crack ratio. And, the carbon contents at which maximum crack ratio is generated are about 0.11wt%C, 0.129wt%C, and 0.132wt%C respectively. The behavior of crack ratio is similar to the results of our field results. But, the carbon contents at maximum crack ratio are different according to experiments. This difference can be explained by the difference of dT_p at different experimental conditions. Because maximum crack ratio can be generated near the transition line. so the carbon contents with maximum crack ratio increase with increasing dT_p. dT_p is affected by cooling rates, steel grades, and the condition of continuous casting machine, etc. So, if dT_p can be calculated by carbon contents with maximum crack ratio on transition line, it is possible to predict the composition range of steels with high crack ratios. As a result, it is possible to suggest conditions that can reduce the risk of crack generations through alloy design and adjustment of operating conditions.

(a)

(b)
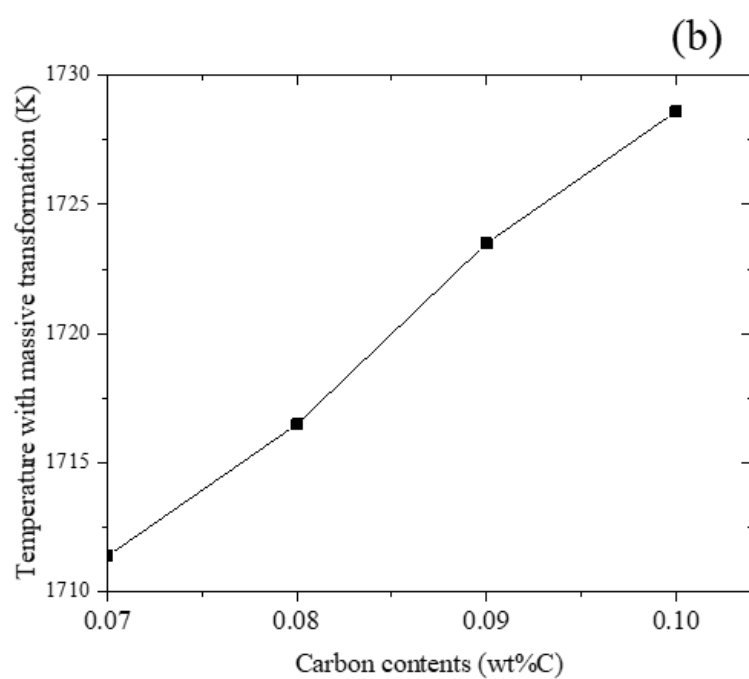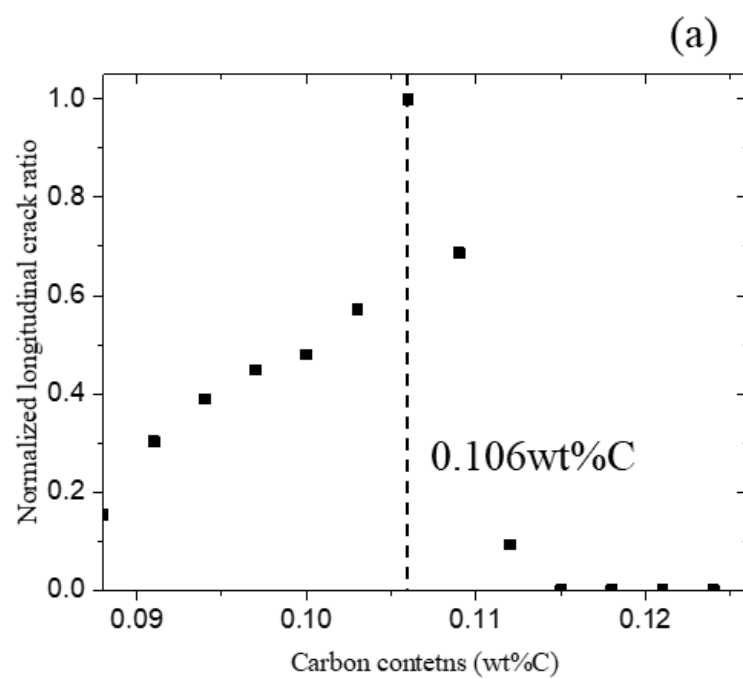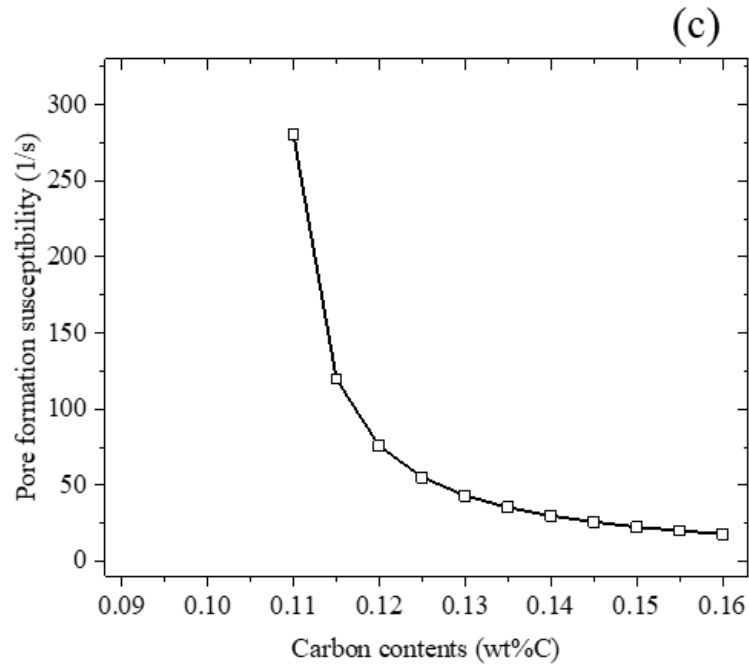
Fig. 5.4 Analyzing the (a) longitudinal crack ratio according to effective carbon contents with temperature at which (b) massive transformation starts and (c) pore formation susceptibilities when dTp is 11K.

5.3 Effects of casting speeds and alloy elements for the behaviors of crack generation on continuous casting

Through the phase transformation model, crack generation prediction model, and stress model for hypo peritectic steel developed in this study, the mechanisms of crack generation and the conditions with high probability of crack generation in the continuous casting process were suggested. As a result, it could be suggested that there is a transition line in which the behaviors of phase change and mechanisms of crack generation are changed, and the probability of crack generation at the carbon composition and dT_p near the transition line is maximized. That is, it can be suggested that effective carbon composition and normalized dT_p of the experimental or continuous casting processes are the main variables for understanding the behaviors of crack generation. In this section, we will show the effects of alloying elements (silicon and manganese) and casting speed to the cracking behavior by the change of carbon contents at which maximum crack ratio according to contents of alloy elements and casting speed.

5.3.1 Effects of Silicon and manganese

Fig. 5.5 shows the change of carbon contents at which maximum crack ratio occurs according to silicon contents in two different continuous casting works. It is showed that the carbon contents at which maximum crack ratio occurs increase, when silicon contents increase. Also, the gradients of the two results are similar to the silicon concentration of about 0.175 wt%C/wt%Si. The increase of carbon contents at which the maximum crack ratio occurs by the increase of silicon concentration may be explained by the effect of the increase in dT_p. In previous section, it was showed that the difference of carbon contents at which maximum crack ratio occurs according to experiments or continuous casting process can be explained by the difference of dT_p. So, it can be suggested that silicon increases dT_p, so the carbon contents at which maximum crack ratio occurs increase.

These results may show that silicon affects the behaviors of phase transformation not only thermodynamically but also kinetically in respect of the behaviors of crack generation. The behaviors of phase transformation according to alloying elements is considered thermodynamically by calculating the crack generation ratio according to the effective carbon composition. Additionally, dT_p is the amount of undercooling of

formation of γ phase. So, it can be suggested that the increase of dT_p is caused by additional delay of formation of γ phase. As a result, silicon may delay the formation of γ phase, so increase dT_p.

The effects of manganese can also be suggested. The average manganese concentrations of Work1 and Work2 are 1.48wt%Mn and 0.97wt%Mn, respectively as shown in Fig. 5.5. And, when the silicon contents are 0wt%Si, the carbon composition(0.115wt%C) at which the maximum crack ratio occurs at Work 1 is greater than that(0.0934wt%C) of Work 2. This result may suggest that the carbon contents at which maximum crack ratio occurs decrease, when manganese contents increase. From these results of the crack generation behaviors, it can be suggested that manganese accelerates the formation of γ phases. In other words, manganese may decrease dT_p.
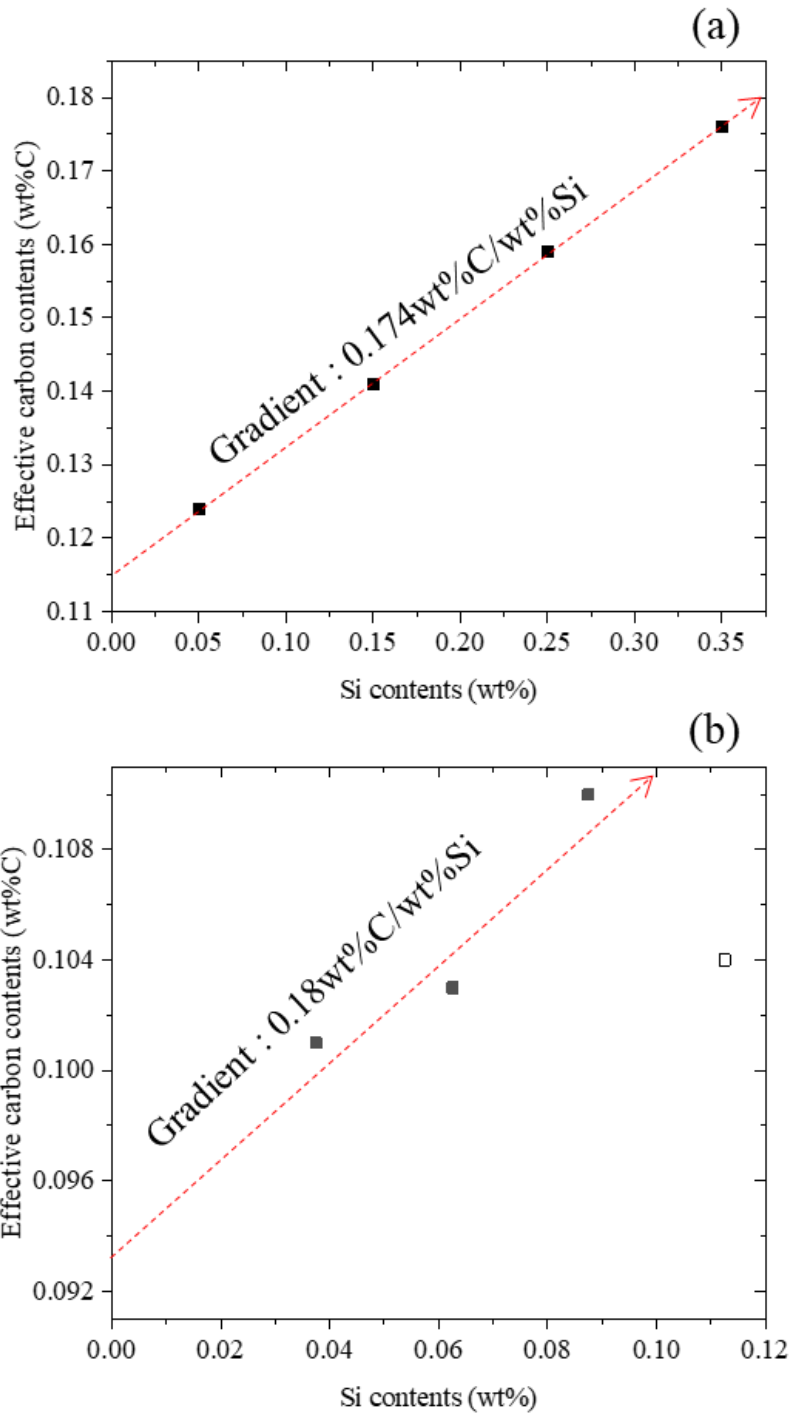
Fig. 5.5 Carbon contents at which maximum crack ratio according to
Si contents (a) Work 1, (b) Work 2

Manganese has the opposite effect with silicon on dT_p. From Fig. 4.18, the possibilities of crack generation can be the largest near the transition line, so carbon contents with maximum crack ratio can change according to dT_p along the transition line. Therefore, it can be suggested that the increased dT_p by increasing silicon contents increases the carbon contents at which the maximum crack ratio occurs. And manganese can easily generate γ phase at the L/d interface, thereby decreasing dT_p. As a result, if we analyze the crack generation behavior according to various alloying elements in this way, it may be possible to suggest the effect of alloying elements on the formation of γ phase and the direction of crack reduction.

5.3.2 Effects of casting speed

Fig. 5.6 shows the carbon contents at which maximum crack ratio occurs according to casting speed, when silicon contents are between 0 and 0.04wt%. The effects of casting speed for the behaviors of crack ratio are analyzed in the limited silicon contents range, because the behaviors of crack generation are heavily affected by silicon contents as shown at Fig. 5.5. The carbon contents at which maximum crack ratio increases with increasing casting speed like the effects of silicon. This results shows that casting speed can increase dT_p. Because casting speed can increase cooling rate normally, so, more undercooling of formation of γ phase (dT_p) is possible during the same time. As a results, it can be suggested that increasing casting speed may increase the carbon contents at which maximum crack ratio occurs by increasing dT_p.
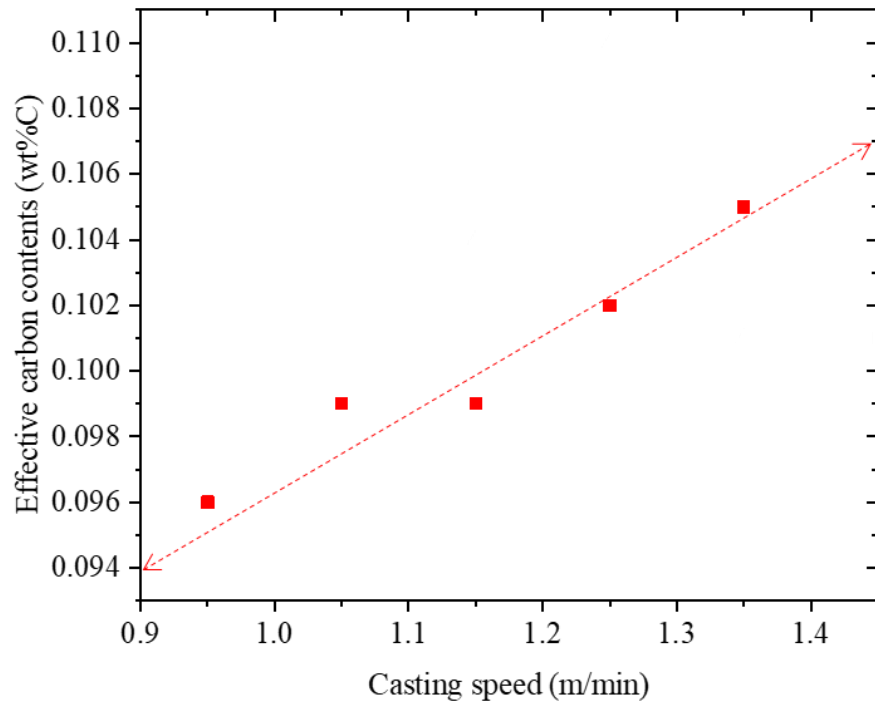
Fig. 5.6 Carbon contents at which maximum crack ratio according to casting speed, when silicon contents are between 0 and 0.04wt% (Work 2)

Chapter. 6 Summary and Conclusion

The quality of the slabs in the continuous casting process is strongly influenced by the steel grade. In particular, it is known that hypo peritectic steel has high probabilities of crack generation during continuous casting So, first, a model of phase transformation of hypo peritectic steel is developed. In this model of phase transformation of hypo peritectic steel, we consider the behaviors of phase transformation until molten steel becomes γ phase, and the diffusion of carbon is the main mechanism of phase transformation. Additionally, based on the various experimental results suggested by many researchers, the model of phase transformation includes massive transformation from δ phase to γ phase and undercooling for the formation of γ phase from the peritectic temperature (dT_p). We show the phase change behavior according to various carbon compositions and dT_p, and the speeds of the δ/γ and L/γ interfaces. As a result, it can be showed that the behaviors phase transformation of the hypo peritectic steel have two paths. First, when solidification ends without peritectic transformation before T_{ps} $(=T_p(peritectic temperature)-dT_p)$, the γ phase is formed by massive transformation. On the contrary, when peritectic reaction starts with liquid, the peritectic transformation starts at L/δ interface, and the formation of γ phase is generated by diffusion controlled transformation.

By using the results of phase transformation model, new models of crack generation of hypo peritectic steel are developed for predicting possibility of crack generation in continuous casting such as strain rates in solid, volume contraction rate during solidification, and pore formation susceptibilities. In addition, by developing a stress model, the stress distributions in the solidified shell are calculated. As a result, there are two main mechanisms of crack generation, which are massive transformation in solid phase and peritectic transformation with small liquid fraction during solidification. In addition, it is showed that there is the linear relation between the carbon composition and dT_p as border line for dividing the two mechanisms of crack generation. Also, it can be suggested that the possibilities of crack generation are maximized near the transition boundary between the two mechanisms by the temperatures at which massive transformation starts and pore formation susceptibilities.

Finally, the crack generation ratios of the field data are analyze by using the results of the developed models. An equation of effective carbon contents is suggested to analyze the crack ratio of steels with alloying elements. As a result, as the carbon contents increase, the crack generation ratios according to the effective carbon composition increase to the

maximum crack generation ratio and then decrease. These crack ratios could be analyzed by the temperatures at the start of the massive transformation and the pore formation susceptibilities at a specific dT_p. As a result, the results of varying the carbon contents when the crack ratios were maximized according to the experiments could be explained as the difference in the normalized dT_p of each process.

Furthermore, the effects of silicon, manganese and casting speed on the cracking behavior were analyzed. As a result, an increase in the silicon concentration and the casting speed increases the effective carbon composition having a maximum crack ratio. And an increase in the concentration of manganese decrease the effective carbon composition having a maximum crack ratio. We analyze this behaviors in terms of the interfacial energy that must be overcome in order to form the γ phase at the L/δ interface. As a result, silicon increases the interfacial energy of δ/γ, thereby increasing dT_p. Manganese, on the contrary, decreases the interfacial energy of δ/γ, thereby decreasing dT_p. And It is suggested that the casting speed increases the undercooling to the γ phase formation(dT_p) by increasing the cooling rate. As a result, it can be suggested that the casting rate and silicon may crack in the higher range of carbon contents and manganese in the lower range of carbon

contents. In addition, it is possible to suggest the direction to avoid crack generation in the alloy design process.

Bibliography

[1]   "World Steel In Figures 2019," *World Steel Association,* 2019 2019.

[2]   S. Seetharaman, *Treatise on process metallurgy, volume 3: industrial processes*. Newnes, 2013.

[3]   M. Alizadeh, H. Edris, and A. Shafyei, "Mathematical modeling of heat transfer for steel continuous casting process," *International Journal of Iron & Steel Society of Iran,* vol. 3, no. 2, pp. 7-16, 2006.

[4]   A. Moitra, "Thermo-mechanical model of steel shell behavior in continuous slab casting," 1994.

[5]   B. Iron, S. R. Association, and S. Dvision, *Definitions and Causes of Continuous Casting Defects*. Iron & Steel Institute, 1967.

[6]   H. Hiebler, "Gmelin-Durrer, Metallurgy of Iron," in *Practice of Steelmaking 3: Continuous casting*, vol. 11: Springer-Verlag Berlin, 1992.

[7]   R. Gray, A. Perkins, and B. Walker, "Quality of Continuously Cast Slab," in *Solidification and Casting of Metals₩ Proc. Conf.₩, Sheffield, England, July 1977*, 1979, pp. 300-305.

[8]   F. Camisani-Calzolari, I. Craig, and P. Pistorius, "A review on causes of surface defects in continuous casting," *IFAC Proceedings Volumes,* vol. 36, no. 24, pp. 113-121, 2003.

[9]   H. F. Schrewe, *Continuous casting of steel: fundamental principles and practice*. Verlag Stahleisen, 1989.

[10]   N. McPherson and S. McIntosh, "Mold powder related defects in some continuously cast steel products," 1987.

[11]   J. Savage and W. Pritchard, "The problem of rupture of the billet in the continuous casting of steel," *Journal of the Iron and Steel Institute,* vol. 178, no. 3, pp. 269-277, 1954.

[12]   D. M. Stefanescu, "Microstructure evolution during the solidification of steel," *ISIJ international,* vol. 46, no. 6, pp. 786-794, 2006.

[13]   J. Xu, S. He, X. Jiang, T. Wu, and Q. Wang, "Analysis of crack susceptibility of regular carbon steel slabs using volume-based shrinkage index," *ISIJ international,* vol. 53, no. 10, pp. 1812-1817, 2013.

[14]   M. H. Trejo, E. A. Lopez, J. J. R. Mondragon, M. d. J. C. Roman, and H. S. Tovar, "Effect of solidification path and contraction on the cracking susceptibility of carbon peritectic steels," *metals and materials international,* vol. 16, no. 5, pp. 731-737, 2010.

[15]   H. Mizukami, A. Yamanaka, and T. Watanabe, "High temperature deformation behavior of peritectic carbon steel during solidification," *ISIJ international,* vol. 42, no. 9, pp. 964-973, 2002.

[16]   J. Konishi, M. Militzer, I. Samarasekera, and J. Brimacombe, "Modeling the formation of longitudinal facial cracks during continuous casting of hypoperitectic steel," *Metallurgical and materials transactions B,* vol. 33, no. 3, pp. 413-423, 2002.

[17]   H. Shibata, Y. Arai, M. Suzuki, and T. Emi, "Kinetics of peritectic

reaction and transformation in Fe-C alloys," *Metallurgical and Materials Transactions B,* vol. 31, no. 5, pp. 981–991, 2000.

[18]   Y. Ueshima, S. Mizoguchi, T. Matsumiya, and H. Kajioka, "Analysis of solute distribution in dendrites of carbon steel with δ/ɤ transformation during solidification," *Metallurgical Transactions B,* vol. 17, no. 4, pp. 845–859, 1986.

[19]   M. Suzuki and Y. Yamaoka, "Influence of carbon content on solidifying shell growth of carbon steels at the initial stage of solidification," *Materials transactions,* vol. 44, no. 5, pp. 836–844, 2003.

[20]   M. L. Zappulla, L. C. Hibbeler, and B. G. Thomas, "Effect of Grade on Thermal-Mechanical Behavior of Steel During Initial Solidification," *Metallurgical and Materials Transactions A,* vol. 48, no. 8, pp. 3777–3793, 2017.

[21]   S. Koric and B. G. Thomas, "Thermo-mechanical models of steel solidification based on two elastic visco-plastic constitutive laws," *journal of materials processing technology,* vol. 197, no. 1–3, pp. 408–418, 2008.

[22]   C. Li and B. G. Thomas, "Thermomechanical finite-element model of shell behavior in continuous casting of steel," *Metallurgical and MAterials transactions B,* vol. 35, no. 6, pp. 1151–1172, 2004.

[23]   K.-h. Kim, T.-J. Yeo, K. H. Oh, and D. N. Lee, "Effect of carbon and sulfur in continuously cast strand on longitudinal surface cracks," *ISIJ international,* vol. 36, no. 3, pp. 284–289, 1996.

[24]   J. Borland, "Generalized theory of super-solidus cracking in welds," *Br. Weld. J.,* vol. 7, pp. 508–512, 1960.

[25]   T. Clyne, M. Wolf, and W. Kurz, "The effect of melt composition on solidification cracking of steel, with particular reference to continuous casting," *Metallurgical Transactions B,* vol. 13, no. 2, pp. 259–266, 1982.

[26]   E. A. López, M. H. Trejo, J. J. R. Mondragón, M. d. J. C. Román, and H. S. Tovar, "Effect of C and Mn variations upon the solidification mode and surface cracking susceptibility of peritectic steels," *ISIJ international,* vol. 49, no. 6, pp. 851–858, 2009.

[27]   J. J. R. Mondragón, M. H. Trejo, and M. d. J. C. Román, "Description of the hypo-peritectic steel solidification under continuous cooling and crack susceptibility," *ISIJ international,* vol. 48, no. 4, pp. 454–460, 2008.

[28]   S. C. Moon, R. Dippenaar, and S.-Y. Kim, "The peritectic phase transition of steel during the initial stages of solidification in the mold," in *AISTech Conference*, 2015.

[29]   S. Griesser, C. Bernhard, and R. Dippenaar, "Effect of nucleation undercooling on the kinetics and mechanism of the peritectic phase transition in steel," *Acta Materialia,* vol. 81, pp. 111–120, 2014.

[30]   H. Yasuda *et al.*, "Massive transformation from δ phase to ɤ phase in Fe-C alloys and strain induced in solidifying shell," in *IOP conference series: materials science and engineering*, 2012, vol. 33, no. 1, p. 012036: IOP Publishing.

[31]   S.-C. Moon, R. Dippenaar, and S.-H. Lee, "Solidification and the δ/ɤ

phase transformation of steels in relation to casting defects," in *IOP Conference Series: Materials Science and Engineering*, 2012, vol. 27, no. 1, p. 012061: IOP Publishing.

[32] Y.-M. Won and B. G. Thomas, "Simple model of microsegregation during solidification of steels," *Metallurgical and Materials Transactions A,* vol. 32, no. 7, pp. 1755-1767, 2001.

[33] D. Phelan, M. Reid, and R. Dippenaar, "Kinetics of the peritectic phase transformation: In-situ measurements and phase field modeling," *Metallurgical and Materials Transactions A,* vol. 37, no. 3, pp. 985-994, 2006.

[34] S.-C. Moon, "The Peritectic phase transition and continuous casting practice," 2015.

[35] M. Yoshiya *et al.*, "Impacts of Interface Energies and Transformation Strain from BCC to FCC on Massive-like δ-ɣ Transformation in Steel," in *IOP Conference Series: Materials Science and Engineering*, 2015, vol. 84, no. 1, p. 012049: IOP Publishing.

[36] Y. N. a. H. Esaka, *Tetsu-to-Hagané,* vol. 67, p. S140, 1981.

[37] T. Kawawa, "Tekko-no-Gyoko (Solidification of Steel), ed. by Solidification Comm. of ISIJ," *ISIJ, Tokyo,* pp. S32-S50, 1977.

[38] N. El-Kaddah, J. Szekely, and G. Carlsson, "Fluid flow and mass transfer in an inductively stirred four-ton melt of molten steel: a comparison of measurements and predictions," *Metallurgical Transactions B,* vol. 15, no. 4, pp. 633-640, 1984.

[39] H. D. Brody, "Solute redistribution in dendritic solidification," Massachusetts Institute of Technology, 1965.

[40] C. Cicutti and R. Boeri, "Analysis of solute distribution during the solidification of low alloyed steels," *steel research international,* vol. 77, no. 3, pp. 194-201, 2006.

[41] M. Yoshiya *et al.*, "Concurrent ɣ-Phase Nucleation as a Possible Mechanism of δ-ɣ Massive-like Phase Transformation in Carbon Steel: Numerical Analysis Based on Effective Interface Energy," *Materials transactions,* vol. 56, pp. 1467-1474, 2015.

[42] R. B. Bird, "Transport phenomena," *Applied Mechanics Reviews,* vol. 55, no. 1, pp. R1-R4, 2002.

[43] I. Jimbo and A. Cramb, "The density of liquid iron-carbon alloys," *Metallurgical Transactions B,* vol. 24, no. 1, pp. 5-10, 1993.

[44] K. Harste, "Investigation of the shrinkage and the origin of mechanical tension during the solidification and successive cooling of cylindrical bars of Fe-C alloys," *Clausthal: Technical University of Clausthal,* 1989.

[45] K. Harste, A. Jablonka, and K. Schwerdtfeger, "Shrinkage and formation of mechanical stresses during solidification of round steel strands," in *4 th International Conference Continuous Casting. Preprints.*, 1988, vol. 2, pp. 633-644.

[46] L. C. Hibbeler, K. Xu, B. G. Thomas, S. Koric, and C. Spangler, "Thermomechanical modeling of beam blank casting," *Iron & steel technology,* vol. 6, no. 7, p. 60, 2009.

[47] R. Pierer and C. Bernhard, "High Temperature Behavior during

Solidification of Peritectic Steels under Continuous Casting Conditions," *MATERIALS SCIENCE AND TECHNOLOGY- ASSOCIATION FOR IRON AND STEEL TECHNOLOGY-,* vol. 5, p. 793, 2006.

[48]   N. K. Gakkai, "Kikai Kogaku Binran," *A6-167,* 1987.

[49]   Y. M. Won, H. N. Han, T.-j. Yeo, and K. H. Oh, "Analysis of solidification cracking using the specific crack susceptibility," *ISIJ international,* vol. 40, no. 2, pp. 129-136, 2000.

[50]   J. Weiner and B. Boley, "Elasto-plastic thermal stresses in a solidifying body," *Journal of the Mechanics and Physics of Solids,* vol. 11, no. 3, pp. 145-154, 1963.

[51]   J. Risso, A. Huespe, and A. Cardona, "Thermal stress evaluation in the steel continuous casting process," *International Journal for Numerical Methods in Engineering,* vol. 65, no. 9, pp. 1355-1377, 2006.

[52]   S. Koric and B. G. Thomas, "Efficient thermo-mechanical model for solidification processes," *International journal for numerical methods in engineering,* vol. 66, no. 12, pp. 1955-1989, 2006.

[53]   J. Boehmer, G. Funk, M. Jordan, and F. Fett, "Strategies for coupled analysis of thermal strain history during continuous solidification processes," *Advances in Engineering Software,* vol. 29, no. 7-9, pp. 679-697, 1998.

[54]   H. Zhu, "Coupled Thermal-Mechanical Finite-Element Model Witb Application 10 Initial Solidification [D]," *Illinois: University of Illinois,* 1993.

[55]   R. W. Lewis, K. Morgan, H. Thomas, and K. N. Seetharamu, *The finite element method in heat transfer analysis.* John Wiley & Sons, 1996.

[56]   P. F. Kozlowski, B. G. Thomas, J. A. Azzi, and H. Wang, "Simple constitutive equations for steel at high temperature," *Metallurgical Transactions A,* vol. 23, no. 3, p. 903, 1992.

[57]   L. Anand, "Constitutive equations for hot-working of metals," *International Journal of Plasticity,* vol. 1, no. 3, pp. 213-231, 1985.

[58]   L. Anand, "Constitutive equations for the rate-dependent deformation of metals at elevated temperatures," 1982.

[59]   ANSYS, "ANSYS Mechanical User's Guide," *ANSYS Mechanical User's Guide,* p. 886, 2013.

[60]   H. Mizukami, K. Murakami, and Y. Miyashita, "Mechanical properties of continuously cast steels at high temperatures," *Tetsu-to-Hagane,* vol. 63, no. 146, p. 652, 1977.

[61]   S. B. Brown, K. H. Kim, and L. Anand, "An internal variable constitutive model for hot working of metals," *International journal of plasticity,* vol. 5, no. 2, pp. 95-130, 1989.

[62]   A. Huespe, A. Cardona, N. Nigro, and V. Fachinotti, "Visco-plastic constitutive models of steel at high temperature," *Journal of Materials Processing Technology,* vol. 102, no. 1-3, pp. 143-152, 2000.

[63]   J. Xu, S. He, T. Wu, X. Long, and Q. Wang, "Effect of elements on peritectic reaction in molten steel based on thermodynamic analysis," *ISIJ international,* vol. 52, no. 10, pp. 1856-1861, 2012.

[64]   Y. Miyashita, M. Suzuki, K. Taguchi, S. Uchida, H. Sato, and M.

Yamamoto, *Nippon Kokan Tech. Rep.,* vol. 93, p. 178, 1982.

[65]   M. H. T. Ueda, Y. Kato, T. Watanabe, M. Hashio, Y. Kato, T. Watanabe, and K. Matsui, *Tetsu-toHagané,* vol. 67, p. A37, 1981.

국문 초록

연속 주조 공정에서 아포정강은 복잡한 상변화와 높은 크랙 발생 비율을 갖는다. 이를 이해하기 위해, 우선 아포정강의 상변화 거동을 모사할 수 있는 상변화 모델을 개발하였다. 이 새로운 아포정강의 상변화 모델은 열역학, 실험식, 탄소의 확산을 고려하였으며, 연속 냉각 중의 상변화 거동을 예측하고자 하였다. 특히 δ 상에서 γ 상으로의 매시브 변태와 포정 온도에서부터 γ 상 생성까지의 과 냉(dT_p)이 상변화 모델에 포함되었다. 그 결과, 아포정강의 상변화 거동은 크게 두 가지 경로를 가짐을 확인하였다. 온도가 $T_{ps}(=T_p$(포정 온도)$-dT_p$)에 도달하기 전에 모두 δ 상으로 포정 변태 없이 응고가 완료되는 경우, 응고된 δ 상은 매시브 변태에 의해 γ 상으로 상변화가 이루어진다. 이와는 달리, 온도가 T_{ps}에 도달하기까지 응고가 완료되지 않았을 때, L/δ계면에서 포정 변태가 시작하는 경우, 포정 변태로 인한 γ 상의 성장은 주로 탄소의 확산에 의해 이루어진다.

아포정강의 상변화 모델 결과를 이용하여, 연속 주조 공정에서의 크랙 발생 메커니즘을 규명하고자 하였다. 이를 위해 고상에서의 변형률 속도, 응고 도중 부피 수축 속도 및 공공 생성 가능성을 모델링 하였다. 추가적으로 응력 해석 모델을 개발함으로서, 응고된 쉘 내의 응력 분포를 계산하였다. 그 결과 고상에서의 매시브 변태와, 응고 도중 발생하는 포정 변태가 주된 크랙 발생 메커니즘으로 판단되었다. 또한 이 두 크랙 발생 메커니즘은 탄소 조성과 dT_p 사이의 선형적인 관계를 기준으로

천이됨을 파악하였으며, 두 메커니즘이 천이되는 경계 근처에서 크랙 발생 가능성이 가장 크다는 것을 보여 주었다.

크랙 발생 예측 모델 결과를 이용하여 연속 주조 공정에서의 면세로 크랙 발생 비율 거동을 분석하였다. 이때, 앞서 진행 한 모델링 연구들을 합금강에 적용하기 위해서 유효 탄소 조성 식을 도출하여 사용하였다. 그 결과, 다양한 실험들의 유효 탄소 조성에 따른 크랙 발생 비율 거동을 특정 dT_p에서의 매시브 변태 시작 시 온도와 공공 발생 가능성을 이용하여 분석이 가능하였다. 나아가 크랙 발생 거동에 대한 실리콘, 망간, 주조 속도의 영향을 분석하였다. 실리콘 농도와 주조 속도의 증가는 최대 크랙 발생 비율을 갖는 유효 탄소 조성을 높이며, 망간 농도의 증가는 최대 크랙 발생 비율을 갖는 유효 탄소 조성을 낮추었다. 우리는 이를 L/δ계면에서 γ상이 생성되기 위해 극복해야 하는 δ/γ 계면 에너지를 계산하여 분석해 보았다. 그 결과 주조 속도, 실리콘 농도, 망간 농도는 γ상의 핵생성에 영향을 주어 dT_p를 변화시킬 수 있다고 판단할 수 있었다. 그리고 이러한 dT_p의 변화는 최대 크랙 발생 비율을 갖는 탄소 조성을 변화 시킬 수 있다고 판단되었다.

주요단어 : 아포정강, 상변태, 크랙 발생 비율, 수치 해석, 연속 주조

학번 : 2014-21448